UNIVERSIDADE D
COIMBRA

Matilde Antunes Palmeira

Implementation of a Customised Light-Sheet Microscope

Thesis submitted to the University of Coimbra in fulfilment of the requirements for the Master's Degree in Biomedical Engineering, specialization in Biomedical Instrumentation, under the scientific supervision of Professor Luísa Maria Oliveira Pinheiro Leitão Cortes and Professor António Miguel Lino Santos Morgado and presented to the Department of Physics of the Faculty of Sciences and Technology.

September 2023

University of Coimbra

Implementation of a Customised Light-Sheet Microscope

Matilde Antunes Palmeira

Thesis submitted to the University of Coimbra in fulfilment of the requirements for the Master's Degree in Biomedical Engineering

Supervisors:
Professor Luísa Maria Oliveira Pinheiro Leitão Cortes
Professor António Miguel Lino Santos Morgado

Coimbra, September of 2023

Agradecimentos

Agradeço aos meus orientadores, a Doutora Luísa Cortes e o Doutor Miguel Morgado, pelo seu apoio e por terem possibilitado a oportunidade de fazer uma tese numa área tão interessante. Nunca teria imaginado que estaria a brincar com Legos nesta fase da minha vida. Obrigada à Doutora Luísa por me acolher durante este ano no MICC, me incentivar a superar os desafios e pela sua empatia.

Um agradecimento especial ao Doutor Julien Colombelli, sem o qual este projeto não seria possível, por todas as horas em que me acompanhou no desenvolvimento do LEMOLish, por explicar detalhadamente todas as dúvidas que tive e pela honra de implementar um microscópio tão curioso.

Fundamentais na minha passagem pelo laboratório, agradeço à Tatiana Catarino e à Margarida Caldeira pela sua amizade, pelo seu humor, por me ensinarem a usar pipettes e me dizerem onde estão os reagentes, e por me apoiarem continuamente neste projeto. Agradeço ainda ao Nuno Beltrão pelo seu apoio no laboratório e por me ajudar na montagem um cérebro de ratinho particularmente gelatinoso.

Agradeço a quem me apresentou ao mundo da investigação e sempre me motivou a ir mais longe - um grande obrigada ao Doutor Rui Travasso, ao Marcos Gouveia, ao Marco Louro e à Catarina Peneda. Agradeço ainda à Sofia Faria, a minha companheira de estágio, por me inspirar com os seus feitos.

Estes cinco anos foram enriquecidos pela companhia da Disa Palma, Francisca Afonso, Joana Antunes, Laura Ferreira, Lídia Faria e Raquel Gonçalves, com quem partilhei as alegrias e mágoas de estudar Engenharia. Agradeço à Sara Cardoso e à Teresa Sousa, pela sua curiosidade no meu percurso e pelo seu apoio. À Sara Esteves, pela sua amizade e por me mostrar como se trabalha em direção aos nossos objetivos. E um grande agradecimento ao CIAAC, pelas amizades e lições, em especial ao Paulo Nogueira Ramos e à Emília Oliveira que tanto me ensinaram e motivaram.

Não estaria a escrever esta tese sem os meus pais, que possibilitaram os meus estudos e me mostraram o mundo, ouvindo sempre os altos e baixos deste percurso. Agradeço à minha prima Olívia pelo seu sentido de humor e por me incentivar nesta aventura. Agradeço à família Vieira por me receber sempre de braços abertos. Ao meu Jorge, que teve infinita paciência e carinho ao longo destes cinco anos, um enorme obrigada.

E porque não me falhou no decorrer desta tese, agradeço ao meu computador pelo seu esforço e por me acompanhar neste projeto incansavelmente.

Muito obrigada!

Abstract

Light-Sheet Fluorescence Microscopy (LSFM) is an imaging technique that has gained interest due to its ability to image large samples three-dimensionally. The relevance of the LSFM is due to its distinctive feature, the light-sheet, and its architecture, where the illumination path is orthogonal to the detection path. In essence, a plane of light illuminates a section of the sample, which is then captured by the detection unit perpendicular to that plane, therefore performing optical sectioning. This means that only light from the plane in focus is captured, which also minimizes the effects of photobleaching and phototoxicity, as only that section is illuminated.

When discussing LSFM, tissue clearing always arises. It is possible to image entire samples, such as mouse organs, with LSFM. However, if they are opaque, the light-sheet can not penetrate the tissue. For this reason, it is necessary to render the samples transparent. Many tissue clearing protocols have been developed in order to achieve minimal light scattering and absorption, although there is no perfect technique that fits all samples. Different tissues, labels, sample sizes, or other specifications may ask for different approaches.

In this present work, two tissue clearing protocols were explored - iDISCO+, a solvent-based protocol, and CUBIC, an aqueous-based protocol. The results for mouse brain samples and mouse liver samples were photographically documented to showcase the evolution of the samples as they progress through the steps of clearing. The samples were also labelled and imaged with the Confocal Microscope to confirm if the protocols are compatible with fluorescent labelling.

Even though LSFM has gained popularity in the last few years, it may not be available in all research institutes - it would be useful to have a screening tool for cleared and labelled samples at hand. For this reason, in this project, we aimed to assemble the open-source light-sheet microscope LEMOLish, which was created by Julien Colombelli and Sébastien Tosi of the Institute for Research in Biomedicine of Barcelona. To improve the system and increase the openness to the community, Arduino code was developed to control the microscope. Therefore, this thesis describes the assembly of the LEMOLish and the Arduino code in use, as well as documents the three-dimensional images of mouse brain samples obtained with it.

The results presented in this thesis underscore the LEMOLish system's strong potential to successfully achieve its primary objective of screening cleared samples.

Keywords: Light-sheet Microscopy, Fluorescence Microscopy, Tissue Clearing, Prototype

Resumo

A Microscopia de Fluorescência em Folha de Luz (*Light-Sheet Fluorescence Microscope* ou LSFM em inglês) é uma técnica de imagiologia que tem ganho interesse devido à sua capacidade de obter imagens tridimensionais de amostras de grandes dimensões. A relevância da LSFM deve-se à sua caraterística distintiva, a folha de luz, e à sua arquitetura, em que o percurso de iluminação é ortogonal ao percurso de deteção. Essencialmente, um plano de luz ilumina uma secção da amostra, que é depois captada pela unidade de deteção perpendicular a esse plano, realizando assim o seccionamento ótico. Isto significa que apenas é captada a luz do plano em foco, o que também minimiza os efeitos de fotobranqueamento e fototoxicidade, uma vez que apenas essa secção é iluminada.

Quando se discute a LSFM, surge sempre a questão da transparentização de tecidos (*tissue clearing*). É possível obter imagens de amostras inteiras, como órgãos de ratos, com LSFM. No entanto, se estas forem opacas, a folha de luz não consegue penetrar o tecido. Por este motivo, é necessário tornar as amostras transparentes. Foram desenvolvidos vários protocolos de transparentização de tecidos para conseguir uma dispersão e absorção mínimas da luz, embora não exista uma técnica perfeita para todas as amostras. Diferentes tecidos, marcação fluorescente, tamanhos de amostras ou outras especificações podem exigir abordagens diferentes.

No presente trabalho, foram explorados dois protocolos de transparentização de tecidos - iDISCO+, um protocolo à base de solvente, e CUBIC, um protocolo à base de água. Os resultados das amostras de cérebro e fígado de rato foram documentados fotograficamente para mostrar a evolução das amostras à medida que progridem nas etapas de transparentização. As amostras foram também marcadas e visualizadas com o microscópio confocal para confirmar se os protocolos são compatíveis com a marcação fluorescente.

Embora a LSFM tenha ganho popularidade nos últimos anos, pode não estar disponível em todos os institutos de investigação - seria útil ter uma ferramenta para a avaliação das amostras transparentizadas e marcadas. Por este motivo, neste projeto, procedeu-se à montagem do microscópio de folha de luz *open-source* LEMOLish, criado por Julien Colombelli e Sébastien Tosi do Instituto de Investigação em Biomedicina de Barcelona. Para melhorar este sistema e aumentar a sua acessibilidade à comunidade, foi desenvolvido código Arduino para o controlo das várias partes do microscópio. Por conseguinte, esta tese descreve a montagem do LEMOLish e o código Arduino em uso, bem como documenta as imagens tridimensionais de amostras de cérebro de rato com ele obtidas.

Os resultados apresentados nesta tese sublinham o forte potencial do sistema LEMOLish para atingir com sucesso o seu objetivo principal de avaliar amostras transparentizadas.

Palavras-chave: Microscopia de Folha de Luz, Microscopia de Fluorescência, Transparentização de Tecidos, Protótipo

Contents

List of Figures

List of Tables

Acronyms

BABB Benzyl Alcohol/Benzyl Benzoate.

BSA Bovine serum albumin.

CCD Charged-coupled device.

CMOS Complementary metal–oxide–semiconductor.

DBE Dibenzyl ether.

DCM Dichloromethane.

DMSO Dimethyl sulfoxide.

DPSS Diode-pumped solid-state.

EEPROM Electrically Eraseable Programmable Read Only Memory.

LSFM Light Sheet Fluorescence Microscopy.

PBS Phosphate buffered saline.

PFA Paraformaldehyde.

RI Refractive index.

RT Room temperature.

SPIM Selective Plane Illumination Microscopy.

Chapter 1

Introduction

1.1 Context and Motivation

In science, looking beyond what we see is paramount to find answers to what sparked our curiosity . Light microscopy allows us to do just that and has become a fundamental part of research.

Nowadays, research facilities generally employ more than one type of microscope (namely wide-field microscopes, multi-photon microscopes, confocal microscopes and light-sheet microscopes), each having their own strengths and limitations. In Coimbra, there is no Light-Sheet Fluorescence Microscope (LSFM). This means that if a research team is seeking to employ the capabilities of LSFM, they must travel to a research facility outside of Coimbra. For this reason, it would be beneficial to screen samples to verify that they are properly prepared before accessing a different research facility. The LEMOLish, conceived by Julien Colombelli and Sébastien Tosi of the Institute for Research in Biomedicine of Barcelona, is a LEGO® LSFM. This system is an ideal candidate to implement, given that it is simpler and cheaper than commercial options.

To be able to image samples in a LSFM, they must be transparent so that the light-sheet can reach deep into the tissue, and the subsequent emitted light (from fluorescent markers) can be observed through the sample. Samples may be naturally transparent (such as zebrafish), or they may need to be optically cleared. For this reason, it is relevant to this thesis to explore tissue clearing protocols, which, as exposed in the State of the Art section, can be varied in terms of efficiency, safety, complexity, cost, or duration.

1.2 Objectives

This thesis aims to explore the effectiveness of two types of tissue clearing protocols (more precisely, iDISCO+, a solvent-based protocol, and CUBIC, an aqueous-based protocol) to clear different types of tissue, and, subsequently, the implementation of the open-source Light-Sheet Microscope LEMOLish to image cleared samples. This second part of the project also intends to develop the Arduino code required to control the different parts of the LEMOLish. This has not been implemented in the original version, which uses the LEGO-MINDSTORMS® EV3 Intelligent Brick to operate the microscope.

1.3 Workflow

An overview of the distribution of the main stages of this project is presented in Figure 1.1.

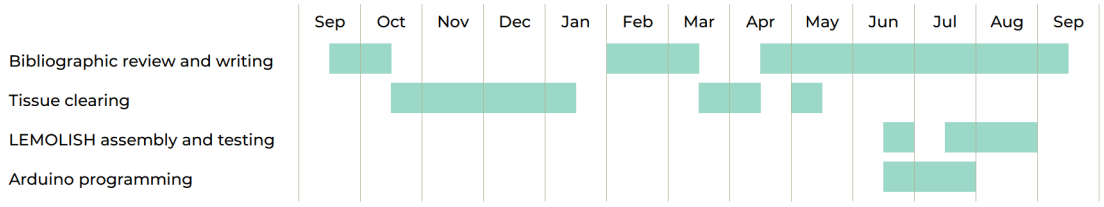

Figure 1.1: Gantt chart of the general stages of the thesis project.

1.4 Thesis Structure

This thesis is composed of five chapters:

- Chapter 1 – Introduction: the present chapter introduces the context and motivation behind the completion of this thesis and the summarized workflow implemented during the project;
- Chapter 2 – Tissue Clearing and Light-Sheet Fluorescence Microscopy – Principles and State of the Art: this chapter overviews the principles of the methodology and technology explored in this thesis, as well as their evolution throughout the decades. It firstly presents the general principles of tissue clearing and gives examples of different types of protocols, and dives deeper into the protocols performed in this thesis, CUBIC and iDISCO+. Then, it delves into Light-Sheet Fluorescence Microscopy and presents its working principles, comparing it to other types of microscopy techniques, and its evolution;
- Chapter 3 – Materials and Methods: in this chapter, the iDISCO+ and CUBIC protocols applied to clear tissue sample are described firstly; in a second part, this chapter details the implementation of the LEMOLish microscope;
- Chapter 4 - Results and Discussion: the results for the tissue clearing protocols and the implementation of the LEMOLish microscope are presented in this chapter;
- Chapter 5 - Conclusion and Future Work: the final, general conclusions are discussed in this sections, as well as the achieved goals and future challenges.

Chapter 2

Tissue Clearing and Light-Sheet Fluorescence Microscopy – Principles and State of the Art

2.1 Tissue Clearing

2.1.1 What is tissue clearing?

Tissue clearing is the process of rendering large biological samples transparent. It has been used in samples with thickness ranging from tens of micrometres to a few centimetres (for example, an entire mouse brain or even a full embryo [1]–[3]). This process alters the optical properties of the sample, allowing the light to propagate throughout the tissue with minimal scattering. Since there is no need to mechanically slice the sample, tissue clearing allows us to see into an intact sample, which is valuable to explore the features and 3D structures of the tissue continuously.

The pursuit of cleared tissues is not new - tissue clearing was first investigated by Werner Spalteholz in the early 1900s, who accomplished cleared biological samples by dehydrating tissues and matching the refractive index (RI) within the tissue with the media surrounding it [4]. Since then, many different methods of tissue clearing have been published with the goal of optimizing the protocols according to the sample and the goal of the study. However, they all follow the same strategy: removing, replacing and/or modifying cellular content and homogenizing the RI of the sample [2], [5].

The great number of protocols that have been put forward since Spalteholz's first experiments try to improve on several criteria, thus each of them have their own advantages and disadvantages. There are many factors to consider, such as uniformity of transparency, autofluorescence, sample shrinkage or expansion, retaining molecules of interest and endogenous fluorescence, structural integrity, porosity, cost, or speed [2], [5], [6].

Even though there are many protocols for tissue clearing, they can be divided into different types of approaches, as presented in the subsection 2.1.4.

2.1.2 The interaction of light and matter

Before explaining what are the fundamentals of tissue clearing protocols, it is important to understand what makes a tissue not transparent. Tissues are composed of many structures, which light interacts with, generating a translucent or opaque sample – for example, light will not propagate through water as it does with lipids or proteins, and will reflect off the surface of the different components of the tissue due to differences in the RI [7]. The fundamental optical processes behind the non-transparency of the tissues are refraction, absorption and scattering.

Refraction and reflection

The refractive index of a material is a property that describes how the material affects the speed of light travelling through it and although it is a complex number, conventionally, it is only expressed as its real part. It corresponds to the ratio between the speed of light in vacuum and the speed of the light travelling through the material:

$$n(\lambda) = \frac{c}{c_m(\lambda)}$$

where c is the speed of light in vacuum, λ is the wavelength of the light, n(λ) is the RI of the material for λ and $c_m(\lambda)$ is the speed of the light in the material [8].

When a photon is propagating through a material and reaches the boundary with another material that has a different RI, refraction and/or reflection can occur. The angle of refraction depends on the angle of incidence, the polarization of the wave and the ratio between the refractive indices. The angle of refraction can be calculated by Snell's law:

$$sin(\theta_2) = \frac{n_1}{n_2} sin(\theta_1)$$

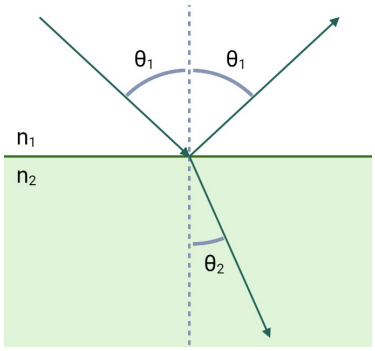

Figure 2.1: Illustration of the incident and reflection angle, θ_1, and the refraction angle, θ_2, as the photon reaches a material with a different RI.

If n_1 is greater than n_2, θ_2 will be greater than θ_1 [8]. To elaborate, the light's path will be deviated, which may result in distortions. When imaging a tissue sample, distortions due to varying RI within the sample would prevent the observer from accurately assessing the configuration of the structures in the sample. If the sample has the same RI all over, the light does not cross boundaries between regions of different RI and therefore is not refracted.

Absorption

The process of absorption involves the energy levels of the electrons in matter. It corresponds to a transition between a lower energy level to a higher energy level due to the atom absorbing a certain amount of energy in the form of a photon that is equal to the difference in energy between these levels, ΔE:

$$\Delta E = h\nu$$

where h is the Planck's constant and ν is the frequency of the photon [8]. This interferes with the excitation light and the fluorescence emission light [7]. The absorbed energy can be later released in the form of heat or by the emission of a photon[8], [9]. The relation between the irradiance of the beam before and after crossing a certain z distance in a medium is given by Beer-Lambert's law:

$$I = I_0 e^{-\mu_a L}$$

where I is the irradiance after the beam crosses the medium, I_0 is the irradiance of the incident beam, μ_a is the absorption coefficient of the medium and L is the distance travelled [10].

Absorption can result in electronic, vibrational, or rotational transitions. An electronic transition is the elevation of the energy level of the particle, occurring in atoms or molecules and, depending on the atoms/molecules, can occur due to light from the ultraviolet to the infrared region of the spectrum. Vibrational transitions are the switch from one vibrational level to another, which can happen in molecules due to light in the infrared region. Rotational transitions are the switch from a rotational state to another, occurring in molecules due to light in the far infrared region [8].

From a biological standpoint, there are many absorbing molecules present in the tissues. Some examples for absorption in the visible spectrum include oxyhemoglobin (for wavelengths raging 400-600 nm) [11], deoxyhemoglobin (400-850 nm) [11] and melanin, whose absorption spectrum ranges from the ultraviolet to the near-infrared (300-800 nm) [12], [13]. DNA absorbs in the ultraviolet region, presenting an absorption band at 260 nm [8], [13]. Examples for longer wavelengths include water and lipids, which absorb in the near-infrared region of the spectrum, with an absorption peak at 980 nm and 930 nm, [8], [13], [14].

Scattering

Scattering consists in the redirection of the light particles' trajectory in a certain angle relative to its original direction of propagation due to non-uniformities in the

medium [9], [10]. The Rayleigh limit, the Mie regime and the geometric limit are important concepts to keep in mind when studying the scattering of light in tissues.

The Rayleigh limit is related to the scattering of light by structures in the tissue that are smaller than the wavelength of the incident photon. In this situation, shorter wavelengths tend to scatter more [7], [9]. Rayleigh scattering is a case of elastic scattering (the scattered energy maintains its energy) [8].

The Mie regime is applicable to particles whose size is comparable to that of the wavelength [7], [9]. Although the Mie theory was conceived for spherical structures [9], it can be applied to cellular components such as mitochondria or vesicles [8].

The geometric limit is applied when the scattering structure's diameter is about ten times larger than the photon's wavelength [9].

Scattering decreases the quality of the image. For the same medium (e.g. tissue sample) and wavelength, the longer the path is, the higher the probability of scattering is, as the incident photons must travel a longer distance. This means that the light to be detected is not a perfect orthogonal image, as some light has been diverted from its original path [7], [8]. In epi-illumination, both the light source and the detector for the fluorescence emission are on the same side of the sample, whereas in trans-illumination the sample is illuminated on one side and the emitted light is detected on the opposite side. Epi-illumination is preferred over trans-illumination as it is more difficult to distinguish the emission light from the source light when using trans-illumination [15]. In the case of light-sheet microscopy, the emitted light is detected perpendicularly to the source light.

2.1.3 The overall steps of tissue clearing

Although there are several different approaches to perform tissue clearing, which will be discussed later (subsection 2.1.4), they are composed of similar major steps: fixation, pre-treatments, delipidation, labelling and RI matching [5], [6]. A summarized view of these steps is present in Figure 2.2

Fixation

Fixation preserves the integrity of the tissue by covalently crosslinking proteins and/or nucleic acids in the tissue, allowing it to withstand harsher steps during the clearing process due to the increased stability of the tissue. The most used fixative is paraformaldehyde (PFA) at a concentration of 3-4% in phosphate-buffered

saline (PBS), which crosslinks the tissue's biomolecules by reacting with amine groups on proteins and nucleic acids; other examples of fixatives are glutaraldehyde, which is chemically similar to PFA, or polyepoxide molecules, such as polyglycerol-3-polyglycidyl ether (P3PE) [6]. For mouse samples, fixation can be performed actively by taking advantage of the mouse's vasculature. In fact, using the standard protocol, blood is washed out after the animal is sacrificed by transcardial perfusion with PBS and followed by perfusion with the fixative solution [1].

It is important avoid underfixation or overfixation. Underfixation reduces stability in the tissue and its ability to withstand clearing, whereas overfixation can prevent labelling due to antigen masking (access to the epitopes is blocked due to the chemical reactions between the fixative and the proteins in the tissue), and can reduce the antibody penetration. [5], [6]

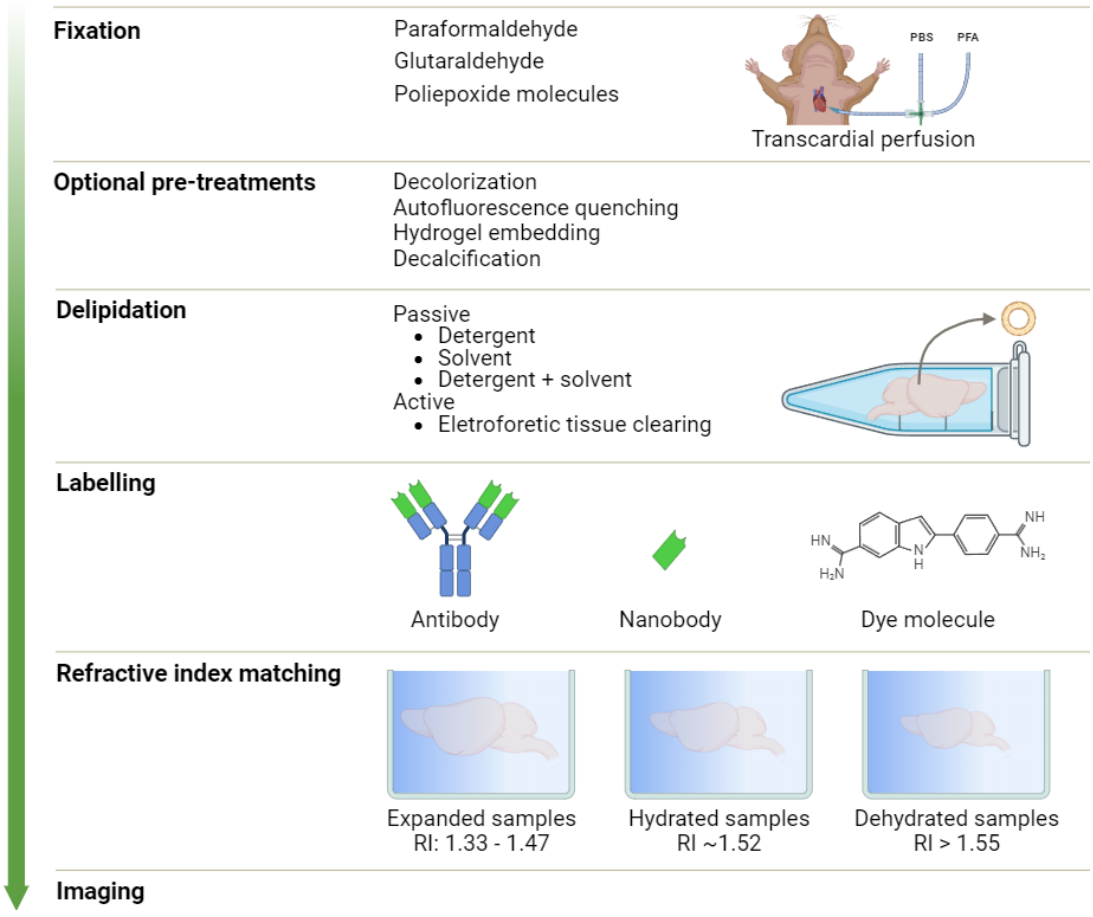

Figure 2.2: Overview of the different steps of tissue clearing. Based on [6].

Pre-treatments

Some tissues, such as larger or pigmented samples, may require additional steps for the clearing to be successful.

Decolourization

Even though the absorption of light is key in fluorescence, there are pigments in tissue samples, such as the haeme group in haemoglobin and myoglobin, which prevent an effective image acquisition by blocking the passage of light [1], [5], [6].

There are many methods to remove pigments from the samples. These include perfusing the animal with PBS to remove its blood, although this method might not be enough to remove all the haeme from blood-rich tissues [6]. Another method is to incubate the sample in hydrogen peroxide, which can be very effective by breaking the chemical bonds of the pigments, but might damage the tissue or alter epitopes, and will quench the tissue's endogenous fluorescence [5], [6]. Amino alcohols are also used to remove haeme and can also contribute to extract lipids, namely N,N,N',N'-Tetrakis(2-hydroxypropyl)ethylenediamine (Quadrol, a component of the CUBIC protocol), N-methyldiethanolamine (NMDEA), and 3-[(3-cholamidopropyl)dimethylammonio]-1-propanesulfonate (CHAPS), or 2,2',2",2"' - (Ethylenedinitrilo)tetraethanol (or THEED) [6]. A different approach to this problem is to use light with wavelengths that the pigments do not absorb [7].

Autofluorescence quenching

Some molecules present in tissues are natively fluorescent and emit light when excited. Examples of endogenous fluorophores that may be present in the sample are aromatic aminoacids, collagen/elastin, NAD(P)H, flavins, fatty acids, vitamin A, protoporphyrin and lipofuscins [16].

This endogenous fluorescence can be useful to study the tissues' morphology and function [16], and can be coupled with fluorescent dyes that emit light in different wavelengths [6]. However, autofluorescence may cover the (exogenous) fluorescent labelling in the sample and reduce the signal-to-noise ratio [5], [6]. Some methods used to decolourize the sample also quench autofluorescence, namely the perfusion of the animal with PBS and the incubation in hydrogen peroxide [5]. Photobleaching is also used to reduce autofluorescence [5], [6].

Hydrogel embedding

First used in the protocol CLARITY, the main purpose of this optional step is to improve the mechanochemical properties of the sample by creating links that hold the molecules in place [2], [6]. However, this method can have other advantages, such as facilitating the expansion of the sample and allowing more elasticity [6], [7]. The protocols that use hydrogel embedding are considered as a separate group of tissue clearing approaches by some authors and is further discussed in subsection 2.1.4.

Decalcification

Bone tissue can be cleared too. This tissue is mainly composed of hydroxyapatite crystals in a collagen matrix and its clearing consists in the elution of the calcium ions that compose hydroxyapatite. Decalcification can be achieved through submerging the tissue in an acidic solution or a chelating reagent (such as EDTA), which is less aggressive on the soft tissues surrounding the bone [1], [6].

Delipidation

As stated in subsection 2.1.2, lipids contribute to the lack of transparency of a sample, and function as a barrier to the delivery of fluorescent probes. Lipids can be removed by organic solvents and/or detergents and can also have the aid of electric fields [1], [6]. Classification of tissue clearing protocols is based on this difference in delipidation approaches and will be further described in subsection 2.1.4.

Labelling

Labelling consists in targeting specific cellular components, commonly by using small molecular dyes, antibodies conjugated with dyes or genetically encoded fluorescent proteins. Due to their size, small molecular dyes or nanobodies (antibody fragments) permeate the tissue quickly, whereas immunostaining (using antibodies, larger molecules) is slower [5], [6]. Because the tissue becomes transparent, it is possible to detect fluorescent emission coming from deeper into the tissue. Therefore, the labelling in cleared tissues allows to extract information about the tissue's structure and cellular organization, such as the spatial distribution of the different cells in the tissue or the expression pattern of a protein of interest.

Some optimization may be necessary to obtain a successful staining of the tissue. Labels that take longer to permeate the tissue may result in an uneven distribution of labelling. Therefore, it might be advantageous to use smaller samples (by mechanically slicing the sample or inducing shrinkage) or one may select smaller molecule labels. Permeabilization of the sample is also important to increase its porosity [5], [6].

RI matching

This is the final step in a tissue clearing protocol – immersing the sample in a solution that matches the RI of the components that were left after the previous

steps. These components are mainly proteins, which have an RI superior to 1.50 [6]. In fact, for many protocols, it is only on this step that the sample exhibits transparency [5]. However, the sample will not be perfectly transparent, as it usually exhibits a slight yellow-brown tint due to the proteins that were retained [5].

As with the previous steps, the RI matching solution must be compatible with the solutions used previously, and with the fluorescent labels, if any were used [6]. The samples are homogenised to a RI in the range of 1.33 to 1.60 depending on the methods used [2], [6]. The lower RI solutions are applied in clearing methods that can expand the sample and lower its RI, such as when using aqueous solutions or hydrogel embedding [6].

After the tissue is cleared, it is possible to do a primary evaluation the quality of the transparency visually by overlaying the sample on a patterned background, such as a grid (as shown in [17]–[19]) , and assessing if it is possible to see the pattern through the sample and if there are distortions.

At this point, the samples components and its surroundings have the same approximate RI, but the microscope's optics should also be taken into consideration to avoid spherical aberration [1], [7]. This is discussed in subsection 2.3.1.

2.1.4 The different approaches to tissue clearing

Since Spalteholz started exploring tissue clearing, many methods have been developed throughout the decades. They can be divided into two main groups – solvent-based or aqueous-based [7]. Hydrogel embedding approaches can be considered as a third group [1], [2], [5]. This partition is not strict, as these approaches can be divided into the different modules that were described in the previous topic and combined to create a new protocol [5], [6].

Solvent-based clearing methods

These methods are the followers to Spalteholz experiments. His protocol followed several steps: after fixation, the tissue was bleached using hydrogen peroxide, followed by dehydration using solutions of consecutively higher percentages of alcohol (the dehydration is necessary because the clearing solution is hydrophobic, but it also permeabilizes the cells' membranes and helps with delipidation [6]). After that, the tissue would be submerged in benzene before being incubated in the clearing solution that contains methyl salicylate and benzyl benzoate (5:3 ratio) combined with wintergreen oil [1], [4]. In general, modern solvent-based clearing methods

follow these steps: dehydration, lipid removal and RI matching.

The dehydration step is composed of several steps of solutions with increasingly higher concentrations of alcohol (0 to 100%), which progressively removes the water content of the sample. Many reagents have been used for this purpose, such as methanol (e.g. iDISCO [20]), ethanol (e.g ethanol-ECi protocol [21]), tetrahydrofuran (e.g. 3DISCO [22]), 1-propanol or tert-butanol (e.g. FluoClearBABB [23]). Methanol, ethanol and THF are strong dehydrators, but they are not recommended if the goal is to keep endogenous fluorescence [6]. The dehydration step already removes part of the lipids, but an additional delipidation step with dichloromethane (DCM) may be necessary [4], [6], [7].

The final step of matching the RI has been achieved with different reagents, namely benzyl alcohol/benzyl benzoate (BABB), dibenzyl ether (DBE), or other less toxic solvents, such as 2,2-thiodiethanol (TDE) and ethyl cinnamate [6].

Solvent-based methods are effective, fast and can clear different types of tissues [2], [7]. However, these techniques have disadvantages. There may be interference with epitopes and fluorescent protein emission may be quenched. Besides that, the chemicals used are often toxic and/or corrosive, and can damage lab equipment, such as microscope objectives that are not prepared for use with this type of chemicals [6], [7].

Aqueous-based clearing methods

The aqueous-based clearing methods were developed in an attempt to avoid the disadvantages of the solvent-based methods. These methods can be further divided into two families: High RI solutions (simple immersion) and hyperhydrating solutions [1], [2], [7].

High RI solutions are used to passively clear the samples by simply immersing them in the high RI medium. Examples of the component of these solutions are sucrose, fructose, glycerol, 2,2'-thiodiethanol (TDE) or formamide [7]. Examples of techniques in this family are FRUIT, immersion in TDE, ClearT2 or SeeDB2, and, commercially, FocusClear or RapiClear [2], [7]. The simplicity and the compatibility with fluorescence dyes of these techniques is interesting, but they have a few downsides, such as a lower clearing efficiency, slow clearing, and, for some techniques that use solutions with high concentrations of sugar or glycerol, the high viscosity [2], [7].

Methods that involve hyperhydration include more steps to achieve a better

clearing result. As the solvent-based methods presented previously, a delipidation step is added, which, in this case, will involve a detergent to remove the lipid layers of the cell [2], [6]. SDS, Triton X-100 and CHAPS are commonly used for this purpose [6]. These aqueous-based methods also use high concentrations of urea [2], [7], [24]. Urea is responsible for the hydration of the sample, including the hydrophobic regions of proteins [7]. This hyperhydration process lowers the RI of the sample, so the final clearing solution can have a slightly lower RI than those used in solvent-based methods [7]. This solution must be hydrophilic, such as sucrose, fructose, iohexol or other newer chemicals like antipyrine and nicotinamide [6], [25]. Aqueous-base clearing methods have the advantage of being simpler, preserving fluorescent proteins and using safer chemicals at the cost of generally taking longer than their solvent-based counterparts [1], [2].

Hydrogel embedding clearing methods

Hydrogel-based protocols try to improve the mechanochemical properties of the sample so that the damage to the tissue is minimal and the proteins are stable [1], [2], [7].

The most used hydrogel embedding techniques are CLARITY, which embeds the tissue in acrylamide and bisacrylamide monomers, and PACT/PARS, which embeds the tissue in acrylamide. These monomers will form polyacrylamide with the paraformaldehyde used in the fixation step [4], [6]. A step of gassing the sample with nitrogen to remove the oxygen can be included for a faster polymerization [4]. The delipidation step can be performed passively or actively – the passive clearing consists in simple immersion in detergent (as in passive CLARITY or PACT), whereas the active clearing uses electrophoresis in a chamber with the clearing solution (as in active CLARITY). PARS uses the vasculature of the animal to infuse the tissue with the monomers and the clearing solution [3].

These techniques show great performance and the effect of tissue expansion can be used as an advantage. However, they can be slow if they have a passive approach, or they require more complex steps for a faster clearing time [2], [7]. Some authors present hydrogel embedding as an optional pre-treatment [6].

2.1.5 The optimization of the CUBIC and DISCO protocols

Tissue clearing has found widespread use across many fields as researchers continuously work on the optimization of tissue clearing protocols so that they can be

applied to their samples' requirements.

In this thesis, two protocols are explored: an aqueous-based protocol, CUBIC, and a solvent-based protocol, iDISCO+. The following sections describe the evolution of these approaches as they are modified for different applications.

CUBIC

The aqueous-based clearing protocol CUBIC (meaning "clear, unobstructed brain imaging cocktails and computational analysis") was first introduced by Susaki et al. in 2014 as a way to transparentize a whole mouse brain [26]. Since then, numerous versions have been put forward to optimize this protocol for the best clearing of many different types of tissue [1], [25].

To create the CUBIC protocol, Susaki et al. thoroughly examined the pre-existing ScaleA2 protocol and tested other possible chemicals that could be used instead of the glycerol, urea or Triton X-100 in that protocol to provide the best results for clearing and fluorescence stability. The final CUBIC protocol presented used two reagents: ScaleCUBIC-1, that is composed of 25 wt% urea, 25 wt% N,N,N',N'-tetrakis(2-hydroxypropyl)ethylenediamine (THEED) and 15 wt% Triton X-100, and ScaleCUBIC-2 that is a mixture of 50 wt% sucrose, 25 wt% urea, 10 wt% 2,2',2"-nitrilotriethanol, and 0.1 %(v/v) Triton X-100. The process begins by immersing a whole mouse brain in reagent 1 at 37 °C for three days, followed by another immersion of fresh reagent 1 for another three to four days. After that, the sample is washed with PBS and then immersed in 20 %(w/v) sucrose in PBS. Then, the sample is immersed in reagent 2 for three to seven days (incubation times are dependent on sample type and size). Finally, the sample can be washed with PBS and kept in 20 %(w/v) sucrose in PBS at -80 °C. The authors reported that the clearing process took two weeks, which is faster than the Scale protocols [26].

As stated before, CUBIC has since been used in other types of tissue. It has been applied to other mice organs such as the heart, mammary glands or bones, and to human tissues from the lung, kidney, spleen, intestines, lymph nodes or brain [1]. Tainaka et al. further analysed the CUBIC protocol, having screened over 1600 chemicals to improve on the efficiency of CUBIC in the delipidation, decolouring, decalcification and RI matching steps [25]. For delipidation and decolourization, the authors include the use of N-butyldiethanolamine, 1-methylimidazole or 1,3-bis(aminomethyl) cyclohexane in the reagent for this step (CUBIC-P includes the first two plus Triton X-100, CUBIC-L includes the first and Triton X-100 and CUBIC-HL, the harshest mixture, includes the latter along with 10 wt% sodium

dodecylbenzenesulfonate). For decalcification, the authors found that a cocktail of EDTA and imidazole is optimal - this is the reagent CUBIC-B. Finally, for RI matching, Tainaka et al. indicate that amides have the best performance and antipyrine avoids tissue shrinkage, using them in the reagents CUBIC-R (with antipyrine and nicotinamide) and CUBIC-RA (with antipyrine and N-methylnicotinamide for better performance with fluorescent proteins).

The protocol implemented in this thesis uses CUBIC-L for delipidation and CUBIC-R+ for RI matching. A representative scheme of the sequence of steps is found in Figure 2.3.

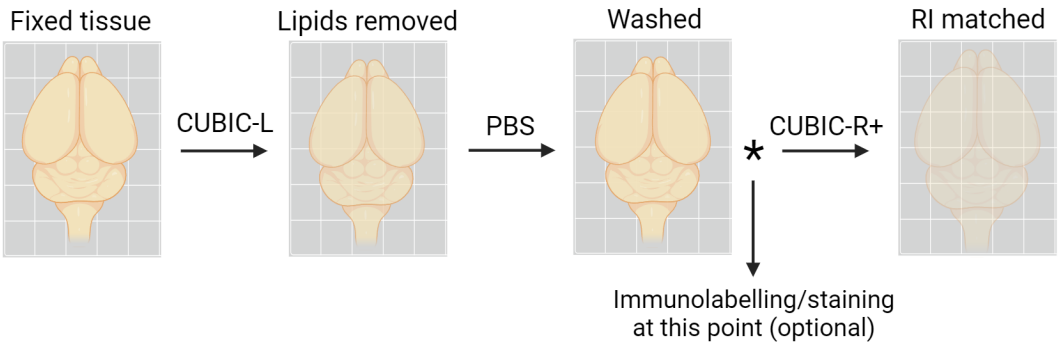

Figure 2.3: Simplified scheme of the application of the CUBIC protocol on a mouse brain. Based on [26] and [27]. Created with BioRender.com

DISCO

The DISCO family encompasses the many protocols that have arisen since Erturk et al. presented the 3DISCO protocol in 2012, meaning "3D imaging of solvent-cleared organs" [22].

Erturk et al. set out to develop a protocol that could successfully clear adult mouse brains and spinal cords. They first implemented a protocol that used alcohol (for dehydration) and BABB (for the optical clearing), but the alcohol degraded the fluorescent signal and this combination could not clear the myelinated tissues of adult mice. Consequently, they scanned multiple chemicals that could replace alcohol and BABB, having selected THF and DBE, respectively. For the delipidation of small samples, DCM was used. With this combination, they were able to successfully clear the adult mice brains and had positive results for other tissues, such as lung, spleen, lymph nodes, mammary glands and tumor tissue [22].

Later, in 2014, Renier et al. published their efforts to improve upon 3DISCO by incorporating key elements from other clearing methods, creating the iDISCO protocol. The goal of iDISCO was to improve on the immunolabelling step and creating

a simple and inexpensive protocol. Renier et al. added a pretreatment to bleach the samples that includes hydrogen peroxide, methanol and DMSO [20]. Then, in 2016, Renier et al. presented iDISCO+, where they used methanol instead of THF and added an extra step with DCM and methanol for further delipidation [28]. The protocol implemented in this thesis is the iDISCO+ with an added decolourization step. A representative scheme of the sequence of steps is found in Figure 2.4.

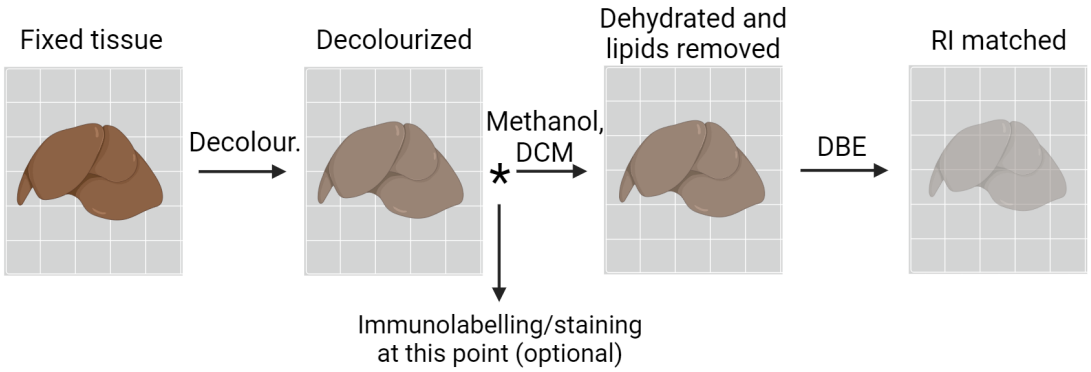

Figure 2.4: Simplified scheme of the application of the iDISCO+ protocol on a mouse liver. Based on [28]. Created with BioRender.com

The DISCOs are solvent-based protocols that cause some shrinkage in the tissue, mainly due to the permeabilization and dehydration steps [1], [6], an effect that Pan et al. explored in uDISCO as an advantage. Using "ultimate DISCO", the authors cleared entire mice bodies while overcoming the difficulties of imaging large volumes and optimizing the preservation of endogenous fluorescence in the sample. uDISCO uses alpha-tocopherol as an antioxidant, tert-butanol instead of THF as a dehydrator (as it is more stable), and a mixture of diphenyl ether (DFE) and BABB to match the RI (instead of DBE, to preserve fluorescence) [19].

In 2018, Li et al. published their results on the improvement of GFP fluorescence with the uDISCO protocol, creating the a-uDISCO protocol that uses an optimized pH values in the tert-butanol and BABB solutions, having reached an optimal value of 9.0-9.5 [29].

A different approach, FDISCO, also improves the preservation of fluorescence in the sample – Qi et al. adjusted the original 3DISCO protocol in terms of temperature and pH of the solutions used to clear the tissue. The authors chose these parameters due to their effect in the stability of green fluorescent protein, and performed all steps at 4 °C, adjusting the THF pH to 9.0 [30].

νDISCO also tries to improve the quality of the fluorescent signal in the cleared tissue. In the 2019 paper, Cai et al. use approaches from other techniques combined with the 3DISCO protocol, such as decolourization with a CUBIC reagent, decalcification with EDTA and using nanobodies in immunolabelling [31].

Other examples that combine reagents and methods from other types of clearing protocols are Dec-DISCO, which introduces CUBIC-L to decolourize the tissue, followed by the 3DISCO protocol [32], or HYBRiD, a protocol that combines the solvent-based protocol with hydrogel based techniques by applying a DISCO protocol for the delipidation steps, followed by the CLARITY protocol [33].

2.2 Fluorescence

Fluorescence, the emission of light due to the excitation of atoms, has a fundamental role in biological and biomedical research, as it can provide valuable information about the location, shape and/or dynamics of cells or cellular components. The object of interest may fluoresce naturally - autofluorescence or primary fluorescence - or it can be labelled with fluorescent markers - secondary fluorescence [15].

This phenomenon occurs when a fluorophore (a fluorescent molecule) absorbs the energy of a photon, releasing it after a very small amount of time (nanoseconds) in the form of another photon of lower energy, and therefore longer wavelength [34], [35]. This process is shown simply in Jablonski diagrams (Figure 2.5).

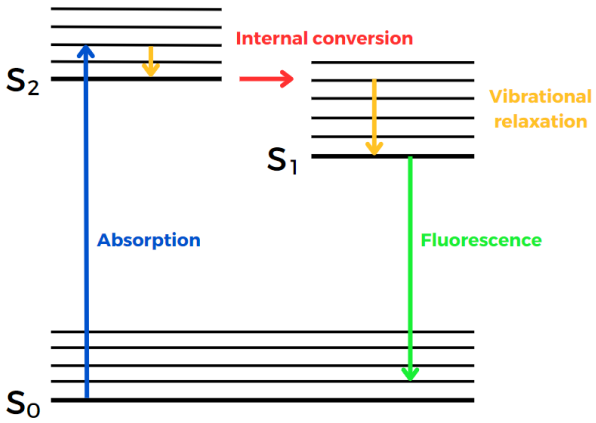

Figure 2.5: Jablonski diagram based on [36]

When a fluorophore that is in the ground state S_0 (a nonexcited state) absorbs a photon, it can transition into a higher energy level and reach an excited state. After the excitation, the fluorophore can return to the ground state in multiple ways, fluorescence being one of the possible mechanisms. After internal conversion and vibrational relaxation takes place, the molecule transitions to the lower level of the excited state. From there, it returns to the ground state, emitting a photon of energy lower than the one that excited the fluorophore - it emits fluorescence [34], [36].

As stated and as shown in the Jablonski diagram (Figure 2.5), the energy of the emitted photon is lower than the energy of the absorbed photon – this is known as the Stokes shift [9], [34]–[36]. The excitation and emission spectra, as well as its Stokes Shift are an inherent property of a given fluorophore, which varies with the properties of its environment [34].

In fluorescence microscopy, several fluorophores can be combined to identify different components in the sample. Therefore, it is necessary to use molecules that are not excited by the same wavelength or that do not emit the same wavelength, as that can create unclear results [15], [36].

2.3 Light Microscopy

Lenses have been used for centuries to observe the details of an object or tissue. The combination of lenses to create a microscope has been reported since the early seventeenth century [37], [38] and, since then, microscopy has been evolving to allow us to see what was never imagined before.

Nowadays, there are many different types of complex microscopes that are applied to different science and technology fields. Whereas a conventional microscope uses light to illuminate the sample, fluorescence microscopes (a type of light microscopes) use the incident light to take advantage of the phenomenon described in section 2.2 that allows to visualize fluorescent molecules in the sample. In fluorescence microscopy, the light that is emitted from the irradiated sample is separated from the excitation light so that the user/detection objective can only receive the emission light [15]. Widefield microscopes, multi-photon microscopes, confocal microscopes and light-sheet microscopes are some of the most commonly found fluorescence microscopes in research facilities [5], [6], [39].

The wide field microscope is the simplest of the four. In this system, the entire field of view is illuminated, leading to the excitation of all fluorophores present in the sample, resulting in the collection of emitted light from different depths of the sample. Therefore, although this system is very efficient to observe a thin specimen, when applied to a thick sample, there will be areas that are lit but are out of focus, resulting in an image of lower resolution. However, this is a fast method with lower costs, and it allows the user to observe the sample in real time [35].

The confocal microscope is characterized by the use of a pinhole that only allows the emission light that comes from the focal plane to be observed, which improves the resolution of the image, especially when observing a thick sample. The excitation

light is normally achieved by laser light, which needs to move across the sample to sequentially scan it so that these data are then compiled to create a tomographic image. Even though this microscope allows for better resolution, it is slower, and even though only the light from the focused point is captured, the excitation light illuminates the sample above and below it, which induces photobleaching [35], [40].

Multi-photon microscopes use more than one photon to excite a fluorescent molecule – for example, two-photon excitation uses two lower energy photons to excite the molecule, instead of a higher energy single photon. This type of microscopy is possible due to the development of fast pulsed lasers. Lower energy photons of longer wavelength scatter less, therefore reaching deeper distances in the sample, and its restricted area of excitation reduces photobleaching [35], [41]. Therefore, multi-photon microscopy has become the preferred tool for deep tissue imaging in thick sections and living animals, allowing to get information from sample depths over 1 mm [42].

The main character of this thesis, the light-sheet microscope, brings a different perspective to the imaging of thick samples. It uses a thin sheet of light to excite an entire plane of a sample at once, as opposed to illuminating the entire sample or scanning the selected plane point by point. Another difference is that the light that is emitted from the plane is captured by a detection objective that is orthogonal to the excitation beam. Since this type of microscope only illuminates the selected sheet and images it at once, there is less photobleaching, the detected light originates only from in focus regions and it has a faster acquisition time [39], [43].

2.3.1 Light-Sheet Fluorescence Microscopy

The essential parts of a Light-Sheet Fluorescence Microscope

A light-sheet fluorescence microscope has the typical components of any microscope, albeit with a specific configuration and optics to create the light-sheet illumination. Figure 2.6 demonstrates the relative positions of light-sheet and the detection objective, characteristic of this type of microscope. It is fundamentally composed of an illumination unit, a platform for the sample, a light detection unit and a computer to control the positioning of the sample and the image acquisition (and image processing) [43]–[45].

The illumination unit generates the light-sheet. It is composed of a laser or lasers that emit a collimated beam of a certain wavelength to excite the fluorophores in a sample (the most commonly used excitation wavelengths in fluorescence microscopy

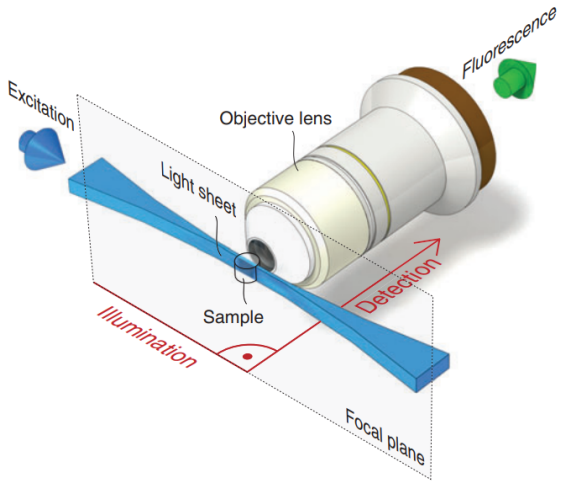

Figure 2.6: LSFM's distinct architecture - the excitation plane is perpendicular to the detection path. Illustration from [44]

are in the range 400-700 nm [35]) and lenses that shape the beam into a thin sheet. Typically, the laser beam first passes through a beam expander to increase the beam's diameter [43], [45]. Then, an optical device creates the light-sheet – a simple and widespread solution is implementing a cylindrical lens [43]–[45], although it may introduce aberrations, which can be attenuated using another objective lens [43], [45]. The sheet can be thinner or thicker depending on the resolution that is needed and on the size of the sample. Thinner light-sheets provide better axial resolution, but they can only be applied to image smaller samples (a few hundred micrometres). Thicker light-sheets (that can be created by a cylindrical lens) in combination with lower numerical aperture (NA) detection lenses are better for large samples, as they are more uniform and allow deeper imaging [6], [7], [44].

The sample is contained in a medium inside a chamber with four clear walls, ideally two times larger than the sample [43]. It can be immersed in a physiological solution in case of live-cell imaging, in the corresponding clearing medium or can be embedded in a gelling agent [1], [45], [46]. Typically, the sample unit is the part that moves the sample along the z-axis [6], [43].

The detection unit is generally composed of an objective lens, filters and a camera [44], [45]. The objective lens can be an air objective or a dipping objective that comes in contact with the immersion solution in the sample chamber. Air objectives may induce chromatic and spherical aberrations if they are not specifically created for observing high RI solutions – nonetheless, they are cheaper and can be used with any kind of immersion solution as they do not come in contact with it, making them a good choice for an optimization phase [5], [6], [45]. Both air objectives and dipping objectives can offer high NA (>0.9) and therefore better resolution, with

dipping objectives offering higher values - however, when using dipping objectives, chemical compatibility or dipping caps are necessary, as they are immersed in the chamber medium [5], [6], [44]. Due to diffraction, a broader disk being emitted from the fluorophore may be observed. These are called Airy disks. If the disks of two or more fluorophores overlap, they cannot be distinguished. To reduce this effect, one can use lenses with higher numerical aperture (NA) [15].

Filters are used to block the excitation light, allowing the fluorescence signal to be detected [45]. The illuminated plane of the sample is captured by a camera, which can be done very quickly with Charged-Coupled Device (CCD) cameras or Complementary Metal–Oxide–Semiconductor (CMOS) cameras [7], [44], [45].

Evolution and state of the art of LSFM

As with tissue clearing, the history of light-sheet microscopy starts in the beginning of the twentieth century. In 1902, Heinrich Siedentopf and Richard Zsigmondy presented the ultramicroscope, which used a light-sheet to observe gold particles that scattered the light in glass [44], [47], [48]. Siedentopf and Zsigmondy's illustrations are adapted in Figure 2.7, showing a specimen holder that is illuminated from the right and imaged from above.

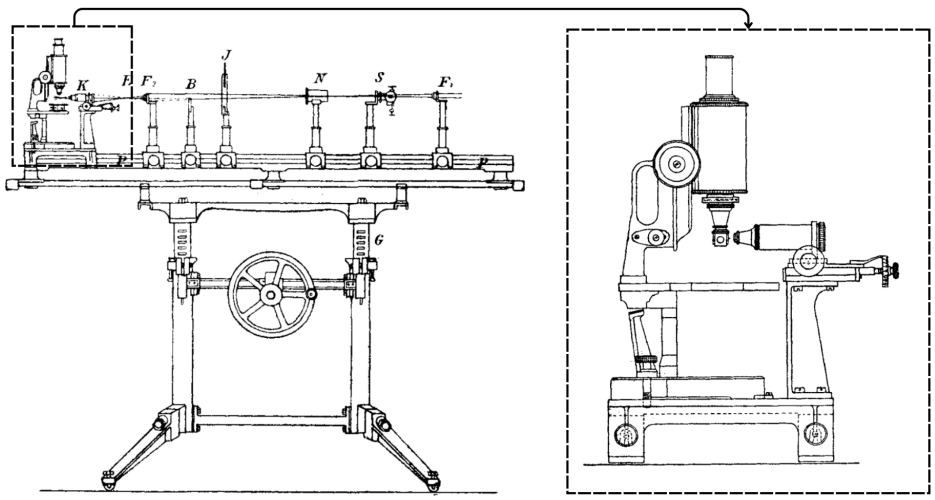

Figure 2.7: Siedentopf and Zsigmondy's illustrations of the ultramicroscope (adapted from [48]).

However, many decades passed before Voie et al. first coupled this type of microscope with fluorescence in 1993, creating the orthogonal-plane fluorescence optical sectioning (OPFOS), which used a cylindrical lens to create the light-sheet and a CCD camera to acquire the image [44], [49]. Another important step for the success of LSFM was done by Huisken et al., by the development of Selective Plane Illumination Microscopy or SPIM, which is considered as the steppingstone for many

of the more well-known versions of LSFM [39], [50]. Its architecture simply consists in a single plane of light that illuminates the sample from one side with a detector at a 90° angle to collect a stack of 2D images [51].

Due to the attenuation of the light-sheet as it travels through the tissue, some LSFMs include bilateral illumination to create a more uniform plane of light, while avoiding some shadows due to particles in the sample [1], [39]. To overcome this issue, Huisken et al. also presented a different solution of pivoting the light-sheet to illuminate the sample at different angles (Multidirectional Selective Plane Illumination Microscopy or mSPIM) [52].

Other architectures use a beam instead of sheet, which has the advantage of having the same intensity in each line of the plane. The Digital Scanned Light-Sheet Microscope (DSLM) and the Confocal Light-Sheet Microscope (CLSM) use a beam to scan the sample horizontally for each z-step [39]. The latter includes a confocal system that only allows the in-focus light to be detected, increasing the signal-to-noise ratio [39], [53].

There are many other examples of different LSFM architectures that address various limitations. For example, Glaser et al. combined mSPIM and DSLM to improve upon the uniformity of the light-sheet and reduce shadow artifacts [50]. Another example is Dual-slit Confocal Light-Sheet Microscopy, which has twice the acquisition rate and improves the signal-to-noise ratio [54]. SCAPE (or Swept, Confocally-Aligned Planar Excitation) also increases the speed of acquisition, and was designed with an oblique illumination that eases the restrictions on sample size and mounting, and does not require physical translation [55].

Applications

Throughout the last three decades, LSFM has gained relevance in the field of biomedical research and has been adapted to image different sample types and sizes, and has applications in ex-vivo, in-vivo and in-vitro studies[39], [44], [56].

LSFM has found use in neuroscience, having been an effective tool in the pursuit of studying the structures of the brain. Digital maps of entire mouse brains have been created, with information about gene expression, neuronal activity, drug distribution, or neurological pathologies [57], [58]. LSFM has also been used with cleared human brain tissue, for example, with the goal of mapping large regions [59] or to assess neural transplant innervation [60].

This imaging technique has also been applied in oncology, with applications in

samples ranging from mouse mammary tumours [61], to cancerous human bladder tissues [62], human pancreatic parenchyma [63], or sentinel lymph nodes from melanoma patients [64].

Developmental biology has also benefited from LSFM imaging. LSFM allows the in-vivo observation of the development of zebra-fish embryo, (imaging organs such as the eye [65], the heart [66], as well as the cardiovascular system [67]), mouse embryos [68], or the ex-vivo imaging of neonatal mouse organs [66].

LSFM is continuously applied to different types of tissues. To illustrate the range of LSFM, a few examples include the gerbil cochlea (resolving internal structures such as hair cells) [69], mouse retinas [70], porcine adipose tissue [71] and even plants, from a subcellular level to whole plant organs [72], [73]. In-vitro examples include imaging tissue mimics (engineered tissues such as spheroids or organoid cultures) [74] and microfluidics [75].

Chapter 3

Materials and Methods

3.1 Tissue Clearing Protocols

3.1.1 Overview

In this part of the project, two types of tissue clearing methods were explored: an aqueous-based method – CUBIC [27] -, and a solvent-based method - iDISCO+ [28]. The optimization of these two tissue clearing methods on mouse brain and liver tissues was divided into four phases:

1. Exploring the efficacy of clearing in different mouse tissues. iDISCO+ was used to clear the front half of a mouse brain, a mouse liver, and a mouse spleen. CUBIC was only used to clear the front half of a mouse brain as it is less efficient (or takes longer) in clearing large and more pigmented samples than solvent-based methods [2], [7], [17]. No immunolabelling was implemented at this phase;

2. Implementing immunolabelling on brain and liver tissue and decolouring in liver tissue. Once again, CUBIC was tested to clear only mouse brain tissue (1mm slices). iDISCO+ was used to clear 1mm brain slices, decoloured liver slices and non-decoloured liver slices. Brain tissue was incubated with anti-Iba-1 primary antibody, targeting protein encoded by the gene AIF1, that is expressed specifically in microglia in the central nervous system [76], and liver tissue was incubated with anti-occludin primary antibody to label the occludin protein that is present in tight junctions of endothelial cells [77], as well as then labelled with an unspecific mouse secondary antibody to label blood vessels;

3. Using iDISCO+ and CUBIC to clear liver tissue slices (decoloured and non-decoloured with iDISCO+, only decoloured with CUBIC) combined with a specific vasculature staining using PECAM-1. PECAM-1 (or platelet/endothelial cell adhesion molecule-1), like occludin proteins, is present in endothelial intercellular junctions [78];

4. Optimization of the concentration of anti-PECAM-1 primary antibody on 40 μm brain slices (no clearing needed).

Figure 3.1 schematizes the order of steps described in the Tissue Clearing Protocols section for each phase, clearing method and type of sample.

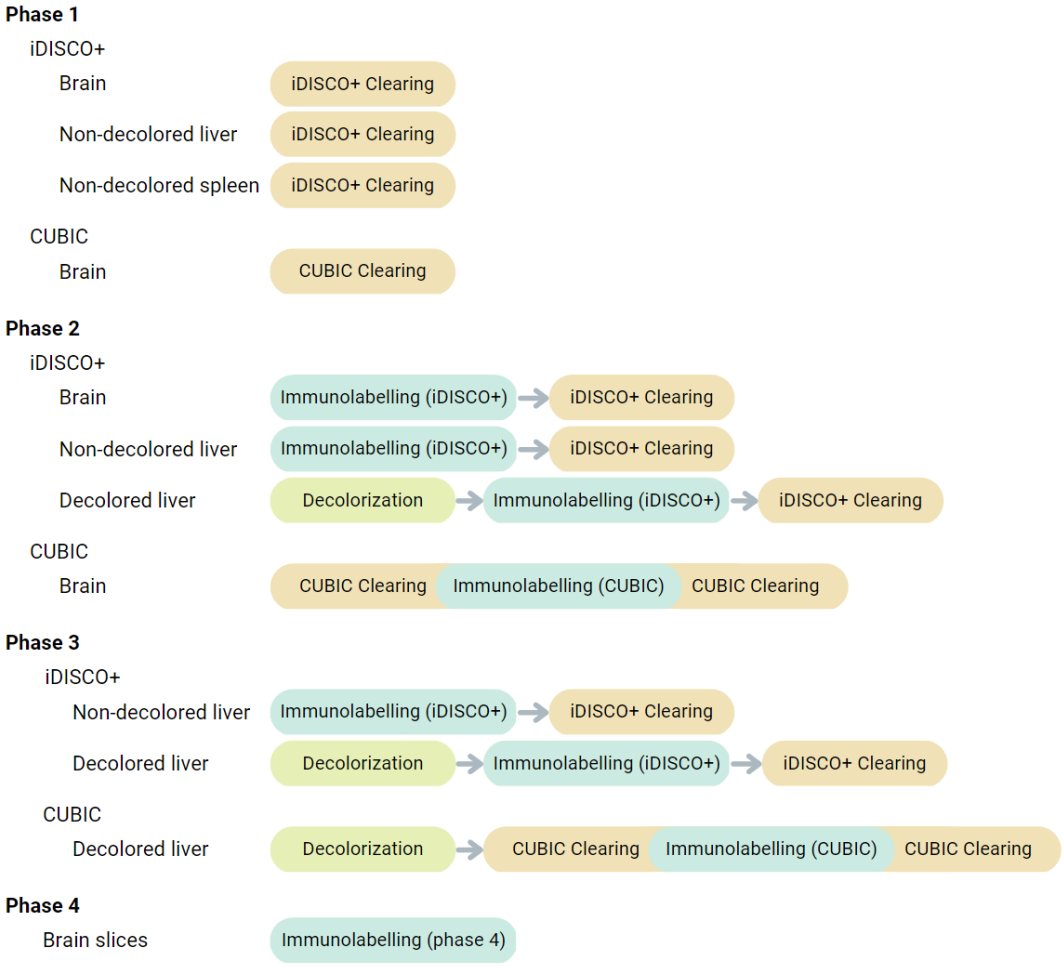

Figure 3.1: Schematization of order of steps described in the Tissue Clearing Protocols section for each phase, clearing method and type of sample. This scheme does not represent the time spent on each step.

3.1.2 Animal samples

The samples used in phases 1, 2 and 3 were extracted from two-month-old female mice, previously fixed with 4% paraformaldehyde in PBS, and were provided stored in 25% saccharose. Before starting the protocols, the samples were washed in PBS three times for 2 hours at room temperature (RT).

The 40 μm brain slices were obtained by cryosectioning a pre-fixed brain of two-month-old male mouse and were washed in PBS once overnight, followed by three times, for fifteen minutes, at RT, before starting the protocols.

Decolouring was performed on mouse liver lobes, which were then sliced into 3 mm slices for immunolabelling and clearing.

3.1.3 Tissue Clearing Protocols

Tissue samples were cleared using the iDISCO+ protocol [28] or with CUBIC protocol [27], with slight modifications, as described.

Decolourization

The decolourization step was based on the information provided on the iDISCO website (`https://idisco.info/`) and by Tainaka et al.'s work [25].

For the first step, the liver lobes selected for decolouring were incubated overnight in a solution of 5 wt% imidazole/10 wt% N-butyldiethanolamine (Sigma-Aldrich, St. Louis, Missouri) in phosphate buffered saline (PBS), at RT. Then, the sample was washed with PBS, for one-hour, at RT, followed by dehydration of the samples by immersing them in solutions of increasing methanol concentrations (Thermo Fisher Scientific, Waltham, Massachusetts) – 20%, 40%, 60%, 80%, 100% - for one hour each, at RT and gentle shaking. Samples were further washed with a 100% methanol solution, for one hour, to ensure the removal of all the water and PBS from the sample. This was followed by incubating the samples, overnight, in a 67% dichloromethane (DCM, Sigma Aldrich)/33% methanol solution, at RT. Then, the liver lobes were washed twice in 100% methanol at RT for one hour and then chilled at 4 °C. The next step was bleaching the samples in a chilled solution of 5% H_2O_2 (Thermo Fisher Scientific) in methanol, overnight at 4 °C. The liver lobes were then rehydrated through immersion in a series of solutions of decreasing methanol concentration – 80%, 60%, 40%, 20% - for one hour, at RT, followed by immersion in PBS for one hour, at RT. Finally, the samples were washed in PTx.2 (0.2% TritonX-100 (Sigma Aldrich), 10% PBS 10X in H_2O) twice, for one hour, at RT.

iDISCO+ clearing

For phase 1, 2 and 3: the samples were dehydrated in a series of methanol/H_2O solutions of increasing methanol concentration – 20%, 40%, 60%, 80%, 100% - for one hour each, at RT, and gentle shaking. The samples were washed further with a 100% methanol solution and left overnight, at RT. After dehydration, they were incubated in in 67% DCM/33% methanol solution at RT, for three hours. Then, samples were washed in 100% DCM twice, for fifteen minutes, at RT, to remove the methanol in the tissue. Finally, samples were incubated and stored in dibenzyl ether (DBE, Sigma Aldrich), at RT (no shaking). The tissue only becomes cleared in this final step.

CUBIC clearing

For phase 1: Firstly, samples were immersed in the CUBIC-L solution [(10 %(wt) N-Butyldiethanolamine (Sigma Aldrich), 10 %(wt) Triton X-100 (Sigma Aldrich) in H_2O] diluted 1:1 in water, overnight, at RT, followed by immersion in CUBIC-L for four days, at 37 °C. Samples were then washed in PBS, three times, for two hours, at 37 °C. RI-matching was achieved by incubating samples with CUBIC-R+ [45 %(wt) antipyrine (Sigma Aldrich), 30 %(wt) nicotinamide (Sigma Aldrich), 0.5 %(v/v)) N-Butyldiethanolamine in H_2O] - firstly in CUBIC-R+ diluted in water 1:1, for 24 hours at RT, and then in CUBIC-R+ for three days, at RT.

For phase 2: Brain slices were first immersed in diluted CUBIC-L (1:1 dilution in water) overnight, at RT, followed by immersion in CUBIC-L, for two days, at 37 °C. Samples were then washed in PBS three times, for two hours, at 37 °C and left overnight in PBS. The "Immunolabelling and nuclear staining in CUBIC" steps for phase 2 described below were implemented at this point. Following labelling, samples moved on to RI-matching, incubating in diluted CUBIC-R+ (1:1 dilution in water) for 24 hours at RT, and then in CUBIC-R+ for three days, at RT.

For phase 3: the liver slices were first immersed in diluted CUBIC-L (1:1 dilution in water) overnight, at RT, followed by immersion in CUBIC-L for two days, at 37 °C. The samples were then washed in PBS three times, for two hours. The "Immunolabelling and nuclear staining in CUBIC" steps for phase 3 were implemented at this point. Following labelling, the samples moved on to RI-matching, incubating in diluted CUBIC-R+ (1:1 dilution in water) for 24 hours, at RT, and then in CUBIC-R+ for three days, at RT.

Immunolabelling in iDISCO+

Note: in this step the liver lobes were cut in slices of approximately 3mm.

For phase 2: the samples were first incubated in the permeabilization solution [20 %(v/v) dimethyl sulfoxide (DMSO, AppliChem GmbH, Darmstadt, Germany), 2.3 %(w/v) glycine (Sigma-Aldrich) in PTx.2], for two days, at 37 °C and then in blocking solution [10 %(v/v) DMSO, 6 %(v/v) Horse Serum in PTx.2], for two days, at 37 °C. Then, the brain slices were incubated with rabbit anti-Iba1 primary antibody (1:1000, FUJIFILM Wako Chemicals Europe GmbH, Neuss, Germany), and the liver slices were incubated with rabbit polyclonal anti-occludin primary antibody (1:200, Abcam, Cambridge, England); these antibodies were diluted in a solution of PTwH [10 %(v/v) PBS 10X, 0.2 %(v/v) Tween-20 (Thermo Fisher Scientific),

0.1 %(v/v) 10mg/mL Heparin stock solution in H_2O], with 5 %(v/v) DMSO, and 3 %(v/v) Horse Serum and the samples incubated for two days, at 37 °C. After incubating with the primary antibody, samples were washed in PTwH four times, for one hour, and a fifth time overnight. Then, brain slices were incubated in goat anti-rabbit AlexaFluor568 secondary antibody (1:500, Thermo Fisher Scientific), and liver slices were incubated with the former and also with goat anti-mouse AlexaFluor488 secondary antibody (1:500, Thermo Fisher Scientific) to label unspecific targets; these were diluted in a solution of PTwH with 3 %(v/v) Horse Serum for three days at 37 °C. In the final step, samples were washed in PTwH four times, for one hour, and a fifth time overnight.

For phase 3: samples were first immersed in the permeabilization solution for seven hours, at 37 °C, and then in blocking solution for one day, at 37 °C. After that, liver slices were incubated with mouse anti-PECAM-1 primary antibody (1:500, Millipore, Billerica, Massachusetts) diluted in a solution of PTwH with 5 %(v/v) DMSO, and 3 %(v/v) Horse Serum and incubated for two days, at 37 °C. After incubating with the primary antibody, samples were washed in PTwH three times, for one hour, and a fifth time overnight. Then, they were incubated in goat anti-rabbit AlexaFluor568 secondary antibody (1:500, Thermo Fisher Scientific) diluted in a solution of PTwH with 3 %(v/v) Horse Serum for two days, at 37ºC. The final step was washing the samples in PTwH, three times, for one hour, and a fifth time overnight.

Immunolabelling and nuclear staining in CUBIC

For phase 2: brain slices were first immersed in staining buffer [10 mM HEPES (Sigma Aldrich), 10 %(v/v) Triton X-100 (Sigma Aldrich), 200 mM NaCl (Sigma-Aldrich), 0.5 %(w/v) Casein (FUJIFILM), 0.05 % NaN_3 (Sigma Aldrich) in H_2O] for 1.5 hours, at RT. Afterwards, the slices were incubated with rabbit anti-Iba1 primary antibody (1:1000, FUJIFILM) diluted in staining buffer, for three days, at RT, and then incubated with goat anti-rabbit AlexaFluor568 secondary antibody (1:500, Thermo Fisher Scientific) also diluted in staining buffer, for four days, at RT. After incubating with antibodies, the samples were washed in 0.1 M PBT [0.1 M PB, 10 %(v/v) Triton X-100 (Sigma Aldrich) and 0.05 % NaN_3 in H_20] twice for 30 minutes at RT and finally washed in 0.1 M PB [6.04 g sodium hydrogen phosphate (Nacalai Tesque), 1.18 g sodium dihydrogenphosphate dehydrate (Nacalai Tesque) and 0.05% NaN_3 for a 500 mL solution], for one hour, at RT.

Nuclear staining was also performed after immunolabelling by incubating the samples with DRAQ5 (1:2000, BioLegend Inc., San Diego, California) diluted in a

solution of Scale-CUBIC [25 wt% urea (Merck KGaA, Darmstadt, Germany), 25 wt% Quadrol (Thermo Fisher Scientific) and 15 wt% Triton X-100 in H_2O] with 500 mM NaCl (Sigma Aldrich) overnight, at RT. After nuclear staining, the sample was washed with 10 mM HEPES (Sigma Aldrich) three times for two hours.

After the staining, brain slices were fixed again by incubation in 1% formaldehyde (Nacalai Tesque) diluted in 0.1M PB, for 24 hours, at RT. The samples were then washed in 0.1M PB, for two hours, at RT.

For phase 3: liver slice was first immersed in staining buffer for 1.5 hours, at RT. After that, slice was incubated with mouse anti-PECAM-1 primary antibody (1:500, Millipore) diluted in staining buffer, for three days, at RT, and then washed twice with PBT for 30 minutes. Then, sample was incubated with goat anti-rabbit AlexaFluor568 secondary antibody (1:500, Thermo Fisher Scientific) diluted in staining buffer for two days, at RT. After the incubation with antibodies, the liver slice was washed in 0.1 M PBT twice, for thirty minutes, at RT, and finally washed in 0.1 M PB for one hour, at RT.

In this phase, the fixation step was implemented before the nuclear staining step. The liver slice was immersed in 1% formaldehyde diluted in 0.1 M PB for 24 hours, at RT. The sample was then washed in 0.1 M PB for two hours, at RT.

Nuclear staining was performed using DAPI (1:10000, Thermo Fisher Scientific) diluted in staining buffer for 30 minutes, at 37 °C. After nuclear staining, the sample was washed with 10 mM HEPES (Sigma Aldrich), three times, for two hours.

Immunolabelling and nuclear staining in phase 4

After washing brain slices in PBS overnight followed by three more times for fifteen minutes, brain slices were immersed in blocking solution [0.2% Triton X-100 (Sigma Aldrich) and 3% bovine serum albumin (BSA, NZYTech, Lisbon, Portugal) in PBS] for one hour, at RT. After blocking, the brain slices were incubated in mouse anti-PECAM-1 primary antibody (1:500, Millipore) in two different concentrations, 1:100 and 1:200, diluted in the blocking solution, for 36 hours, at 4 °C. They were then washed in PBS for two, at 4 °C, and two more times for fifteen minutes, at RT. After washing, the samples were incubated with goat anti-mouse AlexaFluor568 secondary antibody (1:500, Thermo Fisher Scientific) in a solution of 0.2% Triton X-100) in PBS, for 24 hours, at 4 °C. Brain slices were then washed in PBS three times for ten minutes, at RT, and then incubated with DAPI (1:5000, Thermo Fisher Scientific) diluted in PBS for thirty minutes. Finally, tissue slices were washed in PBS three times, for ten minutes, and mounted in DAKO mounting medium (Agilent

Technologies Inc., Santa Clara, California).

3.1.4 Imaging

Image acquisition

Brain and liver slices from phases 2 and 3 were mounted on a glass bottom dish (µ-Dish 35 mm, high glass bottom from Ibidi, Gräfelfing, Germany) and covered with a round glass coverslip before imaging.

The samples were imaged on a Carl Zeis LSM confocal point-scanning microscope employing the Zen Black 2012 software. Two objectives were used: the Plan-Apochromat 20X/0.8 air objective and the Plan-Apochromat 63X/1.4 oil DIC M27 objective (the first was used to image the liver samples and the former to image the brain slices and some details on the liver slices). To illuminate the samples, the Argon/2 laser unit (at 488 nm) was used to excite the AlexaFluor488 label, the DPSS 561-10 laser unit was used for the excitation of AlexaFluor568 and the DRAQ5 dye, and the Diode 405-30 to excite the DAPI dye. Z-stack images of tissue slices were acquired. For the brain slices, images along the Z plane were taken (z-stack) to obtain information of the full morphology and distribution of microglial cells. Z-stacks of the liver tissue were also taken.

Image processing

The acquired images were processed with the software IMARIS 9.6 (Oxford Instruments, Oxfordshire, United Kingdom). The *Surfaces* and *Filament Analysis* modules were explored when analysing the cleared brain slices. The *Surfaces* module was used to select and segment the different microglia cells apart from each other and from the background noise – the parameters were saved and used across the different acquired images. Some manual adjustments to the automatic segmentation were necessary. After segmentation, the most complete cell in the z-stack image for each type of tissue clearing protocol (CUBIC or iDISCO+) was selected to create a mask that was then analysed using the *Filament Analysis* module. This module allows the user to perform a morphological analysis of the cell by measuring several parameters, such as dendrite length, dendrite volume or number of Sholl intersections. Some manual adjustments were necessary to make sure that the full lengths of the dendrites were captured or that the software followed the correct path of the dendrites.

3.2 Microscope Implementation

3.2.1 Concept

LEMOLish is a project created by Julien Colombelli and Sébastien Tosi of the Institute for Research in Biomedicine of Barcelona. It aims to introduce Light-Sheet Microscopy to a wider audience through a simple approach with the fundamental components of an LSFM – light-sheet formation, sample translation and rotation, a detection unit, and a control unit - supported by 1400+ LEGO® pieces. Even though this project aims for simplification, it enables an automated imaging of large, cleared samples in the 0.5 to 5 cm range with micrometric precision.

The original LEMOLish project employs the LEGO® MINDSTORMS® EV3 Intelligent Brick to control the motors, the triggering of the laser and camera and other acquisition details such as the platforms' amount of translation. In this thesis, a modified version that uses an Arduino Mega 2560 Rev3 and stepper motors to control the microscope is presented.

3.2.2 System Components

Light-sheet formation unit

This unit is composed of the lasers that illuminate the sample and the lenses that form the light-sheet (Figure 3.2 and Figure 3.3). In this version of LEMOLish, there are two lasers in the green (532 nm) and blue (450 nm) regions of the spectrum. The green laser is a focusable diode-pumped solid-state (DPSS) laser (CW532-020F) and the blue diode laser module (RLDD450-40-5) features a focusable glass lens optic. Both lasers were ordered from Roithner (Roithner Lasertechnik GmbH, Vienna, Austria) and their specifications are detailed in Table 3.1.

Table 3.1: Laser specifications.

Specification	Green Laser	Blue Laser
Central wavelength	532 nm	450 nm
Average power	20 mW	40 mW
Beam shape	1.5mm diameter	Elliptical (1:1.4)
Supply voltage	3 V DC	5 V DC

The laser beam passes through three lenses to shape it into a light-sheet. The beam is first expanded by a thin wall borosilicate glass tube with an outside diameter

(a) CW532-020F (green laser) **(b)** RLDD450-40-5 (blue laser)

Figure 3.2: Laser light sources from Roithner used in LEMOLish.

of 2 mm and inside diameter of 1.56 mm (B200-156-10) filled with water. Then, the beam passes through a cylindrical lens (LJ1695L2-A, Figure 3.3a) from Thorlabs (Thorlabs GmbH, Munich, Germany) with 50 mm focal length to create the light-sheet. The beam then passes through the destriper, an array of solid glass rods with 1 mm diameter (BR-100-10, Figure 3.3b) that expands the sheet once again, creating multiple overlapped planes of illumination, which reduces shadowing in the sample. The glass tubes and rods were ordered from Sutter Instrument (Sutter Instrument, Novato, California, USA). Figure 3.8 illustrates this unit and further information on how these lenses are placed in the LEGO® structure is in section 3.2.2.

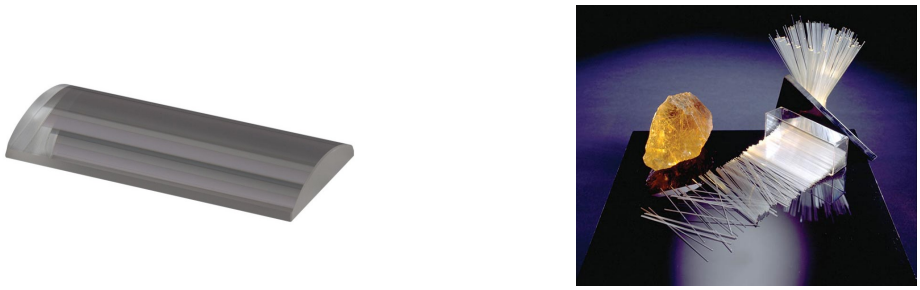

(a) Cylindrical lens **(b)** Glass filaments

Figure 3.3: Lenses used to generate the light-sheet.

Sample unit

The sample is held in a Hellma® quartz glass cuvette with width and depth of 35 mm and height of 32.5 mm (Figure 3.4).

Figure 3.4: Quartz glass cuvette that holds the sample.

Imaging unit

After the sample is excited, its emitted light is captured by the imaging unit. This unit is composed of filters, a zoom lens, and a CMOS camera (as shown in Figure 3.8, along with the light-sheet generation unit and the sample chamber).

The LEMOLish setup was built with two filters – a 495 nm longpass filter (FGL495S) and a 590 nm longpass filter (FGL590S) from Thorlabs. The filters will be applied when using the blue and green lasers respectively, so that the excitation light does not reach the CMOS camera. A representative picture of the filters and their transmission plots are in Figure 3.5 and in Figure 3.6.

(a) 495 nm longpass filter (FGL495S)

(b) 590 nm longpass filter (FGL590S)

Figure 3.5: Filters implemented in this version of LEMOLish.

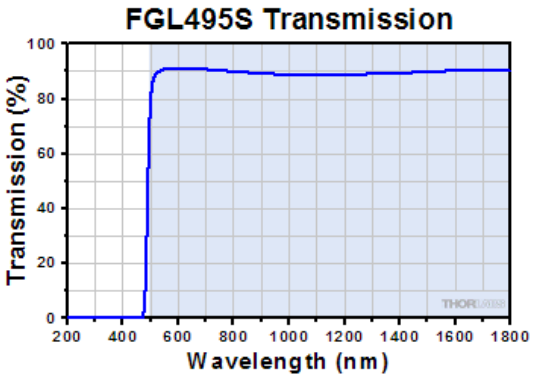

(a) FGL495S transmision plot

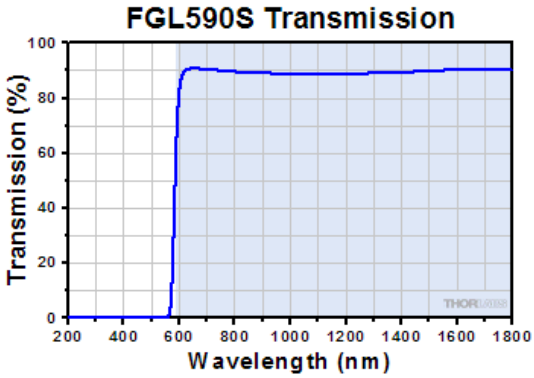

(b) FGL590S transmission plot

Figure 3.6: Transmission plots for the filters.

The CMOS camera is the DFK 33UX174 from The Imaging Source (The Imaging Source Europe GmbH, Bremen, Germany, Figure 3.7a). Its specifications are described in Table 3.2. The trigger and I/O inputs are processed through the Arduino and the collected information is transmitted to a computer through an USB-3.0 interface. The image is visualized with the IC Capture 2.5 software (The Imaging Source).

The zoom lens (Figure 3.7b) has a working distance of 95 mm and a zoom range of 0.7x-4.5x – but as it is also coupled with a 0.5x lens, the final zoom range is

0.35x-2.25x. The zoom lens has a C-mount and was coupled to the CMOS camera. This lens has the same specifications as of the original LEMOLish.

Table 3.2: CMOS camera specifications.

Specification	Value
Number of pixels	1936 (H) x 1216 (V) (approx. 2.35M pixels)
Pixel area	5.86 μm (H) x 5.86 μm (V)
Digitization	10 or 12 bit
Frame rate	164.5 or 128.2 frames/s
Shutter type	Global

(a) DFK 33UX174 CMOS camera. **(b)** Zoom lens.

Figure 3.7: DFK 33UX174 CMOS camera and zoom lens used in LEMOLish.

Figure 3.8 schematizes the configuration of the light-sheet formation unit, the sample unit, and the imaging unit.

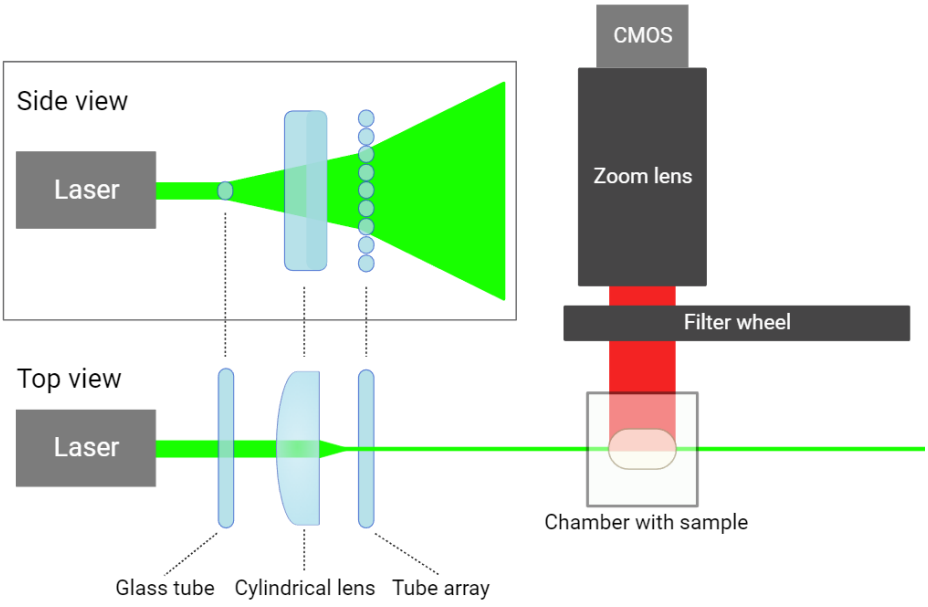

Figure 3.8: Scheme of the light-sheet generation unit, the position of the sample chamber and the imaging unit. Created with BioRender.com

Motion, control and power supply

The LEMOLish employs two separate motors to move the laser platform and the sample platform to refocus the image. As motor 1 (M1) moves the platform that holds the cuvette with the sample, the sample comes out of focus. The authors of LEMOLish do not move the camera and lens to attend to this, so that they remain stable, but they do move the laser platform in the opposite direction that the sample platform moves. The ratio of movement depends on the refractive index of the medium where the sample is immersed, therefore, it will vary according to the clearing method used.

The laser platform and sample platform are translated by stepper motors linked to a driver controlled by the Arduino (LEGO® gears convert the rotation of the motor's spindle into translational motion), and the lasers and camera are triggered by Arduino outputs. The user controls and selects the acquisition parameters by selecting menu options displayed in a 16x2 LCD with the help of four pressure buttons (up, down, select, and back) and by moving the motors with a joystick to choose the start and endpoint. These connections are schematized in Figure 3.9 and details on the Arduino programming are in subsection 3.2.3.

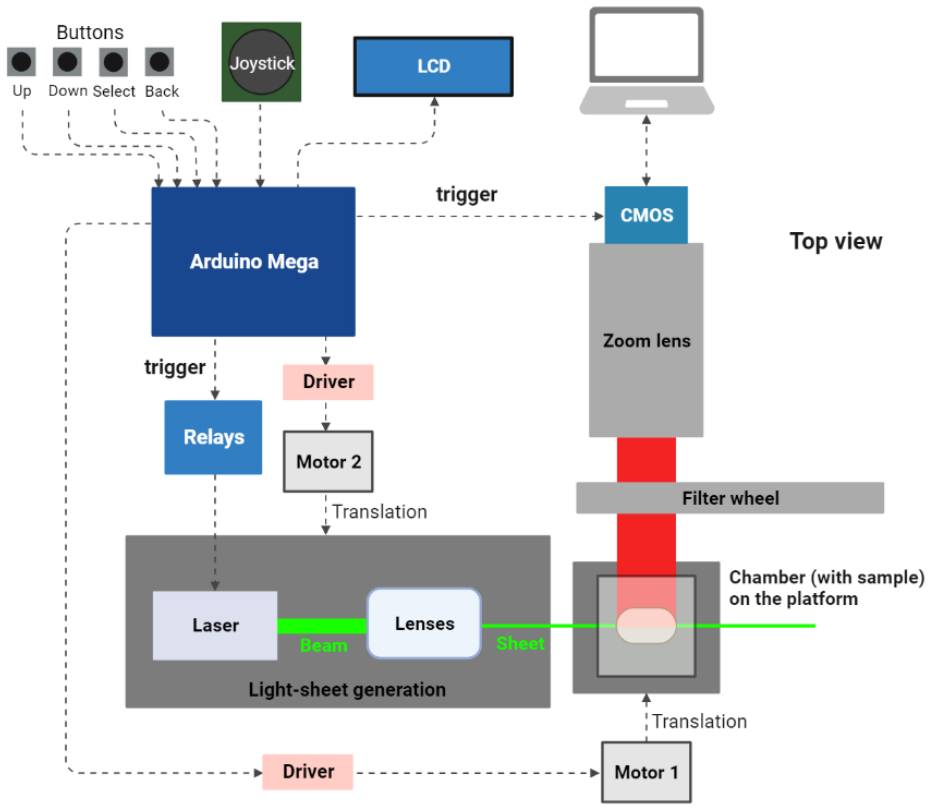

Figure 3.9: Diagram of the LEMOLish LSFM. The Arduino controls the motors, the lasers and the camera with the assistance of the buttons, the joystick and the LCD that shows the menu. Power supplies are not pictured. Created with BioRender.com

The Arduino model is the Mega 2560 Rev3 (Figure 3.10), which contains the ATmega2560 microcontroller and operates at 16 MHz. It has 54 digital input/output pins, 16 analog input pins, 4 hardware serial ports, a USB connection, and a power jack.

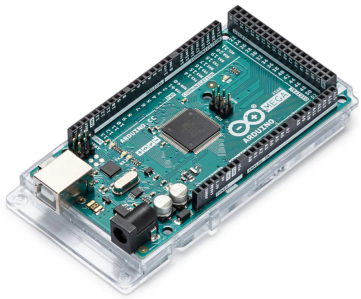

Figure 3.10: Arduino Mega 2560 Rev3

The chosen motor for all three applications is the 17HS4401 stepper motor (from Shenzhen Yousheng Guangcai Electronics Co., Ltd in Guangdong, China, Figure 3.11a) that has 200 steps per full 360° rotation (if no microstepping is applied). This motor has a torque of 41,97 Ncm and a rated current of 1.5 A. As a bipolar motor, it features 4 leads. The torque for this motor was chosen according to the motors in the original LEMOLish setup, which uses servo motors with a rotation sensor that allows a 1° resolution from the LEGO® MINDSTORMS® EV3 kit – it employs two large motors (160-170 rpm, running torque = 20 Ncm, stall torque = 40 Ncm) for the translation operations and a medium motor (240-250 rpm, running torque = 8 Ncm, stall torque = 12 Ncm) for the rotation operation (which was not implemented in this thesis due to time constraints).

To better control the motors, they are coupled with a A4988 driver (Figure 3.11b), which features the A4988 DMOS Microstepping Driver with Translator and Overcurrent Protection from Allegro MicroSystems (Allegro MicroSystems, Inc., Manchester, New Hampshire, USA). Besides the full step mode, this driver allows 1/2, 1/4, 1/8 and 1/16 microstepping modes (Table 3.4), which increases the resolution of the motor's rotation. The A4988 driver operates at a load supply range of 8-35 V (compatible with the stepper motors), a logic supply range of 3.3-5 V (compatible with Arduino) and has a maximum output current of 2 A (compatible with the stepper motors). The driver module has 16 pins, as described in Table 3.3.

The Arduino receives power through the USB cable, while the motors are driven by a separate 12 V external power supply. The CMOS camera is powered using a USB 3.0 cable and is triggered by a 5 V signal from the Arduino. Additionally, the lasers require external power sources of 3 V and 5 V (green and blue laser, respectively). These lasers are connected to relays controlled by the Arduino through 5 V outputs.

Table 3.3: Description of the A4988 driver's symbols.

Symbol	Description
EN	Enables the driver when LOW. LOW by default.
MS1 MS2 MS3	When combined at different logic levels, different microstep resolutions are achieved (Table 3.4).
RESET	When LOW, inputs from STEP are ignored.
SLEEP	When LOW, it reduces power consumption to a minimum.
STEP	A HIGH pulse drives the motor.
DIR	Determines direction of rotation (LOW = clockwise)
VMOT	Supplies the motor (8-35 V)
GND	Ground
2B 2A 1A 1B	Output channels connected to the motor.
VDD	Supplies the internal logic circuit (3.3-5 V)
GND	Ground

Table 3.4: Microstep resolution for the A4988 driver.

MS1	MS2	MS3	Step resolution
Low	Low	Low	Full step
High	Low	Low	Half step
Low	High	Low	Quarter step
High	High	Low	Eighth step
High	High	High	Sixteenth step

(a) 17HS4401 stepper motor

(b) A4988 driver.

Figure 3.11: 17HS4401 stepper motor and the A4988 stepper motor driver.

Microscope Structure

The most intriguing part of this project is indeed it's structure, as it is built entirely out of LEGO® pieces (LEGO System A/S, DK-7190 Billund, Denmark).

To facilitate the assembly, the LEMOLish was divided into modules, and the assembly order was created using the Studio 2.0 software from BrickLink, a trademark from the LEGO Group.

The five different modules have the following functions:

- The motor module translates the rotation of the motor's spindle into the translation in the z-axis of the sample module and the laser module;
- The laser module holds the lasers and the lenses that form the light-sheet;
- The sample module holds the cuvette, which sits in a platform that can be rotated with the help of magnets. This has not been implemented on this version of LEMOLish yet;
- The filter module consists in a wheel that holds the different filters;
- The camera module holds the CMOS camera and the zoom lens, which can be moved up or down, and back and forth.

Motor module

The motor module achieves its function with the help of a 3D printed connector that connects the motor's spindle to a LEGO® cross axle, which in turn transmits its motion to a set of gears that reduce the rotation by a gear ratio of 125:3 (the gears are shown in Figure 3.12). This results in a theoretical displacement of 0.213 μm for every 1° of rotation of the motor.

The motor that moves the sample platform (M1) and the motor that moves the laser platform (M2) are operated at a defined ratio M1/M2 (M1 and M2 corresponding to the angle the motors rotate between each slice). Both platforms are moved in opposite directions so that focus correction is performed by moving them at a ratio that is consistent with the refractive index of the medium the sample is immersed in. In this thesis, the ratios used were in accordance with the ones implemented in the original LEMOLish system (CUBIC implicates M1/M2 = 32/12).

After the motors were coupled to the corresponding platform, tests were performed to check if the sample module and the laser module were being displaced at

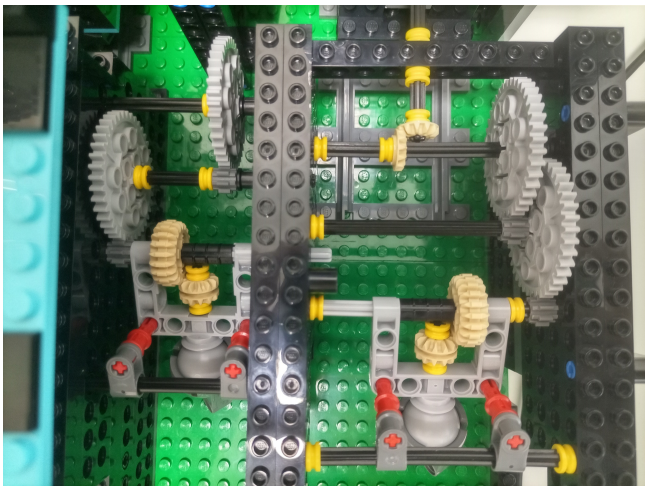

Figure 3.12: Gears that connect to the motors. Worm gears that translate the motors' rotation into translation in the z direction and the motors are not pictured.

a linear speed and at the correct ratio (M1/M2). To do this, the camera (coupled with the zoom lens) was placed on the filter module so that it could image the sample module in front of the laser module (as depicted in Figure 3.13). The motors and camera were controlled normally, as if acquiring images from a sample. The platforms were set to a certain zStart and zStop parameters, and M1 and M2 were kept as 30 and 15, respectively. A stack of images was then acquired as the motors advanced through the "slices". This stack was then analysed on ImageJ, using the TrackMate plugin [79] to segment and track the white region of reference (the segmented areas have a green border depicted in Figure 3.13). Linear regression was then performed on the position of the tracked segmented region (Figure 3.14).

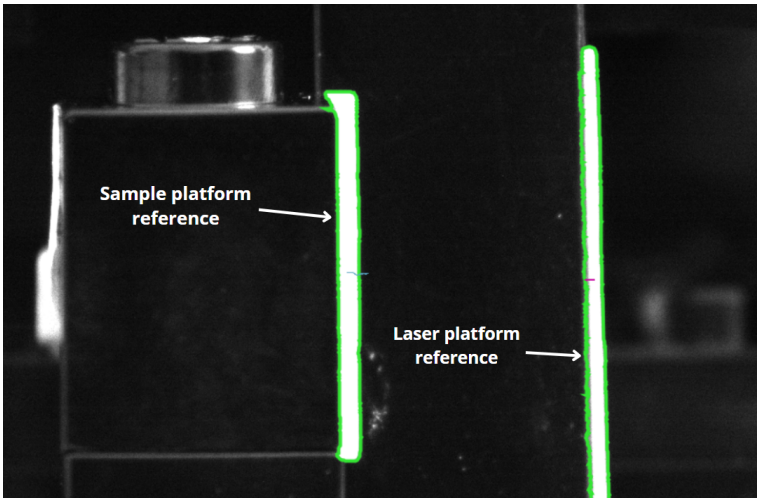

Figure 3.13: Example image captured by the camera to evaluate the relative movement of the platforms with segmentation performed with TrackMate. In the foreground stands the reference piece for the sample module and in the background the reference piece for the laser module.

After several tests, LEGO® pieces were added to provide stability and to prevent other pieces from disconnecting due to the forces exerted on them. Some pieces on

the side wall of the laser module were substituted to ensure the laser's "train" would move more smoothly. Figure 3.14 shows the plots of relative movement of the sample module and laser module, which are moved by motor M1 and motor M2 respectively, after these corrections. The modules move in opposite directions and were dislocated towards and away from each other in two separate acquisitions. In these data, motor M1 travelled 6000 microsteps and M2 travelled half, which theoretically translates to 575.75 μm and 287.87 μm, respectively. The graphs show a linear movement where the slope of the laser module is about half of that of the sample module.

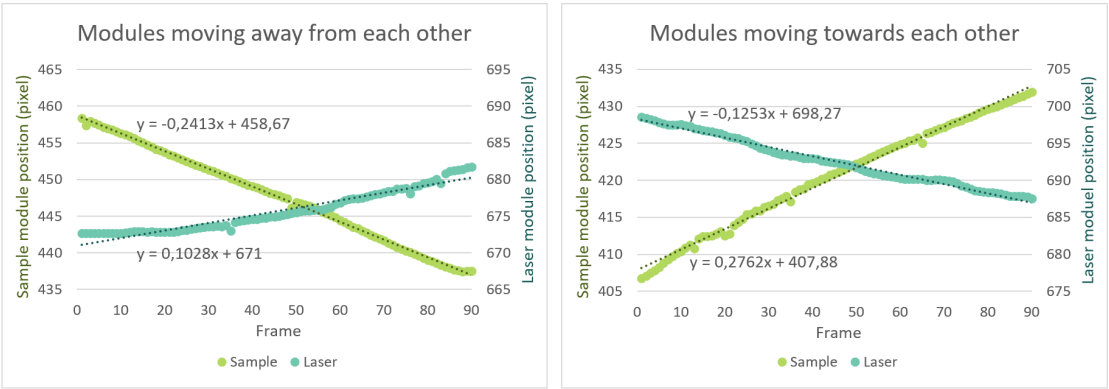

Figure 3.14: Plots of the position of segmented region of the slices as the modules move in relation to each other.

For the first plot (modules moving away from each other), the slopes for the sample and laser module are -0.2413 and 0.1028, (with a linearity error of 0.22% and 0.25% respectively). For the second plot (modules moving towards each other), the slopes for the sample and laser module are 0.2762 and -0.1253 (with a linearity error of 0.27% and 0.11%, respectively).

Laser module

The laser module holds the lasers, the filled capillaries, and the cylindrical lens. This module can hold up to three lasers, mounted on two levels. The bottom level holds one laser, and the top level holds up to two lasers. These two levels are each aligned with a filled capillary that will expand the beam. The capillaries can move slightly up and down as they are held by a pair of LEGO® pistons that the user can manually control. After going through the filled capillary, the beam reaches the cylindrical lens, which is mounted on a balcony outside the laser chamber.

The lasers are held in place by the roof tiles that create a platform for them to lie in. The lasers could be further secured by silicone glue - this step was not yet performed as only the bottom platform was used, and it was useful to have the ability to switch the lasers.

The capillaries were given a slit (made of thin cardboard) that is approximately

2 mm x 30 mm to block any parts of the beam that do not cross the capillary. They were then filled with water with a 200 μL pipette carefully to avoid the formation of air bubbles that would disrupt the laser beam's path. The fully filled capillaries were then sealed with silicone glue, as shown in Figure 3.15. The capillaries were filled and sealed while mounted on the pistons and were left to set overnight.

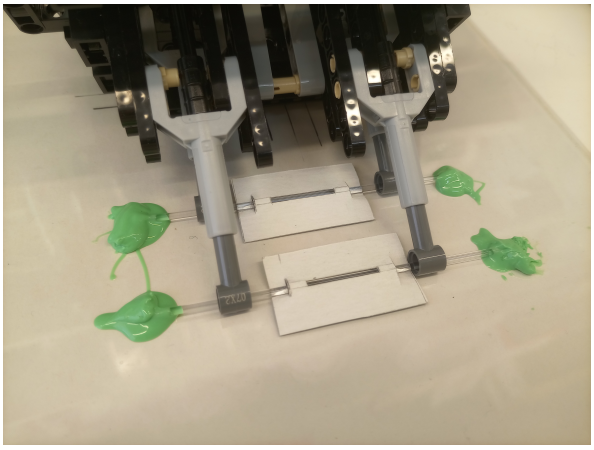

Figure 3.15: Capillaries for beam expansion mounted on the pistons. The piston ends were laid flat on top of an acetate sheet, filled with water and then sealed with silicone glue.

The cylindrical lens sits upright on a balcony outside the laser chamber and is held up by LEGO® pieces, as shown Figure 3.16.

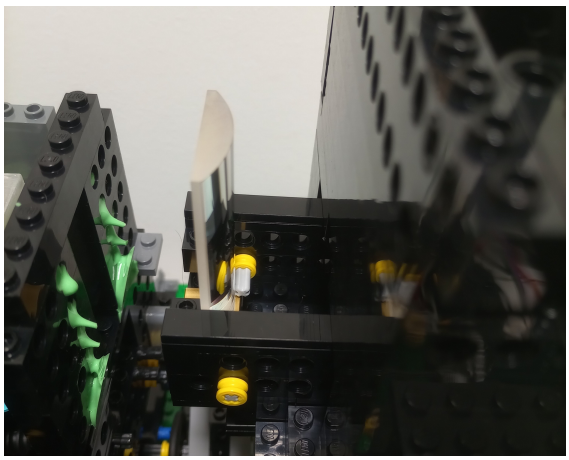

Figure 3.16: Cylindrical lens mounted on its platform.

Sample module

The sample module holds the cuvette that contains the sample and the destriper. It is prepared to have a motor connected to a rotating platform that sits below the platform where the cuvette is placed. The sample in the cuvette is held on top of a magnet (and bearings that allow the magnet to move on the cuvette's floor), which is itself rotated by the magnets attached to the rotating platform. This allows the user to rotate the sample as needed and is shown in Figure 3.17.

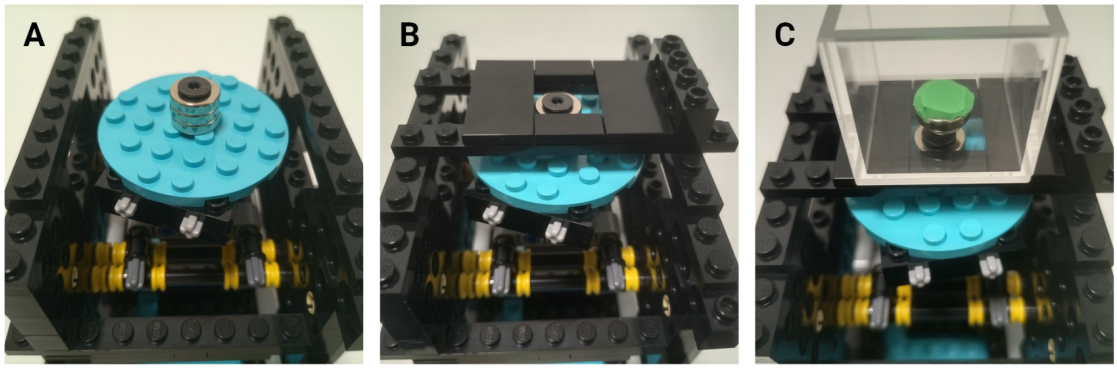

Figure 3.17: Cuvette platform. A – The rotating platform (blue) with the magnets attached. B – The platform where the cuvette sits. C – The cuvette sits on its platform and the sample stand is inside. The sample stand consists of ball bearings, the magnet and a small glob of silicone glue (in green).

The destriper is mounted on this module, on the side of the laser module. To build this part, small glass rods were stacked on a LEGO® structure (a window built with bricks) and secured with silicone glue (Figure 3.18).

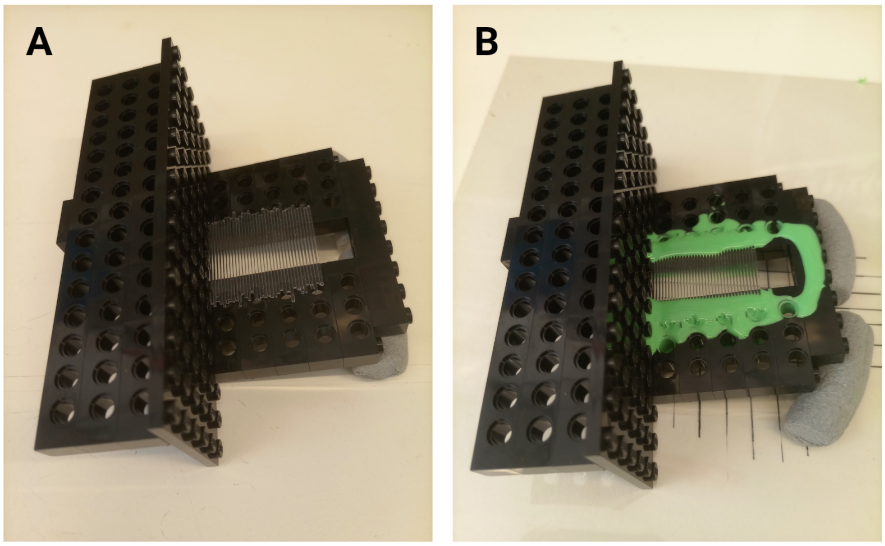

Figure 3.18: Destriper. A – Glass rods were stacked on the window. The platform under the window allows it to lie at an angle that facilitates the stacking and the flow of the silicone glue. B – The destriper after the silicone glue was poured.

Filter module

The filter module, as the name suggests, holds the filters (pictured in Figure 3.19). The filters are mounted onto a wheel that the user can spin to position the correct filter in front of the camera. This module also features a chamber where a motor could be placed to perform the rotation of the magnets that rotate the sample.

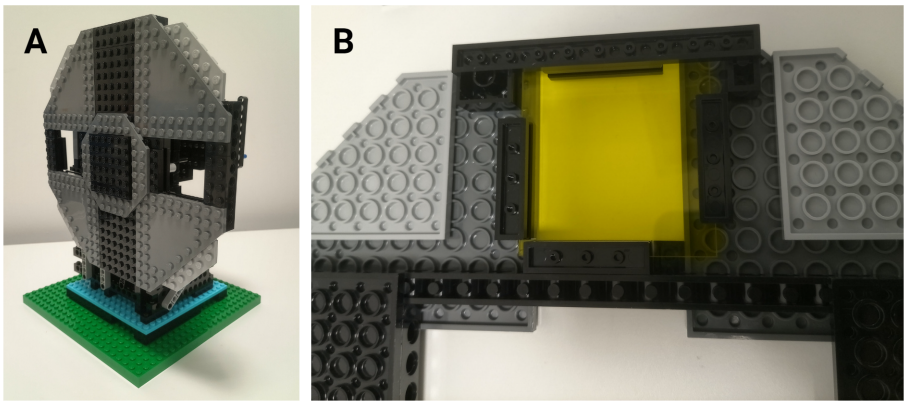

Figure 3.19: Filter wheel. A – The filter wheel module. B – Detail on how the filter is secured to the filter wheel.

Camera module

Lastly, the LEMOLish microscope has a module to hold the camera and zoom lens. This module features pistons that the user controls with a wheel to move the camera up and down. Besides that, a different wheel can make the platform move back and forth in the direction of the sample to focus the image. These mechanisms are shown in Figure 3.20.

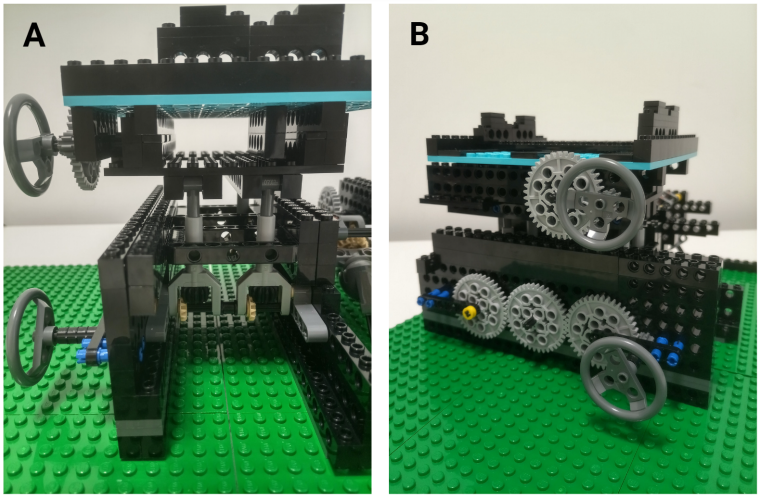

Figure 3.20: Camera module. A – Mechanisms that move the camera platform. The bottom wheel acts on the pistons, raising and lowering the platform. The top wheel moves the platform back and forth. B - Mechanisms that move the camera platform viewed from the side.

The camera platform and cuvette platform had to be aligned, as the cuvette platform was too low. To study this alignment, a wall of bricks with a height that approximately matches the height of the cuvette was labelled with twelve numbers and set where the cuvette would normally be (Figure 3.21 A and B). Then, the camera platform was set at the lowest level to study what was the lowest possible point to image (Figure 3.21 D). If it was too high, the cuvette platform should be

lifted or the camera module should be lowered. In this case, the cuvette platform was raised by a height of two LEGO® plates (Figure 3.21 F).

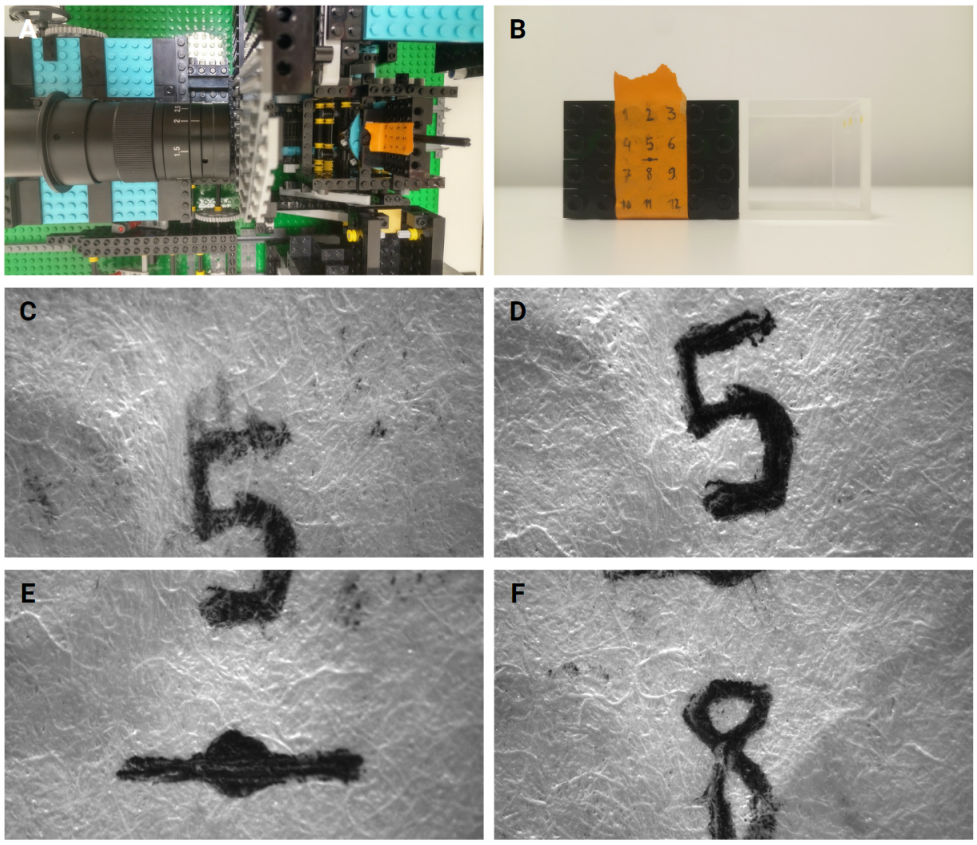

Figure 3.21: Camera and Sample platform alignment. A - Setup for the alignment. B – Size comparison of the number wall and the cuvette. C – What the camera captures when its platform is at approximately middle height before the adjustment. D – What the camera pictures at its lowest level before the adjustment. E – What the camera captures when the cuvette platform is raised by one plate. F – What the camera captures when the cuvette is raised by two plates.

When raised by two plates, the camera, when at its lowest level, imaged the number 8, which is just below the middle of the cuvette. Considering that the sample will be atop its holder, this height is adequate.

Complete setup

Figure 3.22 shows the completed LEMOLish setup, ready to acquire images. In Figure 3.22 A, it is possible to see the cuvette that holds the sample, and Figure 3.22 B illustrates what the user sees when acquiring images. In a real situation, the lights must be off and the microscope can have a dark cover to minimize any light entering the setup and reduce noise in the image. It is not possible to see the sample in Figure 3.22 B as it is entirely illuminated.

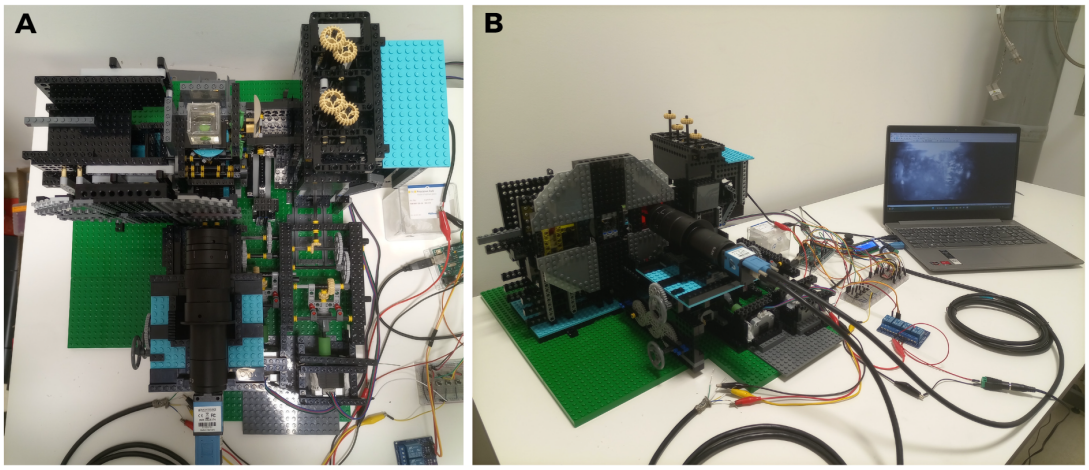

Figure 3.22: Complete setup of the LEMOLish. A - LEMOLish viewed from above, with sample inside the cuvette. B - The entire system, including the visualization of the sample with IC Capture (not visible as it is entirely illuminated by the lights above).

3.2.3 Arduino programming

The Arduino code was developed with Arduino IDE 2.1.0. and can be found in Appendix A.

Arduino connections

The connections and ports employed are described in Table 3.5.

Table 3.5: Arduino connections.

Part	Arduino pin
M1 direction pin	3
M1 step pin	4
M2 direction pin	5
M2 step pin	6
Joystick y direction	A1
Joystick x direction	A2
Joystick pressure button	2
Pressure buttons	10, 11, 12, 13
LCD	SDA and SCL
Relay	8, 9
Camera trigger	7

Libraries

Libraries were used to make the code more efficient. The ezButton library (created by ArduinoGetStarted.com) deals with debouncing and detecting the pressing or releasing of a button. The LiquidCrystal_I2C library (authored by Frank de Brabander) was used to manage what is displayed on the LCD. The driver and stepper motors were controlled with the help of the AccelStepper library (created by Mike McCauley), which supports simultaneous stepper motors and provides many useful functions used throughout the code. Finally, the avr/eeprom library was employed to enable saving values to the Electrically Erasable Programmable Read Only Memory (EEPROM) built in the Arduino (namely the current and start position at certain points in the code so that if the code is interrupted, the motors can be reset. This takes into consideration that the EEPROM can be written to for a limited number of times). This library is particularly useful as it allows to easily save and read large numbers.

Functions

The program can be divided into the several submenus it presents to the user through the LCD: setzStart(), setzStop(), chooseLaser(), setParameters(), showParameters(), startAcquisition() and reset(). The user can scroll through the different options with the up and down pressure buttons and select an option with the select pressure button. To exit a submenu, the user must press the back button.

setzStart()

Here the user can move the motors with the joystick to reach the position where the acquisition starts. By moving the joystick in the y direction, the motors spin clockwise or anticlockwise depending on the direction of the joystick. Moving the joystick in the x direction spins the motor M1 by an increment of 100 steps (clockwise or anticlockwise, which corresponds to 45° or about 9.6 μm. The motor M2 spins at the chosen ratio while M1 spins). The user has the option of turning the lasers on or off to observe the live image captured by the CMOS camera by pressing the select button. To go back to the main menu, the user presses the back button, which also saves the value in steps of the current position to the EEPROM (saved as the start position). The LCD displays the distance travelled.

setzStop()

This function works similarly to the setzStart() function, allowing the user to reach the stop position and turn the lasers on and off, adding the possibility of

setting the current position (in steps) of the motor to 0 by pressing the joystick button. Like setzStart(), the back button also saves the value in steps of the current position to the EEPROM (saved as the current position), besides going back to the main menu.

chooseLaser()

Here, the user chooses what laser or combination of lasers will be used in the acquisition. The user can toggle the lasers on or off with the select button in this mode. The corresponding filter must be set manually by rotating the filter wheel.

setParameters()

This submenu allows the user to select the relative motion of the motors, and the exposure time and number of images acquired per slice. The user chooses the M1 value, the M2 value, which correspond to the angle that the motor will rotate per step (1° of motor rotation is equal to a translation of 0.213μm), or the time value (250ms, 500ms or 1s for single exposures or 2s, 3s, 4s or 5s for repeated exposures, to follow the original setup's parameters).

showParameters()

By selecting this menu, the user can scroll through the acquisition parameters (M1, M2, time, the distance to travel, and number of slices) if they wish to verify their selection.

startAcquisition()

When the user selects this option, acquisition starts. The program first checks if the motors are at the correct start position (taking into consideration the saved values) and will move them if not. Then, it performs a backlash operation to eliminate any gaps in the gears at the start (the motors rotate for 2400 microsteps in the opposite direction of the direction zStart to zStop, and then return to zStart). After the backlash, a cycle is repeated until the total number of slices is reached. In each cycle, the motor moves to the position corresponding to the next slice (the first slice is at zStart), triggers the lasers and the camera, saves the current position to the EEPROM and updates the next position. After this cycle is finished, the motors return to the zStart position, and the current position is saved to the EEPROM. All these operations consider the direction of zStart and zStop and the motors move clockwise or anticlockwise accordingly. This is schematized in Figure 3.23.

To calculate the step size (or the distance between slices) the M1 parameter chosen by the user is translated to the number of microsteps it takes to reach that

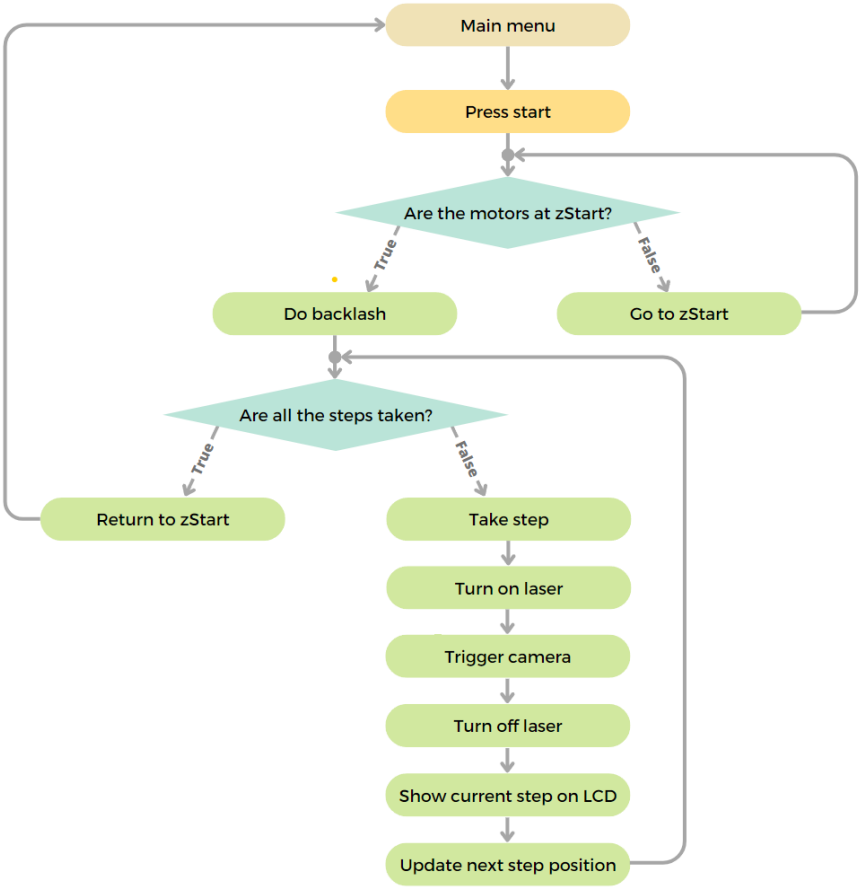

Figure 3.23: Flowchart for the startAcquisition() function.

angle of rotation. Then, because the number of microsteps between zStart and zStop may not be a multiple of M1 (in steps), extra microsteps are distributed by the steps needed to travel between slices. The distance between slices will be the sum of the distance travelled by the sample module and the laser module.

reset()

In this function, the user has three options: go to the zStart position, the zStop position or move to a position that is between zStart and zStop (a slice position that is approximately in the middle of these positions). This last option is particularly useful as zStart and zStop may be positioned outside of the sample, and having a middle position allows the user to return to a certain point of the sample to perform adjustments in image quality or to choose the laser or lasers.

Chapter 4

Results and Discussion

4.1 Tissue Clearing

In this thesis, the iDISCO+ protocol (solvent-based) and the CUBIC protocol (aqueous-based) were used to clear mouse brain and liver samples. This section describes the results for the optimization these protocols, comparing their efficiency in rendering them transparent and evaluating if exogenous fluorescence is compatible with the protocols.

4.1.1 Clearing efficiency

Clearing mouse brain slices with iDISCO+ or CUBIC

The evolution of the slices' cleared state was followed throughout the steps of iDISCO+ and CUBIC. This is represented in Figure 4.1, where images of samples at several steps of iDISCO+ and CUBIC are shown. As mentioned previously by Renier et al. in the iDISCO+ protocol [28], the tissue only becomes transparent on the very last step, which was verified on the pictured sample. In the case of the CUBIC protocol, some clearing is visible after the CUBIC-L step, particularly after labelling, when the sample is embedded in the 10mM HEPES solution. After clearing, we observed that both slices exhibit a good level of transparency.

The iDISCO+ sample became more brittle and is harder to handle due to the dehydration and the organic chemicals used. The CUBIC sample expanded in size after being embedded in CUBIC-L and then again more prominently after the final step. Indeed, it has been reported that CUBIC protocol can induce some swelling [17], [24], [25].

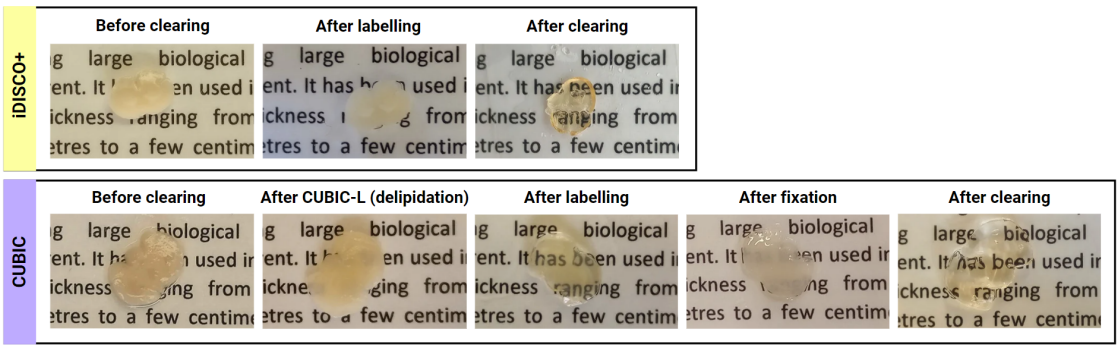

Figure 4.1: Representative pictures of the effect of the iDISCO+ (top row) and CUBIC (bottom row) protocols on brain slices over several steps.

Clearing mouse liver slices with iDISCO+ or CUBIC, and applying the decolourization step

Liver tissue is much more pigmented than brain tissue, primarily due to bile pigments derived from the degradation of hemoglobin. It is expected that a non-decoloured liver sample will not be cleared as effectively as a decoloured liver sample. In fact, as shown in Figure 4.2, we observed that the non-decoloured samples exhibit a brown tint that hinders the observation of the sample text behind the liver slice. The decoloured iDISCO+ liver sample showed much less colouration, exhibiting a yellow-brown tint, which prompted the attempt to clear the liver with CUBIC, which had a lighter yellow tint. These results show the importance of decolouring highly pigmented tissues, allowing them to reach an adequate level of clearing.

As with the brain tissue samples, the CUBIC liver was larger in volume in the post-CUBIC-L and post-RI matching steps of the protocol and showed some transparency after the CUBIC-L step. The iDISCO+ liver only became clear on the last step.

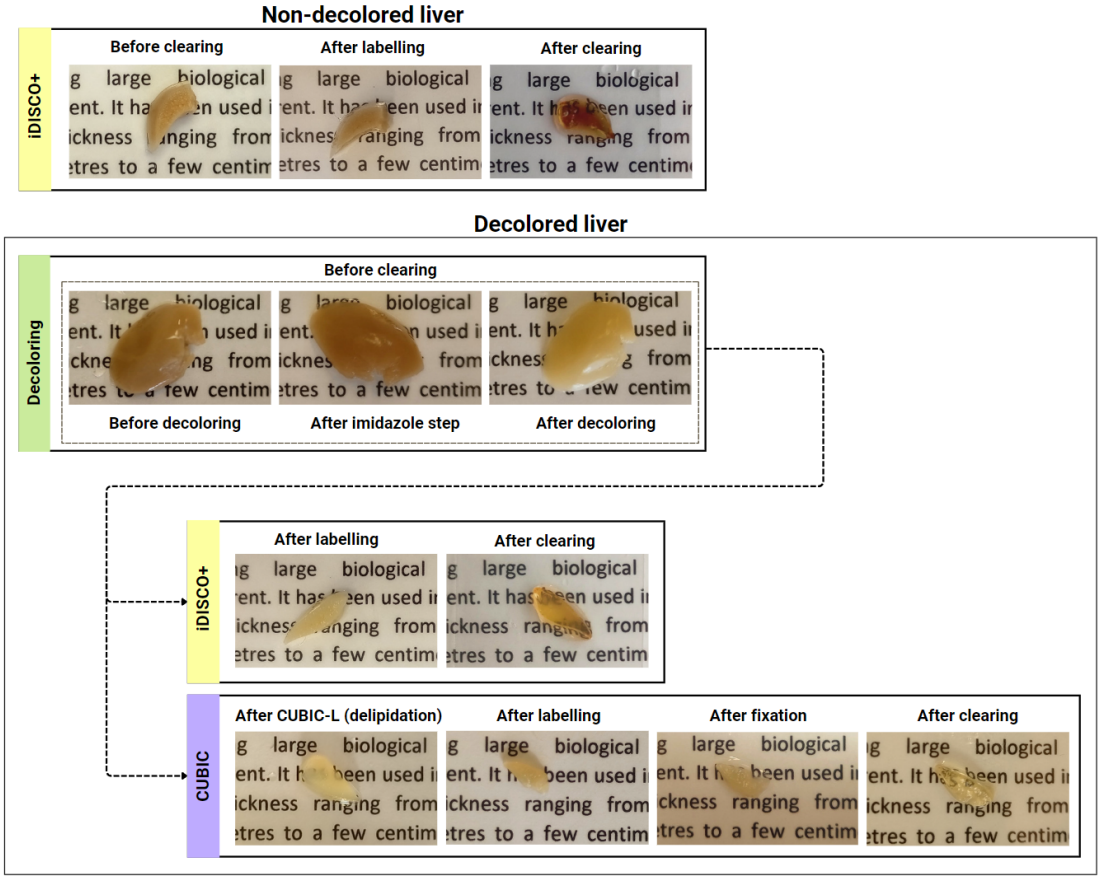

Figure 4.2: Representative pictures of the effect of the iDISCO+ and CUBIC protocols on liver slices over several steps. The first row represents the effect of iDISCO+ on liver slices that were not decoloured. The bottom section shows the effect of decolouring on a liver lobe and the subsequent effect of iDISCO+ and CUBIC on a liver slice.

4.1.2 Immunolabelling results

Immunolabelling in mouse brain tissue cleared with iDISCO+ or CUBIC

During the tissue clearing procedure, brain slides were immunostained using the anti-Iba1 primary antibody, a standard marker for microglia cells in the brain. Both samples were successfully stained using both types of protocol, and imaged using a confocal laser scanning microscope. As shown in Figure 4.3, we were able to clearly image a complex network of microglia cells in both brain slices. The iDISCO+ brain sample presents a denser network, which is in accordance with the fact that the CUBIC brain slice expanded during the protocol. Both images were then processed using the IMARIS software, that allowed to segment individual cells and to remove part of the noise present in the image. Both the raw data and the processed images are presented in Figure 4.3.

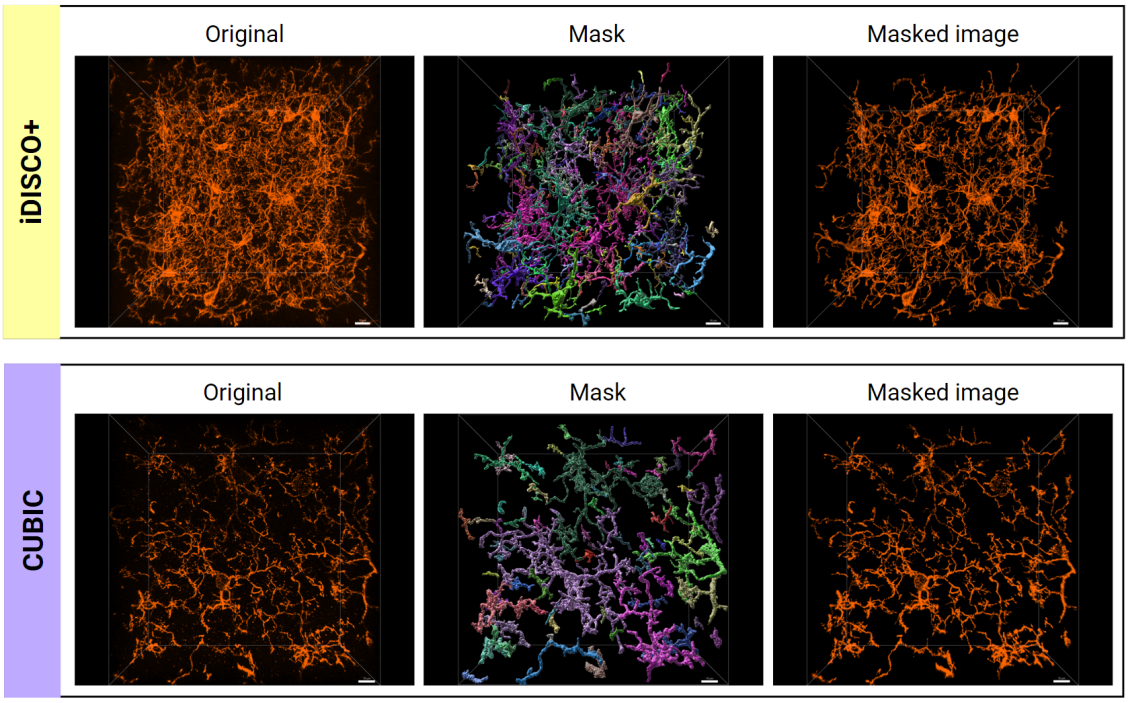

Figure 4.3: Three dimensional images of the immunolabelled brain slices cleared with iDISCO+ (top row) and CUBIC (bottom row). The slices were labelled with anti-Iba1 antibody and imaged with the 63x oil lens on the Carl Zeis LSM 710 confocal microscope. The first image on each row corresponds to the original z-stack image captured on the confocal microscope; the image in the middle shows the sectioning performed with IMARIS; the last image originates from the first when the mask is applied.

To demonstrate the advantage of using tissue clearing methods for the morphological analysis of neuronal cells, allowing to obtain information from the entire cellular structure, a single cell was selected from each dataset and the "Filaments" module of IMARIS was then applied (Figure 4.4).

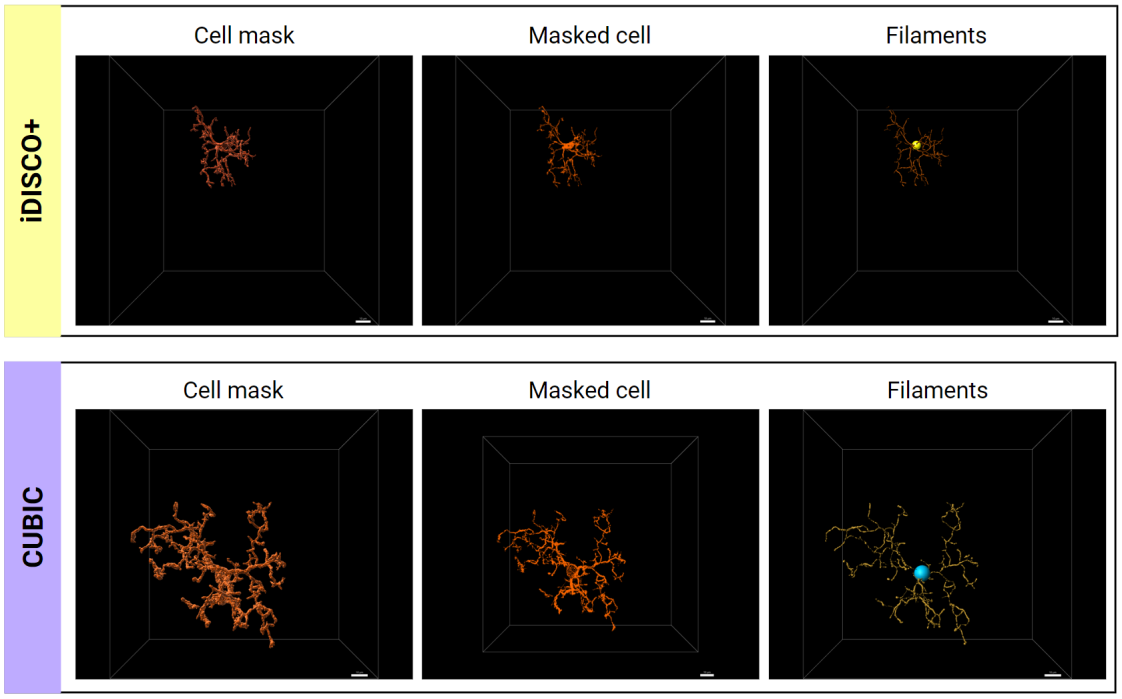

Figure 4.4: Three dimensional images of a selected cell in the immunolabelled brain slices cleared with iDISCO+ (top row) and CUBIC (bottom row). The first image on each row corresponds to the cell segment selected from the corresponding middle image in figure 3; the image in the middle originates from the first when the mask is applied to the original image; the last image shows the cell obtained with the "Filaments" functionality in IMARIS.

After reconstructing cells using the Filament module, morphological data can be extracted to characterize each cell, as summarized in Figure 4.5 and Table 4.1. Sholl analysis is the quantification of intersections of the cell's branches with radial distances at defined intervals (in this case, 5 μm). The graphs of Figure 4.5 show that the cell chosen from the CUBIC sample reaches further into the matrix. The data in Table 4.1 is in agreement with the previous data, as the iDISCO+ cell showed lower values for the sum of all dendrite lengths, area and volume, indicating a smaller cell. As this exercise consists solely of one cell from each sample, no inferences about the average size of the cells can be made.

Table 4.1: Statistics obtained from the IMARIS software characterizing the size of a cell from the iDISCO+ sample and the CUBIC sample.

Statistic	iDISCO+	CUBIC
Dendrite Length (sum)	811.395 μm	1329.69 μm
Dendrite Area (sum)	1497.48 μm^2	3326.74 μm^2
Dendrite Volume (sum)	218.788 μm^3	666.454 μm^3

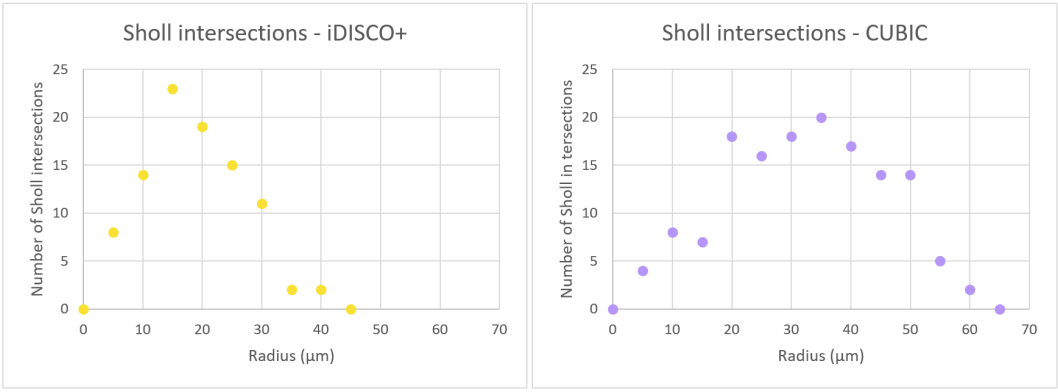

Figure 4.5: Sholl analysis of a cell in the iDISCO+ sample (left) and CUBIC sample (right). The CUBIC cell reaches a longer radius.

Immunolabelling in mouse liver tissue cleared with iDISCO+ or CUBIC

Figure 4.6 and Figure 4.7 present the results for phase 2 (anti-occludin antibody, and unspecific (secondary) antibody) and phase 3 (anti-PECAM-1 antibody) for the iDISCO+ slices. Unfortunately, labelling was not successful on any phase, as only the tissue's autofluorescence is evident in the images. It is still possible to observe some structures, but no vessels are apparent, as it would be expected.

The CUBIC slice shows similar results, having no success in immunolabelling or nuclear staining, as shown in Figure 4.8.

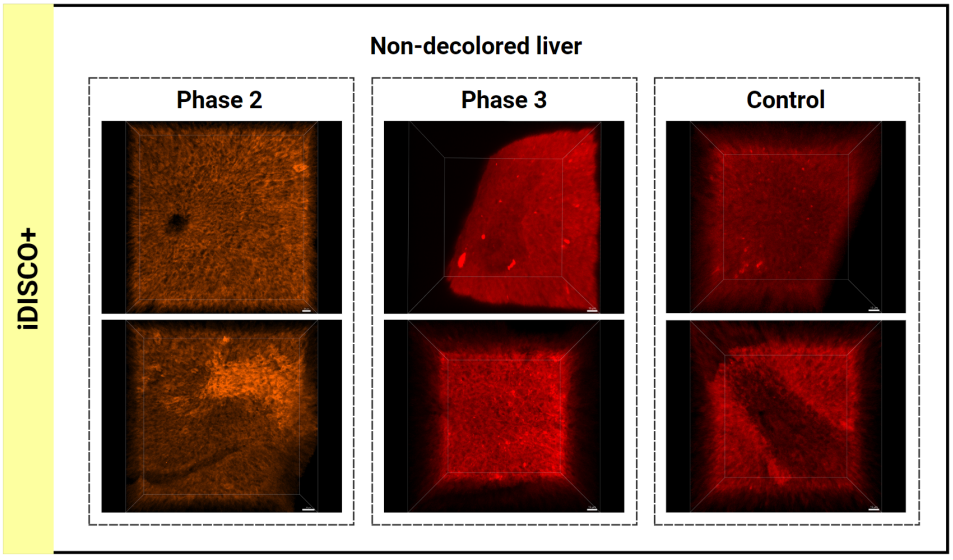

Figure 4.6: Three dimensional images of the immunolabelled non-decoloured liver slices cleared with iDISCO+ from phases 2 and 3, and three-dimensional images from the control liver slice. The sample in phase 2 is labelled with an anti-occludin antibody, as well with an unspecific (secondary) antibody. The sample in phase 3 is labelled with an anti-PECAM-1 antibody. These images were obtained with 23x air lens on the Carl Zeis LSM 710 confocal microscope. The images on each column were obtained from two different regions in each slice.

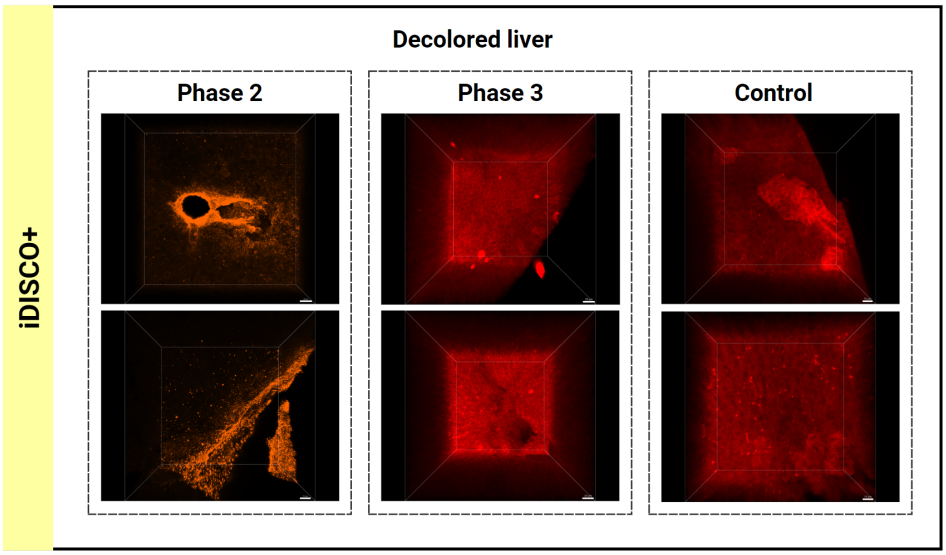

Figure 4.7: Three dimensional images of the immunolabelled decoloured liver slices cleared with iDISCO+ from phases 2 and 3, and three-dimensional images from the control liver slice. The sample in phase 2 is labelled with an anti-occludin antibody, as well with an unspecific (secondary) antibody. The sample in phase 3 is labelled with an anti-PECAM-1 antibody. These images were obtained with 23x air lens on the Carl Zeis LSM 710 confocal microscope, with the exception of the bottom left image, which was obtained with the 63x oil lens. The images on each column were obtained from two different regions in each slice.

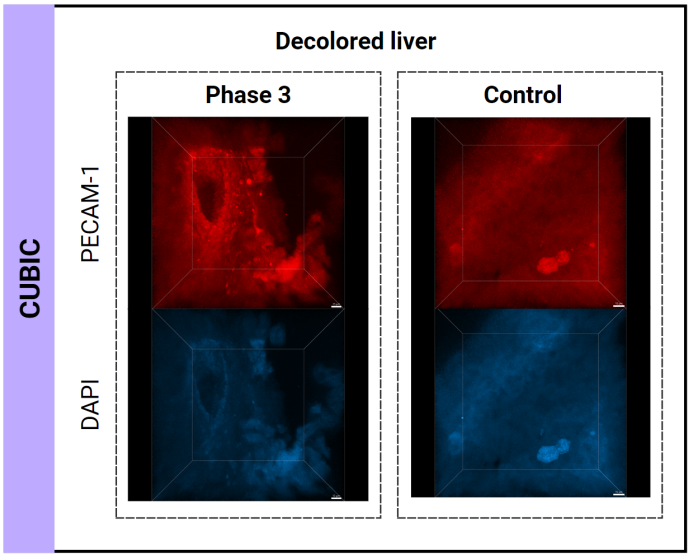

Figure 4.8: Three dimensional images of an immunolabelled decoloured liver slice cleared with CUBIC from phase 3, and three-dimensional images from the control liver slice. The sample in phase 3 is labelled with an anti-PECAM-1 antibody (top) and with the nuclear dye DAPI (bottom). These images were obtained with 23x air lens on the Carl Zeis LSM 710 confocal microscope.

As both phases yielded negative results, phase 4 was implemented on 40 μm brain slices to study how anti-PECAM-1 would label the vessels in these easily permeable samples. It was concluded that the problem laid with the antibodies, as there was no discernible difference when imaging the labelled slices or the control slices.

4.1.3 Discussion

Tissue clearing implemented during this thesis was optically effective using both protocols, iDISCO+ and CUBIC. The CUBIC protocol, which is an aqueous-based clearing method, stands out as it is easier to use due to the safer chemicals that are employed. However, the CUBIC protocol demands a few more days to achieve the best results, in comparison to iDISCO+ (for example, in phase 2, the CUBIC protocol took 15 days and the iDISCO+ protocol took 8 days). The sample expansion observed during the CUBIC protocol can be an advantage since it helps to obtain a more transparent sample, and can help in the diffusion of dyes or antibodies used to stain the sample. However, tissue expansion can be a disadvantage - if the expansion is poorly performed, the tissues' structures may be deformed [5], and there may be some size restraints when mounting the sample.

Tissue clearing was, at a first glance, successful for the brain slices and decoloured livered slices, but it was crucial to evaluate if the protocols were compatible with the immunolabelling step. The confocal microscope revealed that labelling was achieved in brain samples, clearly showing microglia. For the liver samples, it is not possible to conclude the same as the antibodies used may have been the source of the unsatisfactory results.

Due to the safety and effectiveness of CUBIC, this protocol was chosen to clear the samples that would be used in the LEMOLish microscope. This facilitates the positioning of the sample in the designated cuvette and, in case of an accident, the LEGO bricks would not be affected by the chemicals present in the embedding solution.

4.2 Microscope results

Having tested the CUBIC and iDISCO+ clearing protocols, and having built LEMOLish, the next step was to asses the system's performance. This chapter focuses on the evaluation of LEMOLish using unlabelled tissue samples, namely mouse liver and brain. The samples imaged in this chapter are cleared with CUBIC and exhibit only autofluorescence.

4.2.1 Effect of the destriper

When imaging biological samples with light-sheet microscopy, inhomogeneities in the sample (e.g., pigments or cell nuclei) can absorb or scatter light from the excitation beam. This creates shadows behind the obstacle and causes striping artifacts. Therefore, to overcome this problem, we tested a destriper device in the sample module.

Figure 4.9 shows how the introduction of the destriper device in the light path improves the quality of the acquired image. In fact, Figure 4.9 A clearly exhibits stripes, whereas when the destriper is introduced, the acquired image does not feature this pattern, as shown in Figure 4.9 B. All following images were acquired using the destriper.

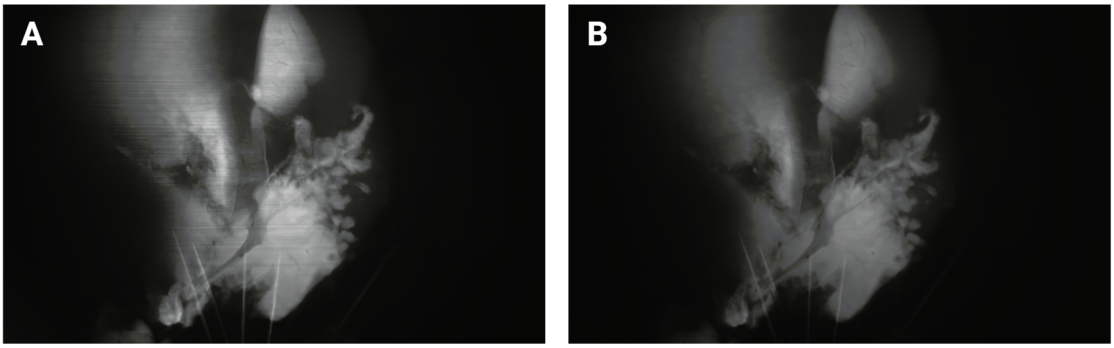

Figure 4.9: The effect of the destriper on a liver sample cleared with CUBIC. View of a slice imaged with the 450 nm (blue) laser. A - Without the destriper. B - With the destriper.

4.2.2 Observable structures in mice brain

The LEMOLish light-sheet microscope allows the user to observe entire cleared mouse organs. In this subsection, three different sections of the brain were selected to illustrate the regions of the brain that are possible to observe with the LEMOLish microscope. The setup of the brain samples, a complete mouse brain and the front

half of a mouse brain are shown in Figure 4.10, mounted inside the cuvette and placed on the sample platform. The light-sheet emerges from the right side of the cuvette.

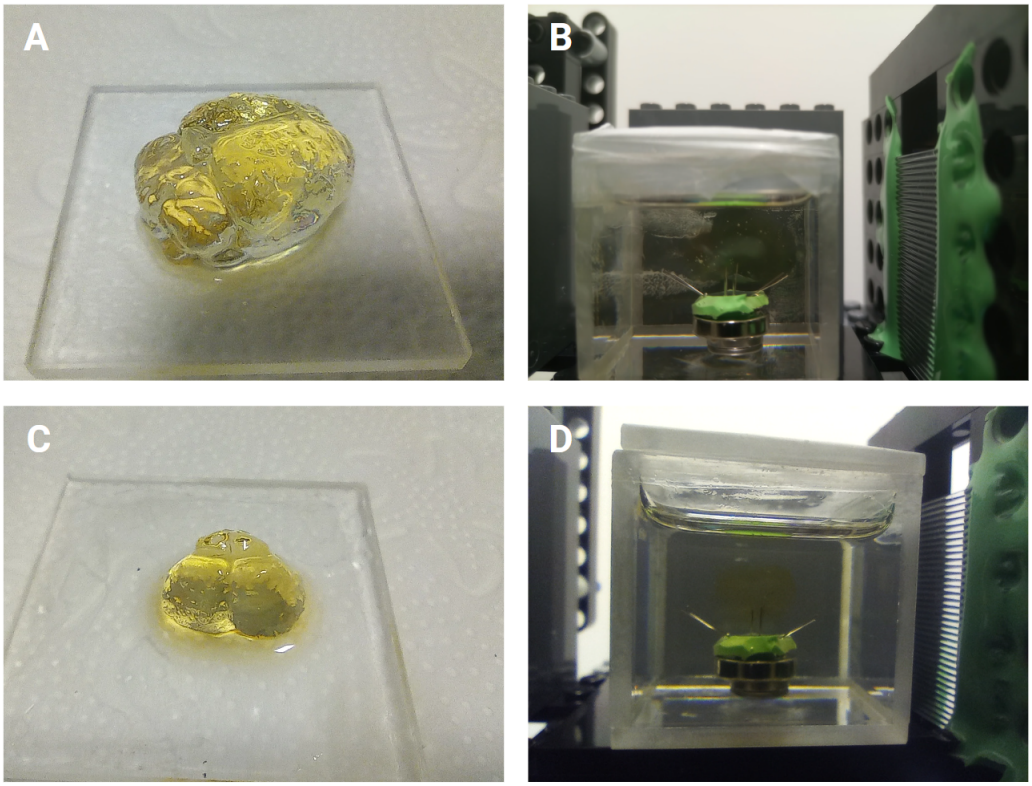

Figure 4.10: Brain samples mounted on the cuvette. A - Complete mouse brain cleared with CUBIC. B - Brain mounted on the cuvette, on its holder. C - Half mouse brain cleared with CUBIC. D - Brain half mounted on the cuvette, on its holder.

Figure 4.11 depicts a sagittal image of the complete mouse brain, along with an anatomical annotation of the same region of the mouse brain atlas. In Figure 4.11 A, it is possible to observe the section entirely, ranging from the cerebellum and hind brain at the left (CB and HB in the anatomical image), to the olfactory bulb at the bottom right (MOB). The brighter parts of this section consist of the caudoputamen (CP in light blue), the hippocampal formation (HPF in light green), the thalamus (TH, salmon coloured), the corpus callosum (cc in grey, the streek above the HPF and CP and below the isocortex (dark green to blue area)) and the anterior commissure, below the caudoputamen region. The CP region exhibits striation, being in fact a part of the corpus striatum (striped body in Latin), a structure belonging to the basal ganglia [80].

Some of the same anatomical structures observed in the mouse sagittal image (Figure 4.11) are also visible when a coronal view of the sample in Figure 4.10 C is imaged, as shown in Figure 4.12 - namely, the corpus callosum (cc in grey), the caudoputamen (CP in light blue) with the notable striation, and the anterior com-

missure fiber tracts (aco in grey, beside the CP). In addition to these structures, the lateral ventricles (VL in dark grey) are also noticeable between the caudoputamen regions, below the corpus callosum.

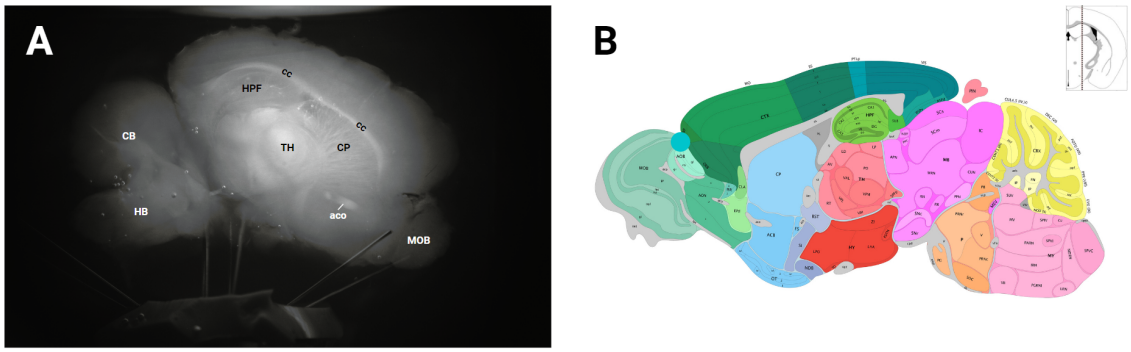

Figure 4.11: Slice of the mouse brain shown in Figure 4.10 A and anatomical annotations of the respective area of the brain. A - View of a brain slice imaged with the 450 nm (blue) laser. B - Respective anatomical annotations adapted from the Allen Mouse Brain Atlas and Allen Reference Atlas – Mouse Brain. Allen Mouse Brain Atlas, mouse.brain-map.org and atlas.brain-map.org.

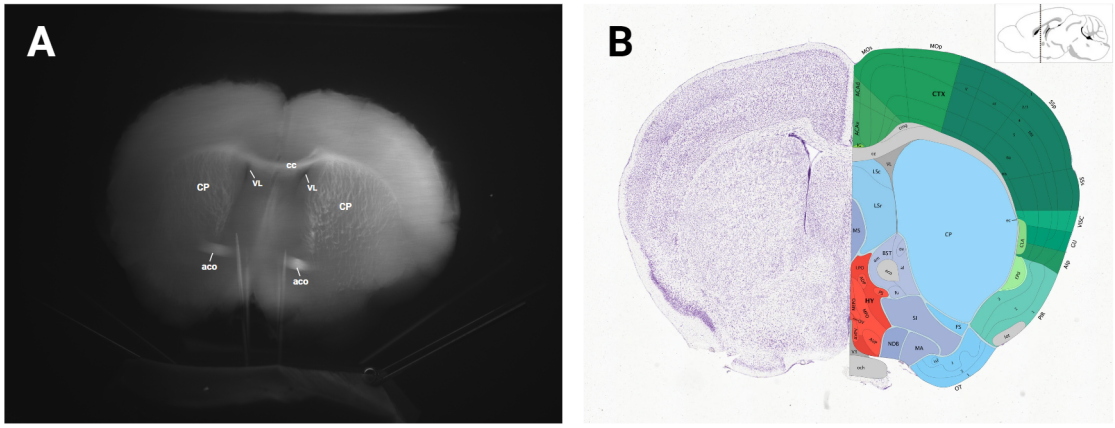

Figure 4.12: Slice of the mouse brain shown in Figure 4.10 C (viewed from the sliced region of the brain) and anatomical annotations of the respective area of the brain. A - View of a brain slice imaged with the 450 nm (blue) laser. B - Respective anatomical annotations adapted from the Allen Mouse Brain Atlas and Allen Reference Atlas – Mouse Brain. Allen Mouse Brain Atlas, mouse.brain-map.org and atlas.brain-map.org.

One of the advantages of the configuration of the light-sheet microscope is the free rotation of the sample, which would be impossible in a conventional light microscope. Therefore, and since the implemented light-sheet microscope has only single side illumination and single side detection, we decide to rotate our sample to image a view from the opposite side of the brain, in relation to Figure 4.12. As shown in Figure 4.13, we successfully imaged the olfactory bulb (below the less bright isocortex). The lateral olfactory tract (lot in grey) can be observed in the periphery of the olfactory bulbs and the anterior commissure (aco in grey) is positioned close to the center of the bulbs.

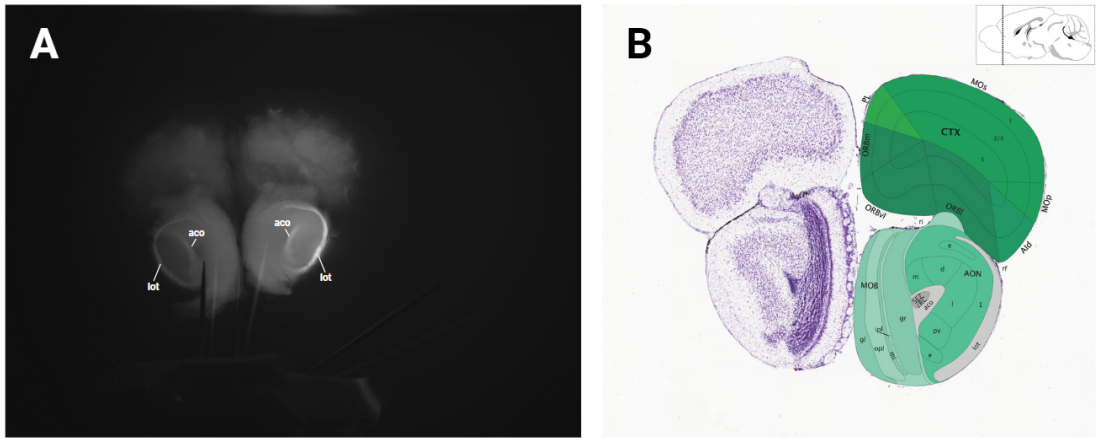

Figure 4.13: Slice of the mouse brain shown in Figure 4.10 C (viewed from the olfactory bulbs side) and anatomical annotations of the respective area of the brain. A - View of a brain slice imaged with the 450 nm (blue) laser. B - Respective anatomical annotations adapted from the Allen Mouse Brain Atlas and Allen Reference Atlas – Mouse Brain. Allen Mouse Brain Atlas, mouse.brain-map.org and atlas.brain-map.org.

4.2.3 Evaluation of microscope performance when repeating acquisitions

After selecting a certain zStart and zStop location, the user can repeat the acquisition between these two points as many times as they need. This is useful as the user may need to switch lasers to observe different labels and later study their co-localization.

To study how the system performs, three consecutive z-stacks were executed on the exact same region interval of the brain pictured in Figure 4.10 C for a range of approximately 1.5 mm. Subsequently, in IMARIS, these image sets were superimposed in a single image as three separate channels - red, green, and blue. If the three image sets fully overlapped, meaning a perfect alignment, a greyscale image should be observed. In fact, that was observed, as shown in Figure 4.14.

On the edges of brighter objects, some colour is visible (resembling chromatic aberration but caused by the slight misalignment between sets). Notably, as the sample is immersed in a liquid medium and samples cleared with CUBIC are soft, a mechanical perturbation (e.g. an accidental bump against the table where the LEMOLish is mounted) could induce minor displacements in its position. Another characteristic visible on this image is that it is brighter on the right side, as that is the side from where the light-sheet illuminates the sample.

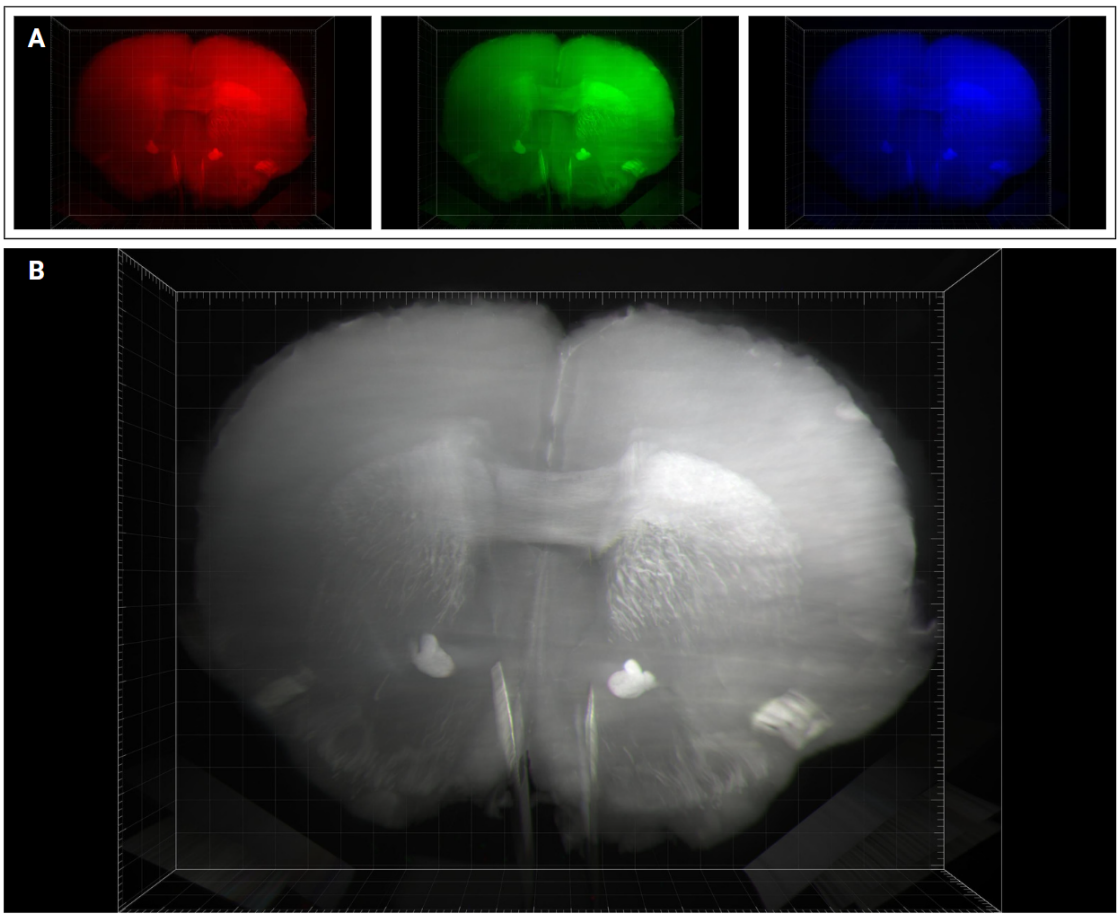

Figure 4.14: Three dimensional render of three superimposed separate runs of the same region of a mouse brain cleared with CUBIC. This sample was not labelled and was imaged with the 450 nm laser, only showing auto-fluorescence. The sets range 1.502 mm, each set being comprised of 161 sections in intervals of 9.3 μm. A - the three sets of images, each given a colour - red, green and blue. B - The resulting image from combining the three channels.

4.2.4 Evaluation of microscope performance in the acquisition of large volumes

After having confirmed that the system is able to image cleared tissue samples and to repeat acquisitions accurately, the next objective was to assess if this LEMOLish setup is able to image a sample for an extended range while maintaining image quality.

To test how the microscope performs when imaging large biological samples, the sample imaged in Figure 4.12, Figure 4.13 and Figure 4.14 was imaged once again, but a greater range was acquired. The brain sample was imaged with the olfactory lobes oriented towards the camera. The imaged distance measured 5.038 mm and 538 sequential images in intervals of about 9.4 μm were acquired. Four sections are depicted in Figure 4.15. The position of the cylindrical lens had been adjusted after

imaging Figure 4.11, Figure 4.12 and Figure 4.13 so that the the thinnest part of the light-sheet waist was positioned in the sample. This improved the resolution of the image.

Figure 4.15 A corresponds to the tip of the olfactory bulbs where acquisition started, and Figure 4.15 B shows the olfactory bulbs more deeply into the cortex, as well as the needles that hold the sample. In Figure 4.15 C and D a darker unfocused ring is noticeable as it is in front of this slice relatively to the camera and blocks the emitted light (it is focused on subfigure B). Shadows cast by the needles are also visible in subfigure C.

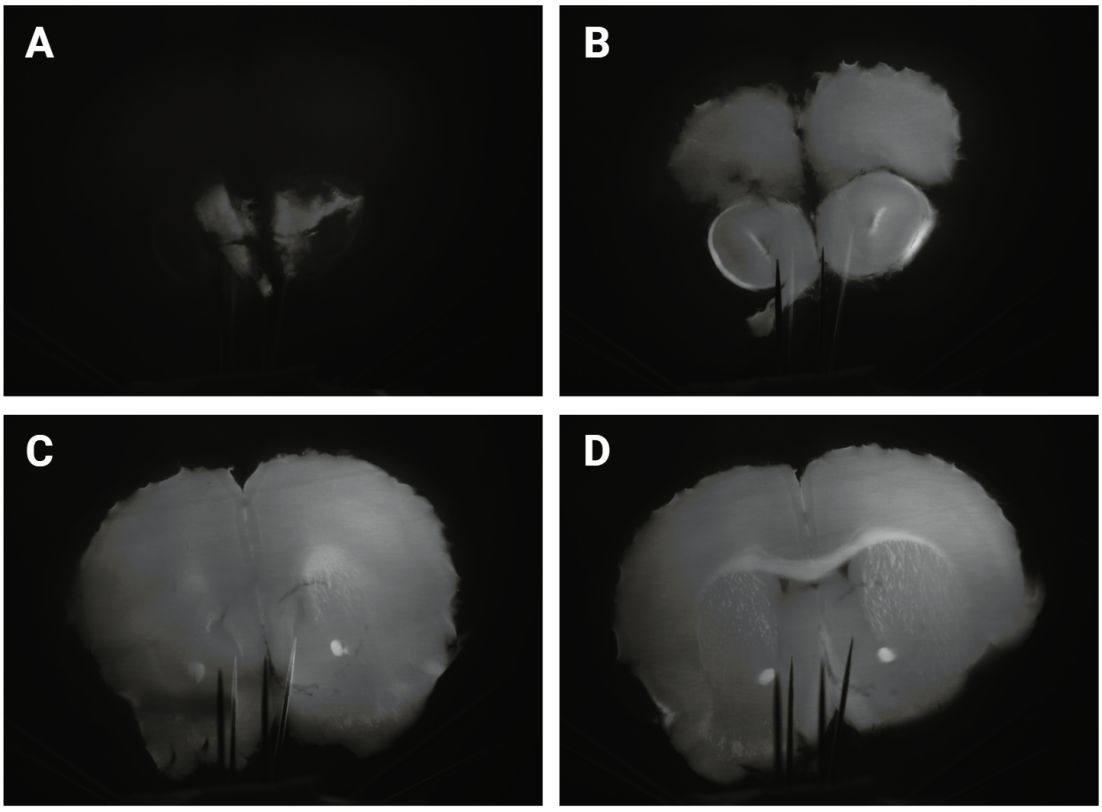

Figure 4.15: Four slices of a longer z-stack of a mouse brain cleared with CUBIC. This sample was not labelled and was imaged with the 450 nm laser, only showing auto-fluorescence. A - the first slice of the stack, at the tip of the olfactory bulbs. B - Slice 219 of 538, the olfactory bulbs are visible. C - Slice 448 of 538, the corpus striatum starts to appear. D - The last slice of the stack.

Using the full image set and the IMARIS software, a three-dimensional rendering of the sample was generated and depicted in Figure 4.16, where Figure 4.16 A and B show the front and back view of the brain sample, respectively. It is possible to discern the structures addressed in subsection 4.2.2. Figure 4.16 C shows the side view reconstructed from the stack of slices, where the depth of the structures visible on Figure 4.16 A and B can be observed, although not as clearly. Some stripes can be seen on subfigure C as some slices were not illuminated, a problem that has been resolved since by using a different relay for the laser trigger action.

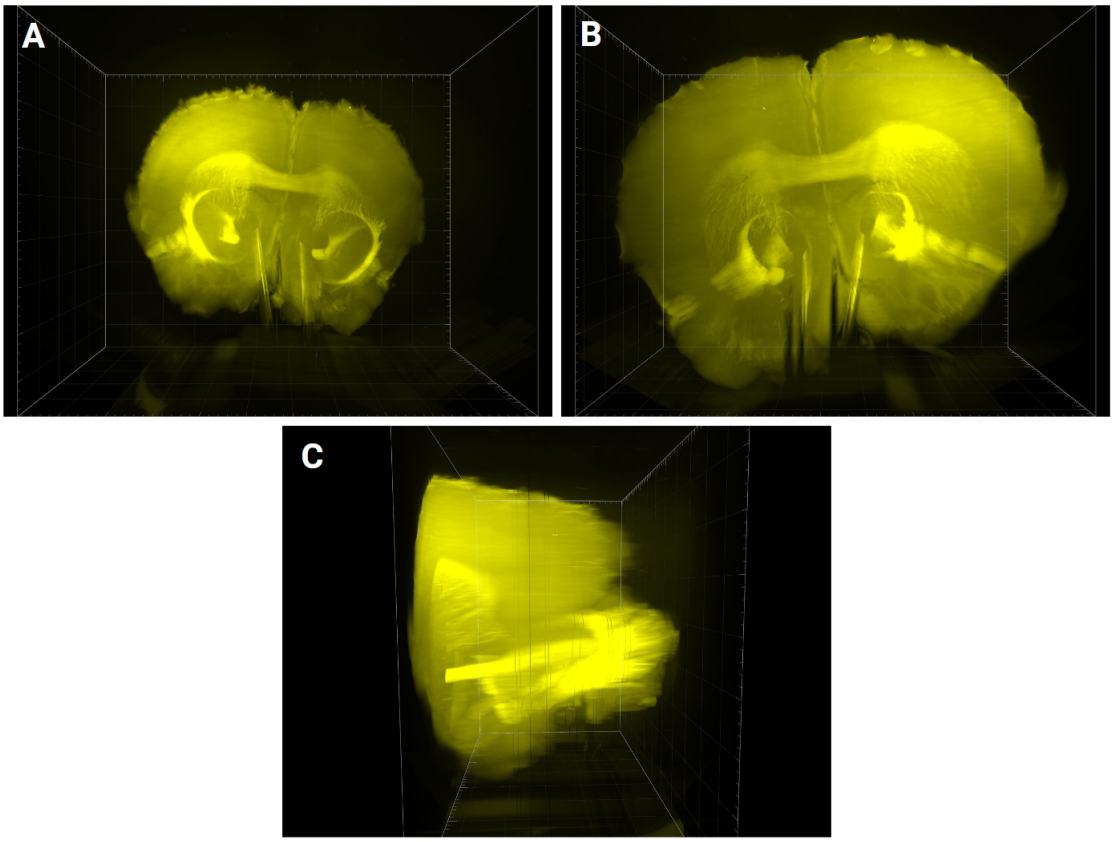

Figure 4.16: Three dimensional render of a longer z-stack of a mouse brain cleared with CUBIC. This sample was not labelled and was imaged with the 450 nm laser, only showing auto-fluorescence. A - View from the side of the olfactory bulbs (closest to the camera). B - View from the opposite side. C - Side view.

4.2.5 Discussion

The figures in the previous section show some artifacts that are commonly found with light-sheet microscopes. Figure 4.11 shows air bubbles in the sample which reflected light and are visible - had they been in the light-sheet's path, a shadow would have originated in that direction [5]. In Figure 4.12 and Figure 4.13, the fading brightness of the light sheet is very apparent, as these large samples are not perfectly clear, and the sheet loses intensity as it crosses the tissue. This artifact can been addressed by implementing bilateral illumination or by pivoting the light-sheet, as seen on novel LSFM architectures [1], [39], [52].

The Arduino software developed for this version of LEMOLish was implemented following closely the original LEMOLish menus, adapting it to the available LCD screen and controls. This setup is easily controllable with a simple joystick and push buttons. To further improve usability, it would be interesting to observe how different users interact with the system to evaluate the intuitiveness of the controls.

The setting of image quality parameters, such as gain and exposure, switching

from live-imaging to trigger based acquisition, and selecting the correct folder to save the images were functionalities controlled with the IC Capture 2.5 software. This occasionally led to some lapses, such as the exposure time not matching between what was set on the Arduino and what was set on IC Capture, or not enabling the trigger mode before starting acquisition.

Some functionalities were not yet implemented in this version of LEMOLish due to time constraints, namely the motorized rotation of the sample and the setup of the two lasers on the top and bottom laser platforms (only the bottom platform was used).

Nevertheless, LEMOLish was able to image z-stacks of mouse brain samples cleared with CUBIC, which were assembled to a three-dimensional image using IMARIS without needing any previous processing. Besides that, it demonstrated that it is capable of imaging sequences potentially large enough to image an entire organ or small specimen such as a mouse embryo.

Chapter 5

Conclusions

5.1 Conclusions

Reiterating the objectives exposed in the beginning of this chapter, this thesis aimed to explore tissue clearing and implementing the open-source light-sheet microscope, LEMOLish.

Two distinct tissue clearing protocols were implemented - iDISCO+, a solvent-based protocol, and CUBIC, an aqueous-based protocol - having been tested on several samples, including mouse brain, liver and spleen.

When applying the standard iDISCO+ protocol [28], the highly pigmented samples, although reaching some transparency, remained pigmented until the final clearing step. This prompted the introduction of decolourization as a pre-treatment step, which significantly improved the clearing results. This step was performed prior to both iDISCO+ and CUBIC protocols and was based on decolourization steps from aqueous-based and solvent-based protocols. In fact, this approach aligns with what was suggested by some authors: that to develop the best protocol tailored for specific samples, steps of different protocols should be evaluated and may be combined [5], [6].

Overall, both protocols yielded comparably positive outcomes. As the CUBIC protocol was relatively easier to handle and safer, it was the preferred choice to use with LEMOLish, as the cuvette needs to be completely filled with the RI matching medium, and therefore any accidental spills are not as dangerous or as damaging to the LEMOLish. CUBIC's expansive properties may be beneficial, increasing the size of small samples, making their structures easier to resolve, and increasing the permeability for immunolabelling, or it may pose a challenge when dealing with already large samples. A sample too large may not fit in the cuvette and, aditionally, as it ranges a large area of the light-sheet, there may be a decrease in image quality away from the focused area of the light-sheet. In addition to that, if the expansion is not equal across the tissue, its structures may be deformed.

While the implemented LEMOLish system is not yet fully optimized, it has successfully captured in-depth images of the provided mouse organ samples. It managed to produce a z-stack with a depth spanning 5 mm, and it repeatedly generated z-stacks within a 1.5 mm range with minimal misalignment. Notably, the LEMOLish system has showcased its capability to image cleared samples, as evidenced by its successful visualization of entire mouse organs, such as liver and brain samples. This underscores the promising potential of the LEMOLish setup to fulfill its primary goal of screening cleared samples. This functionality is useful to verify if the samples are properly cleared and labelled before accessing a commercial or state-of-the-art light-

sheet fluorescence microscope in other national or international microscopy facilities, that will provide researchers with better resolution and magnification.

In addition to the assembling of the LEMOlish system, during the present thesis, a novel Arduino code was developed to control the microscope. This new development will have a great impact in the assembly of this open-source microscope by future builders, since it provides an alternative control system for the microscope, as the originally used LEGO controller and motors have been discontinued and may be harder to find in the future.

5.2 Future Work

Tissue clearing had positive results for the samples tested, although the labelling of the liver samples was not achieved. It was concluded that the problem may lie in the efficacy of the antibodies used as they also failed to label the 40 μm brain slices. It would be interesting to test other antibodies to achieve a successfully labelled liver sample. Furthermore, labelling an entire brain sample (as opposed to 1 mm slices) would provide insights about penetration of the markers into deeper regions of the tissue, which may require further optimization of the protocols.

The current system can image cleared samples but has not been finalized and would benefit from further testing. In some figures in section 4.2, the fading brightness of the light sheet as it traverses the tissue is very apparent. The implementation of the motorized sample rotation, as originally planned, would allow the user to rotate the sample 180° and reimage it. Alternatively, although more expensive as it requires more lasers, a plan for bilateral illumination could be developed.

Another aspect that was not implemented during this thesis was the alignment of the two lasers. The system was assembled so that a laser would be placed on the top platform of the laser module, and another one on the bottom platform. As Figure 4.14 showed that the LEMOLish system is capable of repeating sets of acquisitions, the user would be able to perform an acquisition with one laser, switch the filters, select the other laser, and reimage the sample. This would be beneficial to further evaluate the system's capability of imaging two different fluorophores in the same z-stack of sections, as explored in subsection 4.2.3.

The system was tested with unlabelled brain samples illuminated with the blue laser, therefore only showing autofluorescence. It would be worthwhile to explore its performance when using tissues with fluorescent labelling, and also other types of samples, such as other mouse organs. This is would also be in line with testing

the CUBIC and iDISCO+ protocols with other types of tissues.

Finally, further testing of this system would be valuable to evaluate its axial and lateral resolution, as well as assessing the distance the platforms truly cover when acquiring images. In addition to that, conducting system calibration would enable the determination of the dimensions of the sample imaged by the LEMOLish microscope.

Bibliography

[1] Muge Molbay, Zeynep Ilgin Kolabas, Mihail Ivilinov Todorov, et al. "A guidebook for DISCO tissue clearing." In: *Molecular systems biology* 17 (3 Mar. 2021), e9807. ISSN: 1744-4292. DOI: 10.15252/msb.20209807. URL: http://www.ncbi.nlm.nih.gov/pubmed/33769689%20http://www.pubmedcentral.nih.gov/articlerender.fcgi?artid=PMC7995442.

[2] Pablo Ariel. "A beginner's guide to tissue clearing". In: *The International Journal of Biochemistry & Cell Biology* 84 (Mar. 2017), pp. 35–39. ISSN: 13572725. DOI: 10.1016/j.biocel.2016.12.009. URL: https://linkinghub.elsevier.com/retrieve/pii/S135727251630396X.

[3] Bin Yang, Jennifer B. Treweek, Rajan P. Kulkarni, et al. "Single-Cell Phenotyping within Transparent Intact Tissue through Whole-Body Clearing". In: *Cell* 158 (4 Aug. 2014), pp. 945–958. ISSN: 00928674. DOI: 10.1016/j.cell.2014.07.017. URL: https://linkinghub.elsevier.com/retrieve/pii/S0092867414009313.

[4] Adriano Azaripour, Tonny Lagerweij, Christina Scharfbillig, et al. "A survey of clearing techniques for 3D imaging of tissues with special reference to connective tissue". In: *Progress in Histochemistry and Cytochemistry* 51 (2 Aug. 2016), pp. 9–23. ISSN: 00796336. DOI: 10.1016/j.proghi.2016.04.001. URL: https://linkinghub.elsevier.com/retrieve/pii/S0079633616300043.

[5] Kurt R. Weiss, Fabian F. Voigt, Douglas P. Shepherd, et al. "Tutorial: practical considerations for tissue clearing and imaging". In: *Nature Protocols* 16 (6 June 2021), pp. 2732–2748. ISSN: 1754-2189. DOI: 10.1038/s41596-021-00502-8. URL: http://www.nature.com/articles/s41596-021-00502-8.

[6] Douglas S. Richardson, Webster Guan, Katsuhiko Matsumoto, et al. "Tissue clearing". In: *Nature Reviews Methods Primers* 1 (1 Dec. 2021), p. 84. ISSN: 2662-8449. DOI: 10.1038/s43586-021-00080-9. URL: https://www.nature.com/articles/s43586-021-00080-9.

[7] Douglas S. Richardson and Jeff W. Lichtman. "Clarifying Tissue Clearing". In: *Cell* 162 (2 July 2015), pp. 246–257. ISSN: 00928674. DOI: 10.1016/j.

cell.2015.06.067. URL: https://linkinghub.elsevier.com/retrieve/pii/S0092867415008375.

[8] Tuan Vo-Dinh, ed. *Biomedical Photonics Handbook*. CRC Press, Mar. 2003. ISBN: 9780429214295. DOI: 10.1201/9780203008997. URL: https://www.taylorfrancis.com/books/9780203008997.

[9] Eugene Hecht. *Optics*. 5 ed. Boston: Pearson Education, Inc, 2017. ISBN: 9780133977226.

[10] Frank L. Pedrotti, Leno Matthew Pedrotti, and Leno S. Pedrotti. *Introduction to optics*. 3rd ed. Upper Saddle River, N.J: Pearson/Prentice Hall, 2007. ISBN: 9780131499331.

[11] Julia L. Sandell and Timothy C. Zhu. "A review of in-vivo optical properties of human tissues and its impact on PDT". In: *Journal of Biophotonics* 4 (11-12 Nov. 2011), pp. 773–787. ISSN: 1864-063X. DOI: 10.1002/jbio.201100062.

[12] Rupsa Datta, Tiffany M. Heaster, Joe T. Sharick, et al. "Fluorescence lifetime imaging microscopy: fundamentals and advances in instrumentation, analysis, and applications". In: *Journal of Biomedical Optics* 25 (07 May 2020), p. 1. ISSN: 1083-3668. DOI: 10.1117/1.JBO.25.7.071203. URL: https://www.spiedigitallibrary.org/journals/journal-of-biomedical-optics/volume-25/issue-07/071203/Fluorescence-lifetime-imaging-microscopy--fundamentals-and-advances-in-instrumentation/10.1117/1.JBO.25.7.071203.full.

[13] Inês S. Martins, Hugo F. Silva, Ekaterina N. Lazareva, et al. "Measurement of tissue optical properties in a wide spectral range: a review [Invited]". In: *Biomedical Optics Express* 14 (1 Jan. 2023), p. 249. ISSN: 2156-7085. DOI: 10.1364/BOE.479320.

[14] Steven L Jacques. "Optical properties of biological tissues: a review". In: *Physics in Medicine and Biology* 58 (11 June 2013), R37–R61. ISSN: 0031-9155. DOI: 10.1088/0031-9155/58/11/R37.

[15] Michael W. Davidson and Mortimer Abramowitz. "Optical Microscopy". In: John Wiley & Sons, Inc., Jan. 2002. DOI: 10.1002/0471443395.img074. URL: https://onlinelibrary.wiley.com/doi/10.1002/0471443395.img074.

[16] A.C. Croce and G. Bottiroli. "Autofluorescence spectroscopy and imaging: a tool for biomedical research and diagnosis". In: *European Journal of Histochemistry* 58 (Dec. 2014), p. 2461. ISSN: 2038-8306. DOI: 10.4081/ejh.2014.2461. URL: https://www.ejh.it/index.php/ejh/article/view/2461.

[17] Paweł Matryba, Lukasz Bozycki, Monika Pawłowska, et al. "Optimized perfusion-based CUBIC protocol for the efficient whole-body clearing and imaging of rat organs". In: *Journal of Biophotonics* 11 (5 May 2018), e201700248. ISSN: 1864063X. DOI: 10.1002/jbio.201700248. URL: https://onlinelibrary.wiley.com/doi/10.1002/jbio.201700248.

[18] Katsuhiko Matsumoto, Tomoki T. Mitani, Shuhei A. Horiguchi, et al. "Advanced CUBIC tissue clearing for whole-organ cell profiling". In: *Nature Protocols* 14 (12 Dec. 2019), pp. 3506–3537. ISSN: 1754-2189. DOI: 10.1038/s41596-019-0240-9. URL: https://www.nature.com/articles/s41596-019-0240-9.

[19] Chenchen Pan, Ruiyao Cai, Francesca Paola Quacquarelli, et al. "Shrinkage-mediated imaging of entire organs and organisms using uDISCO". In: *Nature Methods* 13 (10 Oct. 2016), pp. 859–867. ISSN: 1548-7091. DOI: 10.1038/nmeth.3964. URL: http://www.nature.com/articles/nmeth.3964.

[20] Nicolas Renier, Zhuhao Wu, David J. Simon, et al. "iDISCO: A Simple, Rapid Method to Immunolabel Large Tissue Samples for Volume Imaging". In: *Cell* 159 (4 Nov. 2014), pp. 896–910. ISSN: 00928674. DOI: 10.1016/j.cell.2014.10.010. URL: https://linkinghub.elsevier.com/retrieve/pii/S0092867414012975.

[21] Anika Klingberg, Anja Hasenberg, Isis Ludwig-Portugall, et al. "Fully Automated Evaluation of Total Glomerular Number and Capillary Tuft Size in Nephritic Kidneys Using Lightsheet Microscopy". In: *Journal of the American Society of Nephrology* 28 (2 Feb. 2017), pp. 452–459. ISSN: 1046-6673. DOI: 10.1681/ASN.2016020232. URL: https://journals.lww.com/00001751-201702000-00012.

[22] Ali Ertürk, Klaus Becker, Nina Jährling, et al. "Three-dimensional imaging of solvent-cleared organs using 3DISCO". In: *Nature Protocols* 7 (11 Nov. 2012), pp. 1983–1995. ISSN: 1754-2189. DOI: 10.1038/nprot.2012.119. URL: https://www.nature.com/articles/nprot.2012.119.

[23] Martin K. Schwarz, Annemarie Scherbarth, Rolf Sprengel, et al. "Fluorescent-Protein Stabilization and High-Resolution Imaging of Cleared, Intact Mouse Brains". In: *PLOS ONE* 10 (5 May 2015). Ed. by William H. Merigan, e0124650. ISSN: 1932-6203. DOI: 10.1371/journal.pone.0124650. URL: https://dx.plos.org/10.1371/journal.pone.0124650.

[24] Etsuo A Susaki, Kazuki Tainaka, Dimitri Perrin, et al. "Advanced CUBIC protocols for whole-brain and whole-body clearing and imaging". In: *Nature Protocols* 10 (11 Nov. 2015), pp. 1709–1727. ISSN: 1754-2189. DOI: 10.1038/nprot.2015.085. URL: https://www.nature.com/articles/nprot.2015.085.

[25] Kazuki Tainaka, Tatsuya C. Murakami, Etsuo A. Susaki, et al. "Chemical Landscape for Tissue Clearing Based on Hydrophilic Reagents". In: *Cell Reports* 24 (8 Aug. 2018), 2196–2210.e9. ISSN: 22111247. DOI: 10.1016/j.celrep.2018.07.056. URL: https://linkinghub.elsevier.com/retrieve/pii/S2211124718311598.

[26] Etsuo A. Susaki, Kazuki Tainaka, Dimitri Perrin, et al. "Whole-Brain Imaging with Single-Cell Resolution Using Chemical Cocktails and Computational Analysis". In: *Cell* 157 (3 Apr. 2014), pp. 726–739. ISSN: 00928674. DOI: 10.1016/j.cell.2014.03.042. URL: https://linkinghub.elsevier.com/retrieve/pii/S0092867414004188.

[27] Etsuo A. Susaki, Chika Shimizu, Akihiro Kuno, et al. "Versatile whole-organ/body staining and imaging based on electrolyte-gel properties of biological tissues". In: *Nature Communications* 11 (1 Apr. 2020), p. 1982. ISSN: 2041-1723. DOI: 10.1038/s41467-020-15906-5.

[28] Nicolas Renier, Eliza L. Adams, Christoph Kirst, et al. "Mapping of Brain Activity by Automated Volume Analysis of Immediate Early Genes". In: *Cell* 165 (7 June 2016), pp. 1789–1802. ISSN: 00928674. DOI: 10.1016/j.cell.2016.05.007. URL: https://linkinghub.elsevier.com/retrieve/pii/S0092867416305554.

[29] Yusha Li, Jianyi Xu, Peng Wan, et al. "Optimization of GFP Fluorescence Preservation by a Modified uDISCO Clearing Protocol". In: *Frontiers in Neuroanatomy* 12 (Aug. 2018). ISSN: 1662-5129. DOI: 10.3389/fnana.2018.00067. URL: https://www.frontiersin.org/article/10.3389/fnana.2018.00067/full.

[30] Yisong Qi, Tingting Yu, Jianyi Xu, et al. "FDISCO: Advanced solvent-based clearing method for imaging whole organs". In: *Archivio di Studi Urbani e Regionali* 48 (122 2019). ISSN: 19718519. DOI: 10.1126/sciadv.aau8355.

[31] Ruiyao Cai, Chenchen Pan, Alireza Ghasemigharagoz, et al. "Panoptic imaging of transparent mice reveals whole-body neuronal projections and skull–meninges connections". In: *Nature Neuroscience* 22 (2 Feb. 2019), pp. 317–327. ISSN: 1097-6256. DOI: 10.1038/s41593-018-0301-3. URL: https://www.nature.com/articles/s41593-018-0301-3.

[32] Jingtan Zhu, Yilin Ma, Jianyi Xu, et al. "Dec-DISCO: decolorization DISCO clearing for seeing through the biological architectures of heme-rich organs". In: *Biomedical Optics Express* 12 (9 Sept. 2021), p. 5499. ISSN: 2156-7085. DOI: 10.1364/BOE.431397. URL: https://opg.optica.org/abstract.cfm?URI=boe-12-9-5499.

[33] Victoria Nudell, Yu Wang, Zhengyuan Pang, et al. "HYBRiD: hydrogel-reinforced DISCO for clearing mammalian bodies". In: *Nature Methods* 19 (4 Apr. 2022), pp. 479–485. ISSN: 1548-7091. DOI: 10.1038/s41592-022-01427-0. URL: https://www.nature.com/articles/s41592-022-01427-0.

[34] Joseph R. Lakowicz, ed. *Principles of Fluorescence Spectroscopy*. Springer US, 2006. ISBN: 978-0-387-31278-1. DOI: 10.1007/978-0-387-46312-4.

[35] Michael J. Sanderson, Ian Smith, Ian Parker, et al. "Fluorescence Microscopy". In: *Cold Spring Harbor Protocols* 2014 (10 Oct. 2014), pdb.top071795. ISSN: 1940-3402. DOI: 10.1101/pdb.top071795. URL: http://www.cshprotocols.org/lookup/doi/10.1101/pdb.top071795.

[36] Jeff W Lichtman and José-Angel Conchello. "Fluorescence microscopy". In: *Nature Methods* 2 (12 Dec. 2005), pp. 910–919. ISSN: 1548-7091. DOI: 10.1038/nmeth817. URL: https://www.nature.com/articles/nmeth817.

[37] Amir Khodavirdipour, Mahboobeh Mehregan, Ali Rajabi, et al. "Microscopy and its Application in Microbiology and Medicine From Light to Quantum Microscopy: A Mini Review". In: *Avicenna Journal of Clinical Microbiology and Infection* 6 (4 Dec. 2019), pp. 133–137. ISSN: 2383-0298. DOI: 10.34172/ajcmi.2019.24. URL: http://ajcmi.umsha.ac.ir/Article/ajcmi-2145.

[38] Theodore George Rochow and Paul Arthur Tucker. *Introduction to Microscopy by Means of Light, Electrons, X Rays, or Acoustics*. Springer US, 1994. ISBN: 978-1-4899-1515-3. DOI: 10.1007/978-1-4899-1513-9. URL: http://link.springer.com/10.1007/978-1-4899-1513-9.

[39] Pablo Delgado-Rodriguez, Claire Jordan Brooks, Juan José Vaquero, et al. "Innovations in ex vivo Light Sheet Fluorescence Microscopy". In: *Progress in Biophysics and Molecular Biology* 168 (Jan. 2022), pp. 37–51. ISSN: 00796107. DOI: 10.1016/j.pbiomolbio.2021.07.002. URL: https://linkinghub.elsevier.com/retrieve/pii/S007961072100081X.

[40] Adaobi Nwaneshiudu, Christiane Kuschal, Fernanda H. Sakamoto, et al. "Introduction to Confocal Microscopy". In: *Journal of Investigative Dermatology* 132 (12 Dec. 2012), pp. 1–5. ISSN: 0022202X. DOI: 10.1038/jid.2012.429. URL: https://linkinghub.elsevier.com/retrieve/pii/S0022202X15355536.

[41] Alberto Diaspro, Paolo Bianchini, Giuseppe Vicidomini, et al. "Multi-photon excitation microscopy". In: *BioMedical Engineering OnLine* 5 (1 Dec. 2006), p. 36. ISSN: 1475-925X. DOI: 10.1186/1475-925X-5-36. URL: https://biomedical-engineering-online.biomedcentral.com/articles/10.1186/1475-925X-5-36.

[42] David R. Miller, Jeremy W. Jarrett, Ahmed M. Hassan, et al. "Deep tissue imaging with multiphoton fluorescence microscopy". In: *Current Opinion in Biomedical Engineering* 4 (Dec. 2017), pp. 32–39. ISSN: 24684511. DOI: 10.1016/j.cobme.2017.09.004.

[43] Peter A. Santi. "Light Sheet Fluorescence Microscopy". In: *Journal of Histochemistry & Cytochemistry* 59 (2 Feb. 2011), pp. 129–138. ISSN: 0022-1554. DOI: 10.1369/0022155410394857. URL: http://journals.sagepub.com/doi/10.1369/0022155410394857.

[44] Jan Huisken and Didier Y. R. Stainier. "Selective plane illumination microscopy techniques in developmental biology". In: *Development* 136 (12 June 2009), pp. 1963–1975. ISSN: 1477-9129. DOI: 10.1242/dev.022426. URL: https://journals.biologists.com/dev/article/136/12/1963/65234/Selective-plane-illumination-microscopy-techniques.

[45] Emmanuel G. Reynaud, Uroš Kržič, Klaus Greger, et al. "Light sheet-based fluorescence microscopy: More dimensions, more photons, and less photodamage". In: *HFSP Journal* 2 (5 Oct. 2008), pp. 266–275. ISSN: 1955-2068. DOI: 10.2976/1.2974980. URL: https://www.tandfonline.com/doi/full/10.2976/1.2974980.

[46] Miguel M. Lopes, Jacques Paysan, José Rino, et al. "A new protocol for whole-brain biodistribution analysis of AAVs by tissue clearing, light-sheet microscopy and semi-automated spatial quantification". In: *Gene Therapy* 29 (12 Dec. 2022), pp. 665–679. ISSN: 0969-7128. DOI: 10.1038/s41434-022-00372-z. URL: https://www.nature.com/articles/s41434-022-00372-z.

[47] John Girkin. *A Practical Guide to Optical Microscopy*. CRC Press, June 2019. ISBN: 9781315115351. DOI: 10.1201/b22249. URL: https://www.taylorfrancis.com/books/9781351630368.

[48] H. Siedentopf and R. Zsigmondy. "Uber Sichtbarmachung und Größenbestimmung ultramikoskopischer Teilchen, mit besonderer Anwendung auf Goldrubingläser". In: *Annalen der Physik* 315 (1 1902), pp. 1–39. ISSN: 00033804. DOI: 10.1002/andp.19023150102.

[49] A. H. Voie, D. H. Burns, and F. A. Spelman. "Orthogonal-plane fluorescence optical sectioning: Three-dimensional imaging of macroscopic biological specimens". In: *Journal of Microscopy* 170 (3 June 1993), pp. 229–236. ISSN: 00222720. DOI: 10.1111/j.1365-2818.1993.tb03346.x. URL: https://onlinelibrary.wiley.com/doi/10.1111/j.1365-2818.1993.tb03346.x.

[50] Adam K. Glaser, Ye Chen, Chengbo Yin, et al. "Multidirectional digital scanned light-sheet microscopy enables uniform fluorescence excitation and contrast-enhanced imaging". In: *Scientific Reports* 8 (1 Sept. 2018), p. 13878. ISSN: 2045-2322. DOI: 10.1038/s41598-018-32367-5. URL: https://www.nature.com/articles/s41598-018-32367-5.

[51] Jan Huisken, Jim Swoger, Filippo Del Bene, et al. "Optical Sectioning Deep Inside Live Embryos by Selective Plane Illumination Microscopy". In: *Science* 305 (5686 Aug. 2004), pp. 1007–1009. ISSN: 0036-8075. DOI: 10.1126/science.1100035. URL: https://www.science.org/doi/10.1126/science.1100035.

[52] Jan Huisken and Didier Y. R. Stainier. "Even fluorescence excitation by multidirectional selective plane illumination microscopy (mSPIM)". In: *Optics Letters* 32 (17 Sept. 2007), p. 2608. ISSN: 0146-9592. DOI: 10.1364/OL.32.002608. URL: https://opg.optica.org/abstract.cfm?URI=ol-32-17-2608.

[53] Philipp J. Keller, Annette D. Schmidt, Joachim Wittbrodt, et al. "Reconstruction of Zebrafish Early Embryonic Development by Scanned Light Sheet Microscopy". In: *Science* 322 (5904 Nov. 2008), pp. 1065–1069. ISSN: 0036-8075. DOI: 10.1126/science.1162493. URL: https://www.science.org/doi/10.1126/science.1162493.

[54] Zhe Yang, Li Mei, Fei Xia, et al. "Dual-slit confocal light sheet microscopy for in vivo whole-brain imaging of zebrafish". In: *Biomedical Optics Express* 6 (5 May 2015), p. 1797. ISSN: 2156-7085. DOI: 10.1364/BOE.6.001797. URL: https://opg.optica.org/abstract.cfm?URI=boe-6-5-1797.

[55] Matthew B. Bouchard, Venkatakaushik Voleti, César S. Mendes, et al. "Swept confocally-aligned planar excitation (SCAPE) microscopy for high-speed volumetric imaging of behaving organisms". In: *Nature Photonics* 9 (2 Feb. 2015), pp. 113–119. ISSN: 1749-4885. DOI: 10.1038/nphoton.2014.323. URL: https://www.nature.com/articles/nphoton.2014.323.

[56] Stephan Daetwyler and Reto Paul Fiolka. "Light-sheets and smart microscopy, an exciting future is dawning". In: *Communications Biology* 6 (1 May 2023), p. 502. ISSN: 2399-3642. DOI: 10.1038/s42003-023-04857-4. URL: https://www.nature.com/articles/s42003-023-04857-4.

[57] Johanna Perens and Jacob Hecksher-Sørensen. "Digital Brain Maps and Virtual Neuroscience: An Emerging Role for Light-Sheet Fluorescence Microscopy in Drug Development". In: *Frontiers in Neuroscience* 16 (Apr. 2022). ISSN: 1662-453X. DOI: 10.3389/fnins.2022.866884.

[58] Felix A. Kyere, Ian Curtin, Oleh Krupa, et al. "Whole-Brain Single-Cell Imaging and Analysis of Intact Neonatal Mouse Brains Using MRI, Tissue Clearing, and Light-Sheet Microscopy". In: *Journal of Visualized Experiments* (186 Aug. 2022). ISSN: 1940-087X. DOI: 10.3791/64096.

[59] Luca Pesce, Marina Scardigli, Vladislav Gavryusev, et al. "3D molecular phenotyping of cleared human brain tissues with light-sheet fluorescence microscopy". In: *Communications Biology* 5 (1 May 2022), p. 447. ISSN: 2399-3642. DOI: 10.1038/s42003-022-03390-0.

[60] Jonas Doerr, Martin Karl Schwarz, Dirk Wiedermann, et al. "Whole-brain 3D mapping of human neural transplant innervation". In: *Nature Communications* 8 (1 Jan. 2017), p. 14162. ISSN: 2041-1723. DOI: 10.1038/ncomms14162.

[61] Bethan Lloyd-Lewis, Felicity M. Davis, Olivia B. Harris, et al. "Imaging the mammary gland and mammary tumours in 3D: optical tissue clearing and immunofluorescence methods". In: *Breast Cancer Research* 18 (1 Dec. 2016), p. 127. ISSN: 1465-542X. DOI: 10.1186/s13058-016-0754-9.

[62] Nobuyuki Tanaka, Dagmara Kaczynska, Shigeaki Kanatani, et al. "Mapping of the three-dimensional lymphatic microvasculature in bladder tumours using light-sheet microscopy". In: *British Journal of Cancer* 118 (7 Apr. 2018), pp. 995–999. ISSN: 0007-0920. DOI: 10.1038/s41416-018-0016-y.

[63] Seung-Mo Hong, DongJun Jung, Ashley Kiemen, et al. "Three-dimensional visualization of cleared human pancreas cancer reveals that sustained epithelial-to-mesenchymal transition is not required for venous invasion". In: *Modern Pathology* 33 (4 Apr. 2020), pp. 639–647. ISSN: 08933952. DOI: 10.1038/s41379-019-0409-3.

[64] Simon F. Merz, Philipp Jansen, Ricarda Ulankiewicz, et al. "High-resolution three-dimensional imaging for precise staging in melanoma". In: *European Journal of Cancer* 159 (Dec. 2021), pp. 182–193. ISSN: 09598049. DOI: 10.1016/j.ejca.2021.09.026.

[65] Jaroslav Icha, Christopher Schmied, Jaydeep Sidhaye, et al. "Using Light Sheet Fluorescence Microscopy to Image Zebrafish Eye Development". In: *Journal of Visualized Experiments* (110 Apr. 2016). ISSN: 1940-087X. DOI: 10.3791/53966.

[66] Yichen Ding, Jianguo Ma, Adam D. Langenbacher, et al. "Multiscale light-sheet for rapid imaging of cardiopulmonary system". In: *JCI Insight* 3 (16 Aug. 2018). ISSN: 2379-3708. DOI: 10.1172/jci.insight.121396.

[67] Elisabeth C. Kugler, James Frost, Vishmi Silva, et al. "Zebrafish vascular quantification: a tool for quantification of three-dimensional zebrafish cerebrovascular architecture by automated image analysis". In: *Development* 149 (3 Feb. 2022). ISSN: 0950-1991. DOI: 10.1242/dev.199720.

[68] Katie McDole, Léo Guignard, Fernando Amat, et al. "In Toto Imaging and Reconstruction of Post-Implantation Mouse Development at the Single-Cell Level". In: *Cell* 175 (3 Oct. 2018), 859–876.e33. ISSN: 00928674. DOI: 10.1016/j.cell.2018.09.031.

[69] Kendall A. Hutson, Stephen H. Pulver, Pablo Ariel, et al. "Light sheet microscopy of the gerbil cochlea". In: *Journal of Comparative Neurology* 529 (4 Mar. 2021), pp. 757–785. ISSN: 0021-9967. DOI: 10.1002/cne.24977.

[70] Claudia Prahst, Parham Ashrafzadeh, Thomas Mead, et al. "Mouse retinal cell behaviour in space and time using light sheet fluorescence microscopy". In: *eLife* 9 (Feb. 2020). ISSN: 2050-084X. DOI: 10.7554/eLife.49779.

[71] Natalie Theobalt, Isabel Hofmann, Sonja Fiedler, et al. "Unbiased analysis of obesity related, fat depot specific changes of adipocyte volumes and numbers using light sheet fluorescence microscopy". In: *PLOS ONE* 16 (3 Mar. 2021), e0248594. ISSN: 1932-6203. DOI: 10.1371/journal.pone.0248594.

[72] Miroslav Ovečka, Jiří Sojka, Michaela Tichá, et al. "Imaging plant cells and organs with light-sheet and super-resolution microscopy". In: *Plant Physiology* 188 (2 Feb. 2022), pp. 683–702. ISSN: 0032-0889. DOI: 10.1093/plphys/kiab349.

[73] Béatrice Berthet and Alexis Maizel. "Light sheet microscopy and live imaging of plants". In: *Journal of Microscopy* 263 (2 Aug. 2016), pp. 158–164. ISSN: 0022-2720. DOI: 10.1111/jmi.12393. URL: https://onlinelibrary.wiley.com/doi/10.1111/jmi.12393.

[74] Jordi Andilla, Raphael Jorand, Omar E. Olarte, et al. "Imaging tissue-mimic with light sheet microscopy: A comparative guideline". In: *Scientific Reports* 7 (1 Mar. 2017), p. 44939. ISSN: 2045-2322. DOI: 10.1038/srep44939.

[75] Ignacio Albert-Smet, Asier Marcos-Vidal, Juan José Vaquero, et al. "Applications of Light-Sheet Microscopy in Microdevices". In: *Frontiers in Neuroanatomy* 13 (Jan. 2019). ISSN: 1662-5129. DOI: 10.3389/fnana.2019.00001.

[76] Daisuke Ito, Yoshinori Imai, Keiko Ohsawa, et al. "Microglia-specific localisation of a novel calcium binding protein, Iba1". In: *Molecular Brain Research* 57 (1 June 1998), pp. 1–9. ISSN: 0169328X. DOI: 10.1016/S0169-328X(98)00040-0.

[77] Philip M. Cummins. "Occludin: One Protein, Many Forms". In: *Molecular and Cellular Biology* 32 (2 Jan. 2012), pp. 242–250. ISSN: 1098-5549. DOI: 10.1128/MCB.06029-11.

[78] Panida Lertkiatmongkol, Danying Liao, Heng Mei, et al. "Endothelial functions of platelet/endothelial cell adhesion molecule-1 (CD31)". In: *Current Opinion in Hematology* 23 (3 May 2016), pp. 253–259. ISSN: 1065-6251. DOI: 10.1097/MOH.0000000000000239.

[79] Dmitry Ershov, Minh-Son Phan, Joanna W. Pylvänäinen, et al. "TrackMate 7: integrating state-of-the-art segmentation algorithms into tracking pipelines". In: *Nature Methods* 19 (7 July 2022), pp. 829–832. ISSN: 1548-7091. DOI: 10.1038/s41592-022-01507-1.

[80] Catherine E. Hagan, Brad Bolon, and C. Dirk Keene. "Nervous System". In: Elsevier, 2012, pp. 339–394. DOI: 10.1016/B978-0-12-381361-9.00020-2.

Appendix A

Arduino Code

```
#include <ezButton.h>  // library for pressure buttons

#include <LiquidCrystal_I2C.h>  // library for the LCD display

#include <AccelStepper.h>  // library for the stepper motors

#include <avr/eeprom.h> // to save values

int addressStart = 0;
int addressCurrent = 4;

// stepper motors
#define dirPin1 3
#define stepPin1 4
#define dirPin2 5
#define stepPin2 6
#define motorInterfaceType 1 // motor interface type is 1 when using a driver

// joystick
#define y_pin  A1 // Arduino pin connected to Y pin in the joystick
#define x_pin A2
#define up_threshold    400
#define down_threshold  800

// LEDs
#define bottomLaserTrigger 9
#define topLaserTrigger 8
#define cameraTrigger 7

// stepper motors
AccelStepper stepper1 = AccelStepper(motorInterfaceType, stepPin1, dirPin1);
AccelStepper stepper2 = AccelStepper(motorInterfaceType, stepPin2, dirPin2);

// display
LiquidCrystal_I2C lcd(0x27, 16, 2); // I2C address 0x27, 16 column and 2 rows

// pressure buttons
ezButton upButton(13);
ezButton downButton(12);
ezButton selectButton(11);
ezButton backButton(10);
ezButton joystickButton(2);
```

```
43
int menu = 0;
45 long zStart = 0;
long zStop = 0;
47 long midPosition = 0;
long M1_param = 32; //default (CUBIC)
49 long M2_param = 12; //default (CUBIC)
long t_param = 500; //default
51 int yValue = 0 ; // To store value of the Y axis
int xValue = 0;
53 String laserMode = "L1"; //default

55
void setup(){
57   Serial.begin(9600);

59   stepper1.setMaxSpeed(900);
   stepper2.setMaxSpeed(900);
61
   // debouncing for better button function
63   upButton.setDebounceTime(70);
   downButton.setDebounceTime(70);
65   selectButton.setDebounceTime(70);
   backButton.setDebounceTime(70);
67   joystickButton.setDebounceTime(70);

69   pinMode(bottomLaserTrigger, OUTPUT); //blue LED (laser)
   pinMode(topLaserTrigger, OUTPUT); //yellow LED (laser)
71   pinMode(cameraTrigger, OUTPUT); //red LED (camera)

73   lcd.init(); // initialize the lcd
   lcd.backlight();
75
   updateMenu(); // menu that is shown on the LCD
77 }

79 void loop(){
   // must call the loop() function first
81   upButton.loop();
   downButton.loop();
83   selectButton.loop();
   backButton.loop();
85   joystickButton.loop();

87   // up and down buttons scroll through menu
   if(upButton.isReleased()){
89     if (menu > 0) {
         menu--;
91     }
     updateMenu();
93   }
   if(downButton.isReleased()){
95     if (menu < 6) {
         menu++;
97     }
     updateMenu();
99   }

101  // select button starts action displayed in the menu
   if(selectButton.isReleased()){
103    action();
```

```
    updateMenu();
  }
}


void updateMenu() {
  // menu displays as the user scrolls through it with up and down buttons
  switch (menu) {
    case 0:
      Serial.println("Showing menu 0");
      lcd.clear();
      lcd.print(">Set zStart ");
      lcd.setCursor(0, 1);
      lcd.print(" Set zStop ");
      break;

    case 1:
      Serial.println("Showing menu 1");
      lcd.clear();
      lcd.print(">Set zStop ");
      lcd.setCursor(0, 1);
      lcd.print(" Laser      ");
      break;

    case 2:
      Serial.println("Showing menu 2");
      lcd.clear();
      lcd.print(">Laser      ");
      lcd.setCursor(0, 1);
      lcd.print(" Scan param.");
      break;

    case 3:
      Serial.println("Showing menu 3");
      lcd.clear();
      lcd.print(">Scan param.");
      lcd.setCursor(0, 1);
      lcd.print(" Check param.");
      break;

    case 4:
      Serial.println("Showing menu 4");
      lcd.clear();
      lcd.print(">Check param.");
      lcd.setCursor(0, 1);
      lcd.print(" Start");
      break;

    case 5:
      Serial.println("Showing menu 5");
      lcd.clear();
      lcd.print(">Start");
      lcd.setCursor(0, 1);
      lcd.print(" Reset");
      break;

    case 6:
      Serial.println("Showing menu 6");
      lcd.clear();
      lcd.print(" Start");
      lcd.setCursor(0, 1);
```

```
165       lcd.print(">Reset");
          break;
167   }
}
169
void action() {
171   // execute the action selected in the menu (with selectButton)
  switch (menu) {
173     case 0:
          setzStart();
175       break;
        case 1:
177       setzStop();
          break;
179     case 2:
          chooseLaser();
181       break;
        case 3:
183       setParameters();
          break;
185     case 4:
          showParameters();
187       break;
        case 5:
189       startAcquisition();
          break;
191     case 6:
          reset();
193       break;
  }
195 }

197 void setzStart() {
  Serial.println(">Setting position 1");
199   lcd.clear();
  lcd.print(">Rel. step:");
201   float steps_sum1;
  float steps_to_distance1;
203   String str_number_1;


205
  while (!backButton.isReleased()){ // while the user does not press the backButton
207
    // turn lasers on and off
209     // off by default
    if (selectButton.isPressed()){
211       if (digitalRead(bottomLaserTrigger) || digitalRead(topLaserTrigger)){
          digitalWrite(bottomLaserTrigger, LOW);
213         digitalWrite(topLaserTrigger, LOW);
        } else if (!digitalRead(bottomLaserTrigger) && !digitalRead(topLaserTrigger))
    {
215         // check laserMode and turn laser/s and camera on
          if (laserMode.equals("L1")){
217           digitalWrite(bottomLaserTrigger, HIGH);
            digitalWrite(topLaserTrigger, LOW);
219       } else if (laserMode.equals("L2")) {
            digitalWrite(bottomLaserTrigger, LOW);
221         digitalWrite(topLaserTrigger, HIGH);
        } else if (laserMode.equals("L1+2")){
223         digitalWrite(bottomLaserTrigger, HIGH);
            digitalWrite(topLaserTrigger, HIGH);
```

```
225         }
          }
227     }


229
        yValue = analogRead(y_pin); // read joystick input
231     xValue = analogRead(x_pin);

233     // while loop so that motor runs at the selected speed (if loop would make it
        run at the loop speed)
        while (yValue < up_threshold){
235       stepper1.setSpeed(M1_param*10); // speeds have the chosen ratio to dislocate
        the desired amount
          stepper2.setSpeed(M2_param*10);
237       stepper1.runSpeed();
          stepper2.runSpeed();
239       yValue = analogRead(y_pin); // keeps reading joystick input
          zStart = stepper1.currentPosition(); // update the position of the stepper
241     }
        while (yValue > down_threshold) {  // opposite direction
243       stepper1.setSpeed(-M1_param*10); // speeds have the chosen ratio to dislocate
         the desired amount
          stepper2.setSpeed(-M2_param*10);
245       stepper1.runSpeed();
          stepper2.runSpeed();
247       yValue = analogRead(y_pin); // keeps reading joystick input
          zStart = stepper1.currentPosition(); // update the position of the stepper
249     }

251     // to add a fixed number of steps
        if (xValue < up_threshold){
253       int addSteps = stepper1.currentPosition() + 100;
          while(stepper1.currentPosition() < addSteps) {
255         stepper1.setSpeed(M1_param*10); // speeds have the chosen ratio to
        dislocate the desired amount
            stepper2.setSpeed(M2_param*10);
257         stepper1.runSpeed();
            stepper2.runSpeed();
259       }
          zStart = stepper1.currentPosition(); // update the position of the stepper
261       delay(100);
        } else if (xValue > down_threshold) {
263       int removeSteps = stepper1.currentPosition() - 100;
          while(stepper1.currentPosition() > removeSteps) {
265         stepper1.setSpeed(-M1_param*10); // speeds have the chosen ratio to
        dislocate the desired amount
            stepper2.setSpeed(-M2_param*10);
267         stepper1.runSpeed();
            stepper2.runSpeed();
269       }
          zStart = stepper1.currentPosition(); // update the position of the stepper
271       delay(100);
        }
273
        // display is updated with current position each time the user stops the
        joystick
275     // updated outside of the while cycles so the time it takes for the lcd to
        update does not interfere with motor movement
        lcd.setCursor(0, 1);
277     //calculate distance in micrometers
```

```
    steps_sum1 = (stepper1.currentPosition()+(stepper1.currentPosition()*M2_param/
    M1_param));
279     steps_to_distance1 = (steps_sum1*0.45*3*8.885)/125;
    str_number_1 = String(steps_to_distance1)+"    ";
281     lcd.print(str_number_1);

283     backButton.loop(); // backButton is waiting to be pressed
    selectButton.loop();
285     upButton.loop();
  }
287   Serial.print(">> zStart: ");
  Serial.println(String(zStart)+" steps or "+String(steps_to_distance1)+"
    micrometers");
289

291   if (backButton.isReleased()){
    eeprom_update_dword(addressStart, zStart);
293     eeprom_update_dword(addressCurrent, stepper1.currentPosition());
  }
295
  // turn off lasers and camera
297   digitalWrite(bottomLaserTrigger, LOW);
  digitalWrite(topLaserTrigger, LOW);
299 }

301 void setzStop() {
  Serial.println(">Setting zStop");
303   lcd.clear();
  lcd.print(">Rel. step:");
305   float steps_sum2;
  float steps_to_distance2;
307   String str_number_2;

309
  while (!backButton.isReleased()){ // while the user does not press the backButton
311
    // turn lasers on and off
313     // off by default
    if (selectButton.isPressed()){
315       if (digitalRead(bottomLaserTrigger) || digitalRead(topLaserTrigger)){
        digitalWrite(bottomLaserTrigger, LOW);
317         digitalWrite(topLaserTrigger, LOW);
      } else if (!digitalRead(bottomLaserTrigger) && !digitalRead(topLaserTrigger))
    {
319         // check laserMode and turn laser/s and camera on
        if (laserMode.equals("L1")){
321           digitalWrite(bottomLaserTrigger, HIGH);
          digitalWrite(topLaserTrigger, LOW);
323         } else if (laserMode.equals("L2")) {
          digitalWrite(bottomLaserTrigger, LOW);
325           digitalWrite(topLaserTrigger, HIGH);
        } else if (laserMode.equals("L1+2")){
327           digitalWrite(bottomLaserTrigger, HIGH);
          digitalWrite(topLaserTrigger, HIGH);
329         }
      }
331   }

333     yValue = analogRead(y_pin); // read joystick input
    xValue = analogRead(x_pin);
335
```

```
    // while loop so that motor runs at the selected speed (if loop would make it
    run at the loop speed)
337 while (yValue < up_threshold){
      stepper1.setSpeed(M1_param*10); // speeds have the chosen ratio to dislocate
    the desired amount
339   stepper2.setSpeed(M2_param*10);
      stepper1.runSpeed();
341   stepper2.runSpeed();
      yValue = analogRead(y_pin); // keeps reading joystick input
343   zStop = stepper1.currentPosition(); // update the position of the stepper
     }
345 while(yValue > down_threshold) {  // opposite direction
      stepper1.setSpeed(-M1_param*10); // speeds have the chosen ratio to dislocate
     the desired amount
347   stepper2.setSpeed(-M2_param*10);
      stepper1.runSpeed();
349   stepper2.runSpeed();
      yValue = analogRead(y_pin); // keeps reading joystick input
351   zStop = stepper1.currentPosition();
     }
353
    // to add a fixed number of steps
355 if (xValue < up_threshold){
      int addSteps = stepper1.currentPosition() + 100;
357   while(stepper1.currentPosition() < addSteps) {
        stepper1.setSpeed(M1_param*10); // speeds have the chosen ratio to
    dislocate the desired amount
359     stepper2.setSpeed(M2_param*10);
        stepper1.runSpeed();
361     stepper2.runSpeed();
      }
363   zStop = stepper1.currentPosition(); // update the position of the stepper
      delay(100);
365 } else if (xValue > down_threshold) {
      int removeSteps = stepper1.currentPosition() - 100;
367   while(stepper1.currentPosition() > removeSteps) {
        stepper1.setSpeed(-M1_param*10); // speeds have the chosen ratio to
    dislocate the desired amount
369     stepper2.setSpeed(-M2_param*10);
        stepper1.runSpeed();
371     stepper2.runSpeed();
      }
373   zStop = stepper1.currentPosition(); // update the position of the stepper
      delay(100);
375 }
    // display is updated with current position each time the user stops the
    joystick
377 // updated outside of the while cycles so the time it takes for the lcd to
    update does not interfere with motor movement
    lcd.setCursor(0, 1);
379 //calculate the distance in micrometers
    steps_sum2 = (stepper1.currentPosition()+(stepper1.currentPosition()*M2_param/
    M1_param));
381 steps_to_distance2 = (steps_sum2*0.45*3*8.885)/125;
    str_number_2 = String(steps_to_distance2)+"    ";
383 lcd.print(str_number_2);

385 // set current position to the zero position
    if (joystickButton.isReleased()){
387   Serial.println(">>Set to 0");
      stepper1.setCurrentPosition(0);
```

```
389       zStop=0;
      }
391
      backButton.loop(); // backButton is waiting to be pressed
393     selectButton.loop();
      joystickButton.loop();
395   }
    Serial.print(">> zStop: ");
397   Serial.println(String(zStop)+" steps or "+String(steps_to_distance2)+"
        micrometers");

399   if (backButton.isReleased()){
        eeprom_update_dword(addressCurrent, stepper1.currentPosition());
401   }

403   // turn off lasers and camera
    digitalWrite(bottomLaserTrigger, LOW);
405   digitalWrite(topLaserTrigger, LOW);
}
407

409 void chooseLaser() {
    // to choose which laser or lasers to use
411   Serial.println(">Choosing lasers");
    lcd.clear();
413   lcd.print("Laser mode: ");

415   int countLaserMenu = 0;
    String status = "OFF";
417   while (!backButton.isReleased()){ // while the user does not press the backButton
        // to scroll through laser options
419     if (upButton.isReleased()){
        if (countLaserMenu > 0) {
421       countLaserMenu--;
        }
423     }
      if (downButton.isReleased()) {
425       if (countLaserMenu < 2) {
          countLaserMenu++;
427       }
      }
429
      if (selectButton.isPressed()) {
431       if (status.equals("OFF")){
          status = "ON";
433       } else {
          status = "OFF";
435       }
      }
437     lcd.setCursor(0, 1);
      // menu displays as the user scrolls through it with up (left) and down (right)
       buttons
439     switch (countLaserMenu) {
        case 0:
441       lcd.print(">L1   L2   L1+2");
          laserMode = "L1";
443       if (status.equals("ON")){
            digitalWrite(topLaserTrigger, LOW);
445         digitalWrite(bottomLaserTrigger, HIGH);
          } else {
447         digitalWrite(topLaserTrigger, LOW);
```

```
          digitalWrite(bottomLaserTrigger, LOW);
        }
        break;
      case 1:
        lcd.print(" L1  >L2   L1+2");
        laserMode = "L2";
        if (status.equals("ON")){
          digitalWrite(topLaserTrigger, HIGH);
          digitalWrite(bottomLaserTrigger, LOW);

        } else {
          digitalWrite(topLaserTrigger, LOW);
          digitalWrite(bottomLaserTrigger, LOW);
        }
        break;
      case 2:
        lcd.print(" L1   L2  >L1+2");
        laserMode = "L1+2";
        if (status.equals("ON")){
          digitalWrite(bottomLaserTrigger, HIGH);
          digitalWrite(topLaserTrigger, HIGH);
        } else {
          digitalWrite(bottomLaserTrigger, LOW);
          digitalWrite(topLaserTrigger, LOW);
        }
        break;
    }

    // buttons are waiting to be pressed
    upButton.loop();
    downButton.loop();
    backButton.loop();
    selectButton.loop();
  }
  Serial.print(">> Laser Mode: ");
  Serial.println(laserMode);
  digitalWrite(bottomLaserTrigger, LOW);
  digitalWrite(topLaserTrigger, LOW);
}

void setParameters() {
  // to set the parameters of motor 1, motor 2 and acquisition time
  Serial.println(">Setting M1, M2 and time");
  lcd.clear();

  int countParam = 0;
  String param;
  while (!backButton.isReleased()){ // while the user does not press the backButton
    // to scroll through parameters (M1, M2 or time)
    if (upButton.isReleased()){
      if (countParam > 0) {
        countParam--;
      }
    }
    if (downButton.isReleased()) {
      if (countParam < 2) {
        countParam++;
      }
    }

```

```
    // menu displays as the user scrolls through parameters with up (left) and down
     (right) buttons
509 switch (countParam) {
      case 0:
511     lcd.setCursor(0, 0);
        lcd.print("Parameters: ");
513     lcd.setCursor(0, 1);
        lcd.print(">M1   M2   Time");
515     param = "M1";
        break;
517   case 1:
        lcd.setCursor(0, 0);
519     lcd.print("Parameters: ");
        lcd.setCursor(0, 1);
521     lcd.print(" M1  >M2   Time");
        param = "M2";
523     break;
      case 2:
525     lcd.setCursor(0, 0);
        lcd.print("Parameters: ");
527     lcd.setCursor(0, 1);
        lcd.print(" M1   M2  >Time");
529     param = "time";
        break;
531 }

533 int countM1 = 0;
    int countM2 = 0;
535 int countTime = 0;

537 // when user selects a parameter, a sub-sub-menu appears with the possible
    parameter setting
    if(selectButton.isPressed() && param.equals("M1")){
539   // isPressed instead of isReleased as previous button push selected this
    option as well
      Serial.println(">> Selecting M1");
541   lcd.clear();
      lcd.setCursor(0, 0);
543   lcd.print("M1: ");

545   while(!backButton.isReleased()){ // while the user does not press the
    backButton
        // to scroll through parameter values
547     if (upButton.isReleased()){
          if (countM1 > 0) {
549         countM1--;
          }
551     }
        if (downButton.isReleased()) {
553       if (countM1 < 10) {
            countM1++;
555       }
        }
557
        lcd.setCursor(0, 1);
559     // menu displays as the user scrolls through M1 parameter values with up (
    left) and down (right) buttons
        switch (countM1) {
561       case 0:
            lcd.print(">00  18  19  20");
563         M1_param = 0;
```

```
            break;
565       case 1:
            lcd.print(">18  19  20  21");
567         M1_param = 18;
            break;
569       case 2:
            lcd.print(">19  20  21  22");
571         M1_param = 19;
            break;
573       case 3:
            lcd.print(">20  21  22  28");
575         M1_param = 20;
            break;
577       case 4:
            lcd.print(">21  22  28  29");
579         M1_param = 21;
            break;
581       case 5:
            lcd.print(">22  28  29  30");
583         M1_param = 22;
            break;
585       case 6:
            lcd.print(">28  29  30  31");
587         M1_param = 28;
            break;
589       case 7:
            lcd.print(">29  30  31  32");
591         M1_param = 29;
            break;
593       case 8:
            lcd.print(" 29 >30  31  32");
595         M1_param = 30;
            break;
597       case 9:
            lcd.print(" 29  30 >31  32");
599         M1_param = 31;
            break;
601       case 10:
            lcd.print(" 29  30  31 >32");
603         M1_param = 32;
            break;
605     }
      // buttons are waiting to be pressed
607   backButton.loop();
      selectButton.loop();
609   upButton.loop();
      downButton.loop();
611 }
    Serial.print(">>> M1: ");
613 Serial.println(M1_param);
}
615

if(selectButton.isPressed() && param.equals("M2")){
617   // isPressed instead of isReleased as previous button push selected this
    option as well
    Serial.println(">>Selecting M2");
619 lcd.clear();
    lcd.setCursor(0, 0);
621 lcd.print("(-)M2: ");
```

```
623       while(!backButton.isReleased()){ // while the user does not press the
      backButton
          // to scroll through parameter values
625       if (upButton.isReleased()){
            if (countM2 > 0) {
627           countM2--;
            }
629       }
          if (downButton.isReleased()) {
631         if (countM2 < 17) {
              countM2++;
633         }
          }
635
          lcd.setCursor(0, 1);
637       // menu displays as the user scrolls through M2 parameter values with up (
      left) and down (right) buttons
          switch (countM2) {
639         case 0:
              lcd.print(">00  01  02  03");
641           M2_param = 0;
              break;
643         case 1:
              lcd.print(">01  02  03  04");
645           M2_param = 1;
              break;
647         case 2:
              lcd.print(">02  03  04  05");
649           M2_param = 2;
              break;
651         case 3:
              lcd.print(">03  04  05  06");
653           M2_param = 3;
              break;
655         case 4:
              lcd.print(">04  05  06  07");
657           M2_param = 4;
              break;
659         case 5:
              lcd.print(">05  06  07  08");
661           M2_param = 5;
              break;
663         case 6:
              lcd.print(">06  07  08  09");
665           M2_param = 6;
              break;
667         case 7:
              lcd.print(">07  08  09  10");
669           M2_param = 7;
              break;
671         case 8:
              lcd.print(">08  09  10  11");
673           M2_param = 8;
              break;
675         case 9:
              lcd.print(">09  10  11  12");
677           M2_param = 9;
              break;
679         case 10:
              lcd.print(">10  11  12  13");
681           M2_param = 10;
```

```
            break;
683       case 11:
            lcd.print(">11  12  13  14");
685         M2_param = 11;
            break;
687       case 12:
            lcd.print(">12  13  14  15");
689         M2_param = 12;
            break;
691       case 13:
            lcd.print(">13  14  15  16");
693         M2_param = 13;
            break;
695       case 14:
            lcd.print(">14  15  16  17");
697         M2_param = 14;
            break;
699       case 15:
            lcd.print(" 14 >15  16  17");
701         M2_param = 15;
            break;
703       case 16:
            lcd.print(" 14  15 >16  17");
705         M2_param = 16;
            break;
707       case 17:
            lcd.print(" 14  15  16 >17");
709         M2_param = 17;
            break;
711     }
      // buttons are waiting to be pressed
713   backButton.loop();
      selectButton.loop();
715   upButton.loop();
      downButton.loop();
717 }
  Serial.print(">>> M2: ");
719 Serial.println(M2_param);
}
721

if(selectButton.isPressed() && param.equals("time")){
723   // isPressed instead of isReleased as previous button push selected this
  option as well
  Serial.println(">> Selecting time");
725 lcd.clear();
  lcd.setCursor(0, 0);
727 lcd.print("Time step: ");

729   while(!backButton.isReleased()){ // while the user does not press the
  backButton
      // to scroll through parameter values
731   if (upButton.isReleased()){
        if (countTime > 0) {
733       countTime--;
        }
735   }
      if (downButton.isReleased()) {
737     if (countTime < 6) {
          countTime++;
739     }
      }
```

```
741
        lcd.setCursor(0, 1);
743     // menu displays as the user scrolls through time parameter values with up
    (left) and down (right) buttons
        switch (countTime) {
745       case 0:
            lcd.print(">0.25  0.5  1.0 ");
747         t_param = 250; //miliseconds
            break;
749       case 1:
            lcd.print(">0.5  1.0  2.0 ");
751         t_param = 500;
            break;
753       case 2:
            lcd.print(">1.0  2.0  3.0 ");
755         t_param = 1000;
            break;
757       case 3:
            lcd.print(">2.0  3.0  4.0");
759         t_param = 2000;
            break;
761       case 4:
            lcd.print(">3.0  4.0  5.0");
763         t_param = 3000;
            break;
765       case 5:
            lcd.print(" 3.0 >4.0  5.0");
767         t_param = 4000;
            break;
769       case 6:
            lcd.print(" 3.0  4.0 >5.0");
771         t_param = 5000;
            break;
773     }
        // buttons are waiting to be pressed
775     backButton.loop();
        selectButton.loop();
777     upButton.loop();
        downButton.loop();
779   }
      Serial.print(">>> Time: ");
781   Serial.println(t_param);
    }
783 // buttons are waiting to be pressed
    upButton.loop();
785 downButton.loop();
    backButton.loop();
787 selectButton.loop();

789 }
}
791

void showParameters(){
793

  Serial.println(">Showing current parameters");
795 lcd.clear();

797 zStart = eeprom_read_dword(addressStart);

799 int step = (int) round(M1_param/0.45); // steps it must take to complete the M1
      angle
```

```
  float megaSteps = abs((zStop-zStart)/step);

  long int distanceM1_show = zStop-zStart; // steps M1 will take from start to stop
  float total_distance = (distanceM1_show+(distanceM1_show*M2_param/M1_param));
  float steps_to_distance_total = (total_distance*0.45*3*8.885)/125;

  int countShow = 0;
  String showParam;
  while (!backButton.isReleased()){ // while the user does not press the backButton
    // to scroll through parameters
    if (upButton.isReleased()){
      if (countShow > 0) {
        countShow--;
      }
    }
    if (downButton.isReleased()) {
      if (countShow < 3) {
        countShow++;
      }
    }

    String M1str = "M1: " + String(M1_param) + "      ";
    String M2str = "M2: " + String(M2_param) + "      ";
    String timestr = "Time: " + String(t_param) + "    ";
    String stepstr = "Dist.: " + String(steps_to_distance_total) + "    ";
    String slicesstr = "Slices: " + String((int)megaSteps+1) + "      ";
    // menu displays as the user scrolls through parameters with up (left) and down
     (right) buttons
    switch (countShow) {
      case 0:
        lcd.setCursor(0, 0);
        lcd.print(M1str);
        lcd.setCursor(0, 1);
        lcd.print(M2str);
        break;
      case 1:
        lcd.setCursor(0, 0);
        lcd.print(M2str);
        lcd.setCursor(0, 1);
        lcd.print(timestr);
        break;
      case 2:
        lcd.setCursor(0, 0);
        lcd.print(timestr);
        lcd.setCursor(0, 1);
        lcd.print(stepstr);
        break;
      case 3:
        lcd.setCursor(0, 0);
        lcd.print(stepstr);
        lcd.setCursor(0, 1);
        lcd.print(slicesstr);
        break;
    }
    upButton.loop();
    downButton.loop();
    backButton.loop();
  }

}
```

```
void startAcquisition() {
  Serial.println("Acquiring images...");
  lcd.clear();

  // microstepping: 1/4 step = 0.45 degrees
  // the M1 and M2 parameters correspond to the angle step each motor must take
  // so the total microsteps the motor must take is approximately:

  zStart = eeprom_read_dword(addressStart);
  int step = abs((int) round(M1_param/0.45)); // steps it must take to complete the
     M1 angle
  float megaSteps = abs((zStop-zStart)/step); // how many big steps (composed of
    steps)

  // we are dealing with integers
  // so we need to take in consideration that due to rounding, some steps are
    missing:
  int extraSteps = abs((zStop-zStart)) - (step*(int)megaSteps); //

  int extraSteps_per_megaStep = (int) extraSteps/megaSteps; // can we spread the
    extra steps equally
  int remainder_extraSteps = extraSteps%(int)megaSteps; // but sometimes some
    remain
  int extraStepsList[(int)megaSteps];

  for (int i=0; i<(int)megaSteps; i++){
    extraStepsList[i] = extraSteps_per_megaStep; // start with equal extra steps in
     each megastep

  }
  for (int k=0; k<remainder_extraSteps; k++){
    extraStepsList[k]++; // spread the remainding extra steps
  }

  Serial.print("zStart: ");
  Serial.println(zStart);
  Serial.print("zStop: ");
  Serial.println(zStop);
  Serial.print("Step: ");
  Serial.println(step);
  Serial.print("Extra steps needed: ");
  Serial.println(extraSteps);
  Serial.print("Slices: ");
  Serial.println(megaSteps+1);
  Serial.println("Extra steps per Mega step: ");
  for(int j = 0; j < (int)megaSteps; j++)
  {
    Serial.print(extraStepsList[j]);
    Serial.print(" ");
  }
  Serial.println(" ");

  lcd.print(">Working...");
  lcd.setCursor(0, 1);
  String toLCD = "0%              ";
  lcd.println(toLCD);

  int count = 0;
  while (count < 1) { // so that this occurs only once

    // this program only keeps track of the position of motor 1
```

```
915     // because they run in speeds according to the chosen ratio M1/M2
        // this way, they stop at the same time at the correct position for each one
917
        long lastCurrentPosition = eeprom_read_dword(addressCurrent);
919
        // first it is necessary to put the motors in the initial position, if needed
921     if (zStart != lastCurrentPosition) {
          if (stepper1.currentPosition() >= (zStart-lastCurrentPosition)){
923         while (stepper1.currentPosition() != (zStart-lastCurrentPosition)) {
              stepper1.setSpeed(-M1_param*20);
925           stepper2.setSpeed(-M2_param*20);
              stepper1.runSpeed();
927           stepper2.runSpeed();
            }
929       } else {
            while (stepper1.currentPosition() != (zStart-lastCurrentPosition)) {
931           stepper1.setSpeed(M1_param*20);
              stepper2.setSpeed(M2_param*20);
933           stepper1.runSpeed();
              stepper2.runSpeed();
935         }
          }
937       stepper1.setCurrentPosition(zStart);
        } else {
939       if (stepper1.currentPosition() >= zStart){
            while (stepper1.currentPosition() != zStart) {
941           stepper1.setSpeed(-M1_param*20);
              stepper2.setSpeed(-M2_param*20);
943           stepper1.runSpeed();
              stepper2.runSpeed();
945         }
          } else {
947         while (stepper1.currentPosition() != zStart) {
              stepper1.setSpeed(M1_param*20);
949           stepper2.setSpeed(M2_param*20);
              stepper1.runSpeed();
951           stepper2.runSpeed();
            }
953       }
        }
955


957     delay(100);

959     // backlash
        if (zStart >= 0) {
961       while (stepper1.currentPosition() != zStart + 2400) {
            stepper1.setSpeed(M1_param*20);
963         stepper2.setSpeed(M2_param*20);
            stepper1.runSpeed();
965         stepper2.runSpeed();
          }
967       delay(100);
          while (stepper1.currentPosition() != zStart) {
969         stepper1.setSpeed(-M1_param*20);
            stepper2.setSpeed(-M2_param*20);
971         stepper1.runSpeed();
            stepper2.runSpeed();
973       }
        } else {
975       while (stepper1.currentPosition() != zStart - 2400) {
```

```
        stepper1.setSpeed(-M1_param*20);
977     stepper2.setSpeed(-M2_param*20);
        stepper1.runSpeed();
979     stepper2.runSpeed();
      }
981   delay(100);
      while (stepper1.currentPosition() != zStart) {
983     stepper1.setSpeed(M1_param*20);
        stepper2.setSpeed(M2_param*20);
985     stepper1.runSpeed();
        stepper2.runSpeed();
987   }
    }
989
    delay(1000); // 1 second delay after motors are positioned
991
    long int pos_next = zStart;
993 int countMegaStep = 0;

995 //take to position 2
    while (countMegaStep <= megaSteps) { // while motor 1 does not reach the final
    position, zStop
997
      // each step
999   eeprom_update_dword(addressCurrent, stepper1.currentPosition()); //update the
     current position

1001  delay(1000);
      if (zStop>zStart){
1003    while (stepper1.currentPosition() != pos_next){ // while motor 1 does not
    reach end of the step
          stepper1.setSpeed(M1_param*10); //speeds at the chosen ratio
1005      stepper2.setSpeed(M2_param*10);
          stepper1.runSpeed();
1007      stepper2.runSpeed();
        }
1009  } else {
        while (stepper1.currentPosition() != pos_next){ // while motor 1 does not
    reach end of the step
          stepper1.setSpeed(-M1_param*10); //speeds at the chosen ratio
1011      stepper2.setSpeed(-M2_param*10);
          stepper1.runSpeed();
1013      stepper2.runSpeed();
        }
      }
1017
      Serial.print("Current position: ");
1019  float steps_sum_start = (stepper1.currentPosition()+(stepper1.currentPosition
    ()*M2_param/M1_param));
      float steps_to_distance_start = (steps_sum_start*0.45*3*8.885)/125;
1021  Serial.println(steps_to_distance_start);

1023  eeprom_update_dword(addressCurrent, stepper1.currentPosition());

1025  // activate lasers and camera
      delay(900); // a 0.9s delay after the motors stop for mechanical
    stabilization
1027  // checking which lasers to turn on
      if (laserMode.equals("L1")){
1029    digitalWrite(bottomLaserTrigger, HIGH);
        digitalWrite(topLaserTrigger, LOW);
```

```
1031        } else if (laserMode.equals("L2")) {
              digitalWrite(bottomLaserTrigger, LOW);
1033          digitalWrite(topLaserTrigger, HIGH);
            } else if (laserMode.equals("L1+2")){
1035          digitalWrite(bottomLaserTrigger, HIGH);
              digitalWrite(topLaserTrigger, HIGH);
1037        }

1039        delay(500);
            // turn camera on and off according to chose time parameter
1041        if (t_param <= 1000) {
              digitalWrite(cameraTrigger, HIGH);
1043          delay(t_param);
              digitalWrite(cameraTrigger, LOW);
1045          delay(250);
            } else {
1047          int countTimeLoop = 0;
              while (countTimeLoop*1000 < t_param) {
1049            digitalWrite(cameraTrigger, HIGH);
                delay(1000);
1051            digitalWrite(cameraTrigger, LOW);
                delay(250);
1053            countTimeLoop++;
              }
1055        }

1057        delay(250);
            // turn off lasers
1059        digitalWrite(bottomLaserTrigger, LOW);
            digitalWrite(topLaserTrigger, LOW);
1061


1063        lcd.setCursor(0, 1);
            int currentSlice = countMegaStep+1;
1065        int totalSlices = (int) megaSteps + 1;
            String toLCD = (String(currentSlice)+"/"+String(totalSlices)+"    ");
1067        lcd.println(toLCD);

1069        if (zStop>zStart){
              pos_next = pos_next+step+extraStepsList[countMegaStep]; // update next step
1071        } else {
              pos_next = pos_next-step-extraStepsList[countMegaStep];
1073        }

1075        countMegaStep++;
            Serial.println("----------------------");
1077      }

1079      delay(2000); // delay before resetting motor position
          count++;
1081      lcd.clear();
          lcd.print("Resetting...");
1083
          // resetting motors back to the original position
1085      if(zStop>zStart){
            while (stepper1.currentPosition() != zStart) {
1087          stepper1.setSpeed(-M1_param*20);
              stepper2.setSpeed(-M2_param*20);
1089          stepper1.runSpeed();
              stepper2.runSpeed();
1091        }
```

```
    } else {
1093        while (stepper1.currentPosition() != zStart) {
        stepper1.setSpeed(M1_param*20);
1095        stepper2.setSpeed(M2_param*20);
        stepper1.runSpeed();
1097        stepper2.runSpeed();
      }
1099    }

1101    eeprom_update_dword(addressCurrent, stepper1.currentPosition());

1103    delay(500);

1105    // the backButton is waiting to be pressed
    backButton.loop();
1107  }
}
1109


1111 void reset() {

1113   // to choose which laser or lasers to use
   Serial.println(">Resetting");
1115   lcd.clear();
   int countResetMenu = 0;
1117   while (!backButton.isReleased()){ // while the user does not press the backButton
     // to scroll through laser options
1119     if (upButton.isReleased()){
       if (countResetMenu > 0) {
1121         countResetMenu--;
       }
1123     }
     if (downButton.isReleased()) {
1125       if (countResetMenu < 2) {
         countResetMenu++;
1127       }
     }
1129

     // menu displays as the user scrolls through it with up (left) and down (right)
      buttons
1131     switch (countResetMenu) {

1133       case 0: // return to 0
         lcd.setCursor(0, 0);
1135         lcd.print(">Go to 0     ");
         lcd.setCursor(0, 1);
1137         lcd.print(" Go to middle");

1139         if(selectButton.isPressed() ){
           Serial.println(">>Going to 0");
1141           stepper1.setCurrentPosition(eeprom_read_dword(addressCurrent)); //make
    sure stepper is at the right position
           if (stepper1.currentPosition() >= 0){
1143           while (stepper1.currentPosition() != 0) {
             stepper1.setSpeed(-M1_param*20);
1145             stepper2.setSpeed(-M2_param*20);
             stepper1.runSpeed();
1147             stepper2.runSpeed();
           }
1149         } else {
           while (stepper1.currentPosition() != 0) {
```

```
1151              stepper1.setSpeed(M1_param*20);
                  stepper2.setSpeed(M2_param*20);
1153              stepper1.runSpeed();
                  stepper2.runSpeed();
1155            }
              }
1157          eeprom_update_dword(addressCurrent, stepper1.currentPosition()); //
    update the position in the EEPROM
          }
1159        break;
        case 1: // go to position between zStop and zStart
1161        lcd.setCursor(0, 0);
            lcd.print(">Go to middle");
1163        lcd.setCursor(0, 1);
            lcd.print(" Go to zStart");
1165        if(selectButton.isPressed()){
              Serial.println(">>Going to the middle");
1167
              zStart = eeprom_read_dword(addressStart);
1169          stepper1.setCurrentPosition(eeprom_read_dword(addressCurrent));
              int step = abs((int) round(M1_param/0.45)); // steps it must take to
    complete the M1 angle
1171          float megaSteps = abs((zStop-zStart)/step); // how many big steps (
    composed of steps) (zStop=0)

1173          // we are dealing with integers
              // so we need to take in consideration that due to rounding, some steps
    are missing:
1175          int extraSteps = abs((zStop-zStart)) - (step*(int)megaSteps); //

1177          int extraSteps_per_megaStep = (int) extraSteps/megaSteps; // can we
    spread the extra steps equally
              int remainder_extraSteps = extraSteps%(int)megaSteps; // but sometimes
    some remain
1179          int extraStepsList[(int)megaSteps];

1181          for (int i=0; i<(int)megaSteps; i++){
                extraStepsList[i] = extraSteps_per_megaStep; // start with equal extra
    steps in each megastep
1183          }
              for (int k=0; k<remainder_extraSteps; k++){
1185            extraStepsList[k]++; // spread the remainding extra steps
              }
1187
              // the middle position corresponds to a slice in the middle of zStart and
     zStop
1189          // not necessarily exactly in the middle, depends on number and size of
    the steps
              int countMegaStep = 0;
1191          midPosition = zStart;
              for(int cReset = 0; cReset < (int)(megaSteps/2); cReset++){
1193            if (zStop>zStart){
                  midPosition = midPosition+step+extraStepsList[cReset]; // update next
     step
1195            } else {
                  midPosition = midPosition-step-extraStepsList[cReset];
1197            }
              }
1199
              if (stepper1.currentPosition() >= midPosition){
1201            while (stepper1.currentPosition() != midPosition) {
```

```
            stepper1.setSpeed(-M1_param*20);
            stepper2.setSpeed(-M2_param*20);
            stepper1.runSpeed();
            stepper2.runSpeed();
          }
        } else {
          while (stepper1.currentPosition() != midPosition) {
            stepper1.setSpeed(M1_param*20);
            stepper2.setSpeed(M2_param*20);
            stepper1.runSpeed();
            stepper2.runSpeed();
          }
        }

        eeprom_update_dword(addressCurrent, stepper1.currentPosition());
        Serial.println(stepper1.currentPosition());
      }
      break;
    case 2: // return to zStart
      lcd.setCursor(0, 0);
      lcd.print(" Go to middle");
      lcd.setCursor(0, 1);
      lcd.print(">Go to zStart");

      if(selectButton.isPressed() ){
        Serial.println(">>Going to zStart");
        zStart = eeprom_read_dword(addressStart);
        stepper1.setCurrentPosition(eeprom_read_dword(addressCurrent)); //make
    sure stepper is at the right position
        if (stepper1.currentPosition() >= zStart){
          while (stepper1.currentPosition() != zStart) {
            stepper1.setSpeed(-M1_param*20);
            stepper2.setSpeed(-M2_param*20);
            stepper1.runSpeed();
            stepper2.runSpeed();
          }
        } else {
          while (stepper1.currentPosition() != zStart) {
            stepper1.setSpeed(M1_param*20);
            stepper2.setSpeed(M2_param*20);
            stepper1.runSpeed();
            stepper2.runSpeed();
          }
        }
        eeprom_update_dword(addressCurrent, stepper1.currentPosition()); //update
     position in the EEPROM

      }
      break;
  }
  // buttons are waiting to be pressed
  upButton.loop();
  downButton.loop();
  backButton.loop();
  selectButton.loop();
 }
}
```